Material Characterisation and Interface Optimisation of Recycled Carbon Fibre Composites

JACK HOWARTH

A Thesis Presented for the Degree of

Doctor of Philosophy
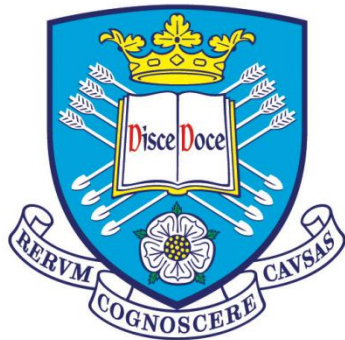
Department of Materials Science and Engineering

Faculty of Engineering

University of Sheffield, UK

December 2012

Acknowledgements

Abstract

Composites manufactured from a novel non-woven veil of recycled carbon fibre were tested in longitudinal tension, 3-point bend and short beam shear to assess their mechanical properties with respect to other commonly available materials. It was found that their mechanical properties were intermediate between 'high-end' unidirectional pre-preg and 'low-end' chopped strand mat, and similar to that of other short-fibre reinforced plastics.

A range of oxygen plasma treatments were carried out on the fibres to improve interfacial performance of the composites. It was found that treatment at an intermediate plasma power of 20 W resulted in the greatest improvement in tensile strength of a 10° off-axis composite. Samples were manufactured from either 2 individual veils (IV) or from 2, 10-layer 'pre-forms' (PF). Both exhibited similar improvements in 10° off-axis strength. Thus shadowing of the fibre within the plasma did not appear to be significant. Overtreatment at higher plasma powers (35 and 50 W for IV and 50 W for PF) resulted in a significant reduction in tensile strength and failure strain.

X-ray Photoelectron Spectroscopy (XPS) showed that plasma treatment at 20 W resulted in the highest level of oxygen functionality on the fibre surface, correlating with the best interfacial performance. Plasma treatment at 10 and 35 W resulted in slightly elevated surface oxygen content, however the off-axis tensile properties of 10 W treated samples were not significantly improved compared to the untreated control.

The poor mechanical performance of the over-treated samples can be attributed to either an overly strong interface resulting from increased adhesion or damage to the fibres as a result of the treatment process. There were large variations in fibre wettability across treatments, such that no discernible pattern was present between wettability and interfacial performance.

XPS and ToF-SIMS analysis showed that there was almost complete coverage of the veil by the binder in the veil-making process, and that silicon contamination on the fibre itself is likely silica based, and that silicon present in the binder is PDMS.

List of Publications

The following publications are based on the work in this project:

1. **J. Howarth and F.R. Jones,** "Interface Optimisation of Recycled Carbon Fibre Composites" *Proceedings of ECCM 15*, Ref 1955, Venice, June 2012.

2. **J. Howarth, F.R. Jones and S.A. Hayes,** "Interface Optimisation of Recycled Carbon Fibre Composites"*, Proceedings of ICCM 18,* Ref IF1953, Jeju-do, August 2011.

The following presentations delivered were based on the work in this project:

1. **J. Howarth and F.R. Jones,** "Interface Optimisation of Recycled Carbon Fibre Composites"*, 15th European Conference on Composite Materials,* Venice, June 2012.

2. **J. Howarth, F.R. Jones and S.A Hayes,** "Interface Optimisation of Recycled Carbon Fibre Composites"*, 18th International Conference on Composite Materials,* Jeju-do, August 2011.

3. **J. Howarth, F.R. Jones and S.A. Hayes,** "Interface Optimisation of Recycled Carbon Fibre Composites Through Surface Treatment"*, 4th International Conference on Sustainable Materials, Polymers and Composites*, Birmingham, July 2011.

4. **M. Jeschke and J. Howarth,** "Advanced nonwoven materials from recycled carbon fibre"*, 1st International Conference on Carbon Fibre Recycling and Reuse,* Hamburg, Germany, November 2009.

Contents

Chapter 1

Introduction

1.1 Introduction

Composite material products are generally of high value, representing a significant investment in raw materials and manufacture. Their high intrinsic value (especially those made with carbon fibre reinforcement) combined with current legislation makes them a viable target for recycling and/or re-use. This has driven the development of several composite recycling technologies, whose focus is on the recovery and re-use of high value components. The nature of such processes results in recyclates that can differ vastly from the original product, and can be detrimental to their value. Composite recycling is a relatively new area of research, and it is important to characterise any recyclate material to assess its potential applications. Processes to retain high recyclate value are of increasing importance in the current economic and environmental climate.

The interface, or interphase, in fibre reinforced composites is the region where loads are transferred from the fibre phase to the matrix phase and vice versa, and is therefore of key importance in the development and performance of composite materials. The dependence of mechanical properties on the interface region has been demonstrated by the differing effects of many surface treatment applications to the fibres (usually anodic oxidation in the case of carbon). Surface treatment (or sizing) conditions need to be

optimised for a particular material system as effects on the interface (and therefore composite performance) can be harmful as well as positive.

Oxygen plasma treatment is a process that that can manipulate fibre surface chemistry and therefore affect interfacial performance in various ways. The main mechanisms for this are through removal of contaminants, changing fibre surface topography, imparting oxygen functionality and removal of weak boundary layers on the fibre surface. There are many varying parameters in oxygen plasma treatments, including plasma power, reactant flow rate, treatment time, temperature and pressure. This demonstrates the many treatment conditions possible using oxygen plasma treatment, and each must be optimised to achieved the desired effects.

There are many techniques by which the interface can be assessed. These range from mechanical testing of composites which provide a direct measurement of material performance, to surface analysis of the fibres themselves in order to quantify surface chemistry and any changes brought about by treatment. In most cases a combination of surface analysis and mechanical testing is performed in order to assess the contribution of any fibre treatments.

1.2 Aims of the Thesis

The initial aim of this work was to characterise the novel reinforcement material – a non-woven veil manufactured from recycled carbon fibre. The characterisation was to encompass an assessment of the mechanical properties of unidirectional composites

manufactured from it (in order to compare their performance with other fibre reinforced composites), and an analysis of the fibre surface chemistry.

The primary aim of this work was to optimise the interface of the resulting composites using oxygen plasma treatment of the fibres, and to characterise the changes in interfacial properties through fibre surface chemistry analysis and mechanical testing of the resulting composites. The work also aimed to assess the sources of contamination and the role of the binder in the fibre surface chemistry.

This work is intended to assess the potential of composites manufactured from this novel reinforcement material and to determine the suitability of oxygen plasma treatment as a means of optimising the interface region in the resulting composites.

Chapter 2

Literature Review

2.1 Composite Materials

A composite can be defined as "any multiphase material that exhibits the properties of each constituent, such that a better combination of properties is realised" [1]. The principle of these materials is to utilise the strengths of each constituent whilst each phase offsets the weaknesses of the other. For example in fibre reinforced plastics (FRPs), high strength, high modulus fibres are incorporated into a polymeric matrix resulting in a composite with properties intermediate between the 2 phases. Specifically $\sigma_f > \sigma_c > \sigma_m$, $E_f > E_c > E_m$ and $\varepsilon_f < \varepsilon_c < \varepsilon_m$ (σ = tensile strength, E = Young's modulus, ε = tensile strain and the subscripts f, c and m denote fibre, composite and matrix respectively).

Composite materials can be classified into several categories according to either the reinforcement or matrix. Based on the matrix there are polymer matrix composites, metal matrix composites and ceramic matrix composites. Based on the reinforcement there are particulate composites and fibrous composites. What sets composite materials apart from other multi-phase materials is that each phase is distinct from the other on the micro/macroscopic level. This is in contrast to for example, metal alloys, where the interaction of constituents at the atomic level mimics a single phase material.

FRPs typically consist of a fibrous reinforcing phase embedded in a polymeric matrix phase [2]. Reinforcing fibres are usually made of carbon, glass or polymer.

2.1.1 Fibre Reinforced Polymer Composites

Reinforcing fibres can be classified as a) continuous, aligned b) discontinuous, aligned or c) discontinuous, random. The appeal of FRPs as engineering materials is not based on their strength and stiffness alone, but on their *specific* strength and stiffness, i.e. their strength and stiffness per unit weight. This gives them a considerable advantage over metals. As a result FRPs are increasingly replacing metals in many applications. For example the new Boeing 787 Dreamliner is 50% composite by weight (including the wings and fuselage) whereas its previous jet the 777 is just 12%. [3]. Another example is that a continuously aligned carbon fibre/epoxy resin composite with a fibre volume fraction (V_f) of 60% has a specific stiffness and a specific tensile strength approximately 5 times that of a high strength Al-Zn-Mg alloy [4].

However this gives rise to an important drawback of FRPs. The carbon fibre/epoxy resin composite mentioned above only has high strength and stiffness when the load is applied parallel to the fibre direction. When loaded transversely to the fibre axis, the strength and stiffness are significantly lower ($\sigma_{clu} \gg \sigma_{ctu}$). That is to say that FRPs reinforced with aligned, unidirectional fibres are highly *anisotropic*. Anisotropy is the property of being directionally dependent, as opposed to *isotropy*, where properties are the same in all directions (for example metals). An example of the anisotropy of fibres is that in high strength carbon fibre, tensile strength is around 1.2 GPa when the fibres are loaded longitudinally but drops to around 40 MPa when loaded transverse to the alignment axis [1].

The anisotropy of FRPs can be overcome by stacking plies at different orientations, the simplest solution being to stack an equal number of plies at 90° to the alignment axis as parallel to the alignment axis (0°). This gives the panel similar load-bearing capabilities in 2 directions as opposed to one in the case of a unidirectional lay-up. However, the tensile strength will be approximately halved as only 50 % of the fibres are bearing longitudinal load. The 90° plies are adding weight, so the gain in having high strength in 2 directions is offset by a loss of *specific* strength.

Further complications arise when load needs to be carried in more than 2 directions. Plies can be laid up in any combination of orientations; however each differently oriented layer reduces the *specific* strength in any one direction. Designers can overcome this problem through a better understanding of how their component will bear load. With this knowledge the stacking sequence and orientation of the plies can be optimised for specific parts. There are numerous examples of modelling and algorithms being used to optimise the orientation of plies in a laminate [5, 6].

2.1.2 Fibres

Fibres used in FRPs are usually one of 3 types; carbon, glass or high performance polymeric. More recently natural fibres have grown in production due to their sustainability. The most common types are flax, hemp and jute. The Nova Institute estimates that in 2010 natural fibre reinforced plastics (NFRPs) accounted for approximately 13% of the E.U. composites market by weight, and that by 2020 this could increase to around 28% [7].

The most common synthetic polymer fibres are aromatic polyamides or "aramid," and were developed by DuPont in the U.S. and marketed mainly as Kevlar and Nomex. Kevlar 49 fibres for example, have a tensile strength of 3 GPa and Young's Modulus of 112.4 GPa [8]. Thus their stiffness is lower than that of carbon fibres, however Kevlar 49 fibres have a strain to failure of 2.4% [8]. This is very high compared to carbon which is much more brittle and this inherent toughness of aramid fibres makes them ideal in applications where toughness is paramount, for example in ballistic protection. They also have excellent temperature resistance compared to other organic polymers. This is due to the conjugated π-electron system (giving the polymer many stabilising resonance structures). The polymer chains are largely oriented parallel to the fibre axis, this has been shown by crystallography [9]. As such their strength and stiffness is highly dependent on the strength of the covalent linkages in the chain. The chains are linked together through relatively weak Hydrogen Bonding between the carbonyl oxygen of one chain and the H atom on the N-H of a neighbouring chain. As a result they are highly anisotropic with good properties in the longitudinal direction but poor properties in the transverse direction.

Glass fibre reinforced plastics (GFRPs) are by far the most commonly used in the composites industry, accounting for 90% of the world market [10]. The most common type of glass fibre, E-glass, has a tensile strength of approximately 2 GPa and Young's modulus of 76 MPa [2]. These are much lower than for carbon and aramid fibres, yet compare well with many metals. This in combination with glass fibres being much cheaper than carbon or aramid fibres accounts for them dominating the global composites market. When tested bulk glass fails at much lower stresses than theoretically possible and this is due to the presence of surface flaws which lead to

crack propagation [11]. Glass fibres have a high surface/volume ratio so the population of critical flaws is lower. Therefore glass fibres have a higher strength than the bulk. GFRPs are used in a wide range of applications with a focus on good properties *and* low cost. Examples include the manufacture of boats, bath tubs, sports equipment and piping.

Carbon fibres are the reinforcement of choice for high strength and stiffness, and can be classified into 2 main types; high modulus and high strength. The properties depend on the manufacturing process and nature of the pre-cursor. Polyacrylonotrile (PAN) is the main precursor, though pitch and rayon have also been used. Carbon fibres are 7-8 µm in diameter and consist of small crystallites of turbostratic graphite [4]. The difference between turbostratic graphite and graphite single crystals is that the layer planes are not regularly packed in the c-axis direction [4]. The carbon atoms in the layer planes are held together by covalent bonds, longitudinal to the fibre axis. In the transverse direction the planes are held together by weak intermolecular Van der Waal's forces resulting in the high anisotropy of carbon fibres.

Whether carbon fibre is high modulus or high strength depends on the final graphitisation temperature. High modulus fibres are graphitised at higher temperatures than high strength fibres [12] (resulting in better alignment of the layer planes), and as a result there is a trade-off between whether strength or stiffness is optimised. Although even high strength fibres have a slightly lower tensile strength than Kevlar 49, they are much stiffer. As a result carbon fibre reinforced plastics (CFRPs) are a widely used engineering material at the 'high-end' of the composites industry. Their main applications are in the aerospace and automotive industries.

Table 2.1 compares the properties of the typical fibre types mentioned above. Figures are obtained from Hull [4] and DuPont's Kevlar Technical Guide [8].

Table 2.1 – Comparison of the mechanical properties of different reinforcing fibre types.

Fibre Type / Property	Tensile Strength (GPa)	Longitudinal Modulus (GPa)	Transverse Modulus (GPa)	Strain to Failure (%)
High modulus C	2.2	390	12	0.5
High strength C	2.7	250	20	1
E-Glass	1.4-2.5	76	76	1.8-3.2
Kevlar 49	2.8-3.6	112	-	2.2-2.8

Table 2.1 illustrates how carbon fibres have lower strength to Kevlar 49 but vastly superior stiffness and so CFRPs dominate the aerospace and automotive industries, whereas the superior strain to failure of Kevlar 49 makes it an attractive material for applications where toughness is important. E-glass also has a high strain to failure but is inferior to Kevlar 49 in strength and stiffness and so is generally used where cost is paramount.

The anisotropy of carbon fibres is highlighted by the vastly differing values of modulus when parallel or transverse to the alignment axis ($E_{fl} \gg E_{ft}$). This is in contrast to E-glass fibres (and indeed other glass fibre types) which are isotropic ($E_{fl} = E_{ft}$). With the choices on offer, designers can optimise their material selection depending on their product requirements.

2.1.3 Matrices

Just as important as fibre selection in the manufacture of an FRP is the incorporation of an appropriate matrix phase. In some composites the matrix phase can be metallic or ceramic, but in the case of FRPs they are almost universally polymeric in nature. The matrix phase holds the fibres together, transfers load to the fibres and imparts ductility, flexibility and corrosion resistance to a composite.

There are 2 main classifications of polymer matrices, those derived from thermo-plastics and those from thermo-sets. Both types are used in composites, although thermo-sets dominate. Thermo-plastics, such as polypropylene and polycarbonate, are high molecular weight polymers which are not cross-linked. Their strength and stiffness arise from the properties of the monomer units. They are traditionally used in conjunction with short fibre reinforcing phases, although more recently they are being combined with continuous reinforcements [13]. Thermo-sets, such as epoxy and unsaturated polyester, are highly cross-linked polymeric systems whose properties arise from the degree of cross-linking. A key property difference is that when heated thermo-plastics will soften, whereas thermo-sets will only char and break down. This is due to thermo-plastics having only weak intermolecular forces present between the polymer chains, whereas thermo-sets are highly cross-linked throughout with covalent bonds. Table 2.2 [4, 14] compares the properties of typical resin systems of both types.

Table 2.2 – Comparison of the mechanical properties of common resin systems.

Resin Type/Property	Density (g cm^{-3})	Young's Modulus (GPa)	Tensile Yield Stress (MPa)	Strain to Failure (%)
Polypropylene	0.9	1-1.4	25-38	>300
Polycarbonate	1.1-1.2	2.2-2.4	45-70	50-100
Epoxy	1.1-1.4	3-6	35-100	1-6
Unsaturated Polyester	1.2-1.5	2-4.5	40-90	2

Thermo-sets dominate the composites industry due to their wide availability and ease of processing [15]. However thermo-plastics have some advantages; quality control is easier as they are usually in pelletized form or monomer units in solution. This is in contrast to some thermo-set epoxies which require hardeners, catalysts and viscosity modifiers [16]. Thermo-plastic matrices also exhibit greater toughness, however the processing of them usually involves high temperature and pressure (e.g. injection moulding) which increases component production costs.

An epoxy resin system was chosen as the matrix phase for this work due to its good compatibility with carbon fibre. Epoxy is a very general term satisfied by the presence of at least one epoxy group in each monomer unit of resin. Therefore there is scope for a wide range of epoxy resins and also the hardeners used to cure them. However most commercial epoxies are glycidyl ethers or amines synthesised from epichlorohydrin.
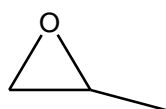
Fig 2.1 – General structure of the epoxy group

It can be seen from Figure 2.1 that the epoxide ring is under a high degree of bond strain, with bonding angles of around 60° compared to the standard 120° for a sp^3 hybridised carbon. Consequently it is highly reactive, and this feature is utilised for curing.

Although there is great diversity in available epoxies, hardeners and curing agents in practice the diglycidyl ether of bisphenol A (DGEBA) is the most common starting epoxy. It is made by reaction of bisphenol A with epichlorohydrin in the presence of sodium hydroxide (Fig 2.2).
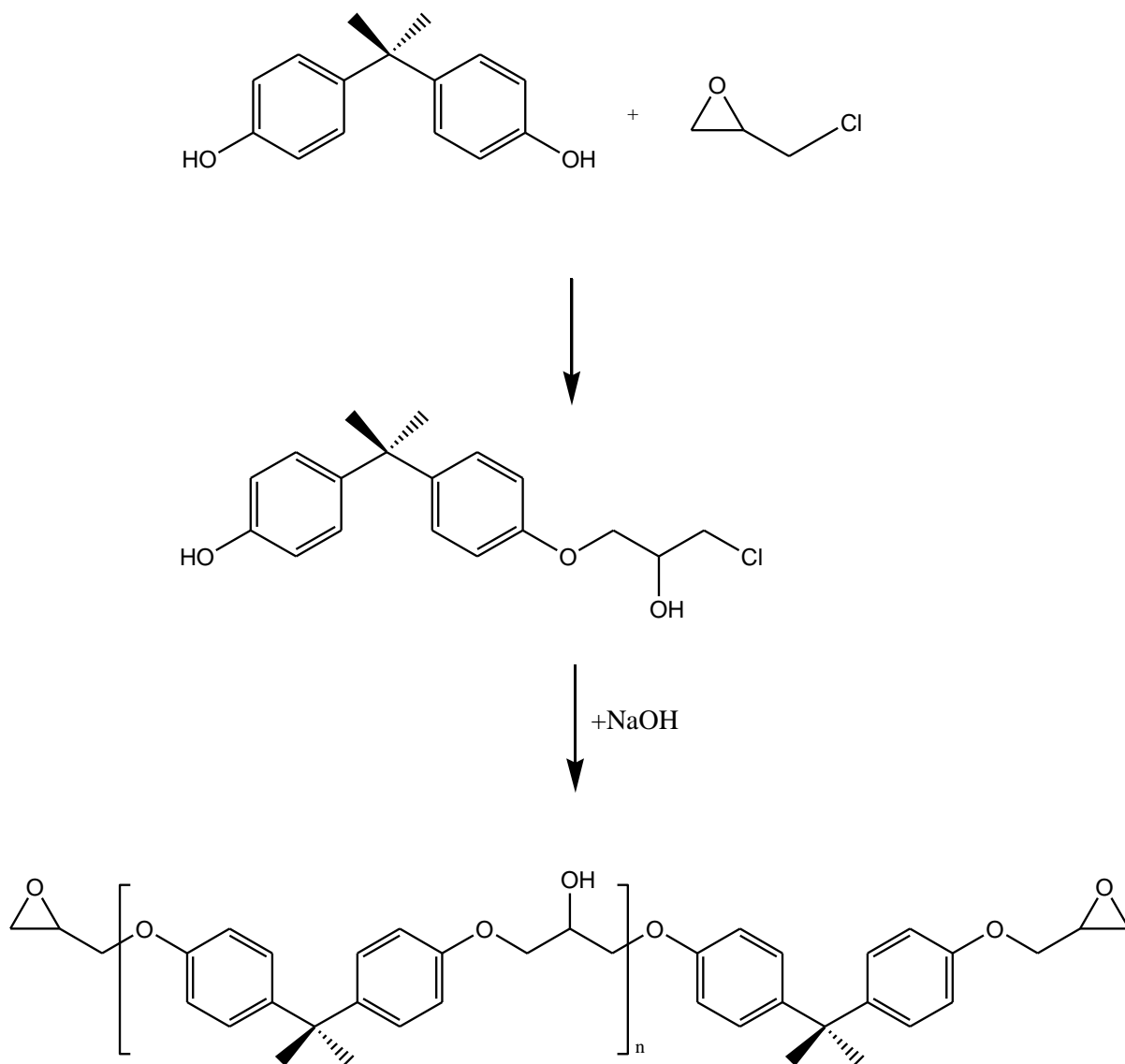
Fig 2.2 – Synthesis of epoxy resin from bisphenol A and epichlorohydrin

In practice *n* usually = 0-4 for epoxy resins, higher values of *n* lead to high viscosity and processing problems. *n* is usually fractional owing to the various oligomers produced on the reaction depicted in Figure 2.2.

Epoxies can react with each other (homopolymerisation) to form a polyether. A catalyst may be used to initiate chain growth polymerisation, for example BF_3 (cationic) or

tertiary amines (anionic). Copolymerisation can be achieved using an anhydride hardener. Hardeners for epoxy resins typically contain an active hydrogen atom [14], which adds to the epoxy group like so:
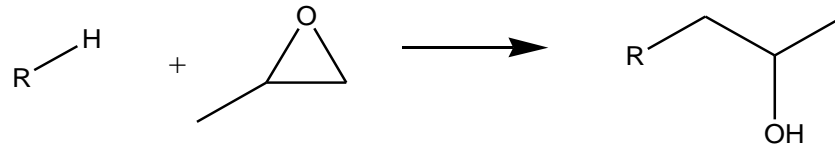
Fig 2.3 – Addition curing reaction of a typical hardener to epoxy group

It can be seen form Figure 2.3 that a precise concentration of hardener must be added in order to react with all the epoxy groups and not leave any excess hardener in the system. More specifically, the hardener is added at a stoichiometric concentration dependent on the molar mass per functional epoxy group and the molar mass of the hardener [14]. For example in Epikote 828, 90g of nadicmethylenetetrahydrophthalic anhydride (NMA) hardener must be added for every 100g of epoxy resin.

Although epoxies have good strength and stiffness properties they do have their limitations. They are sensitive to moisture, and can absorb water to approximately 10% by weight [17]. This has a huge effect on the glass transition temperature T_g, which reduces by around 20 ^oC per 1% by weight moisture adsorption [17].

2.1.4 Composite Mechanics

The simplest way to predict composite stiffness is to consider a composite containing a single fibre embedded in the matrix, under longitudinal load and assuming perfect interfacial bonding. Assuming that both phases deform elastically, in this model the

strain in the fibre is equal to the strain in the matrix (and as a result equal to the strain in the composite):

$$\varepsilon_c = \varepsilon_f = \varepsilon_m \tag{2.1}$$

Under elastic deformation the tensile strength of the composite is equal to its stiffness (Young's modulus) multiplied by its strain:

$$\sigma_c = E_c \varepsilon_c \tag{2.2}$$

The stiffness and strain in the composite depend on the relative contributions of stiffness and strain from each of the fibre phase and the matrix phase. The stress is equal to force/area ($\sigma = F/A$). Equation 2.2 can be re-written as:

$$\sigma_c = V_f E_f \varepsilon_f + (1 - V_f) E_m \varepsilon_m \tag{2.3}$$

As the strain in each phase and in the composite is equal (equation 2.1), dividing each term through by strain gives equation 2.4:

$$E_c = V_f E_f + (1 - V_f) E_m \tag{2.4}$$

This equation is known as the rule of mixtures, and its prediction of composite stiffness is highly valid for continuously aligned FRPs (where there are equal strains under elastic deformation). Complications arise when predicting stiffness for composites

reinforced with discontinuous and/or imperfectly aligned fibres, where fibre length and orientation efficiency factors are required to validate the rule of mixtures [4].

The fibre orientation efficiency (or Krenchel) factor, η_0, is given by the following equation [2]:

$$\eta_0 = \sum a_n cos^4\theta \qquad\qquad [2.5]$$

where a_n is the proportion of total fibre content and θ the angle of the fibres. The Krenchel factor varies from ⅜ for a randomly oriented reinforcement to 1 for a continuously aligned reinforcement.

Composites reinforced with short fibres can approach the strength of those reinforced with continuous fibres, providing the fibres exceed a critical length l_c. Load is transferred to the fibres through shear across the interface. The stress in the fibre increases from zero at the ends to a maximum value in the centre according to the Shear Lag model [18]. The critical fibre length l_c is defined as the minimum length at which the centre of the fibre reaches σ_{fu} when the matrix is at maximum shear stress, and is calculated from the following equation:

$$l_c = \frac{(\sigma_{fu} \times d_f)}{IFSS} \qquad\qquad [2.6]$$

Where σ_{fu} = fibre tensile strength, d_f = fibre diameter and $IFSS$ = interfacial shear strength. When $l < l_c$ the fibre cannot fail, the stress increases linearly from the ends to the fibre mid-point. When $l > l_c$, the fibre fibre will fail (and can continue to fail) until a

saturation point is reached (when $l < l_c$). When $l >> l_c$, the fibres can be considered as continuous with respect to length, giving the fibre length factor (η_l) a value of 1.

2.1.5 Common Manufacturing Routes

There are many ways of manufacturing composite artefacts, depending on the starting materials (fibre and matrix), their processability, the desired product performance/application and the costs involved.

The most common method of composite manufacture with thermo-setting resins is the *wet lay-up method* [19]. This is the method of choice for fibreglass/polyester composites, the most commonly produced material in the industry [10, 20]. The reinforcement, in the form of a fabric, mat or veil, is laid onto a mould or plate and wet resin is then worked into it. The resin can be applied in several ways, commonly it is worked into the reinforcement using a paint brush, and a rolling technique is applied to ensure even distribution and removal of air bubbles. Another reinforcement layer is placed on top and the cycle is repeated until the desired thickness has been reached. The resin is then left to cure. In some cases this can be aided by vacuum consolidation depending on the performance required and the costs involved.

When high performance of a composite is critical the part is usually made by the *pre-preg lay-up method*. Pre-pregs are sheets of reinforcement that have been pre-impregnated with resin which has been partially cured to aid in handling and lay-up. The relative amounts of fibre and matrix can be highly controlled in pre-preg manufacture. The partially cured resin has a 'tack' which allows a lay-up to be made without there being slippage between layers. The degree of tack is determined by the

17

resin type and the extent of cure, and can be controlled by addition of thermo-plastic in the resin formulation. This has the added benefit of controlling viscosity and increasing fracture toughness [21]. Extent of cure also affects the material's *drape*, its ability to conform to shapes which is important for lay-up onto moulds [22], although this is generally controlled by the weave of the reinforcement. In lay-up, sheets are cut and stacked according to the required reinforcement orientations and part thickness. Curing involves at the very least vacuum consolidation and often autoclaves are used.

Another technique finding increasing use in industry is resin transfer moulding (RTM). The process involves placing the reinforcing phase into a mould and injecting resin into the mould under pressure or under vacuum. Large, complex shapes can be made quickly and cheaply this way however the final properties tend to not be as good as parts made from pre-preg.

Other common techniques for composite manufacture are filament winding, pultrusion (both utilising fibre tows) and matched-die moulding (for sheet moulding compounds [SMCs] and bulk moulding compounds [BMCs]).

2.2 Composites Recycling

As a result of the current economical and environmental climate, technologies are being developed to recycle some end of life waste composites as an alternative to landfill. Such technologies are increasing in importance in Europe due to environmental legislation. Applicable to composites are the End-of-Life Vehicle Directive (ELV) [23]

and Waste Electric and Electronic Equipment Regulations (WEEE) [24]. The ELV states that by 2015 all vehicles will need to have a reuse and recovery rate of no less than 95%. The WEEE makes responsible manufacturers and distributors for the collection and recycling of their waste.

Suitability for recycling is affected by many factors, but generally there needs to be a market for the recyclate and the process of recycling must be economically viable. Initially the end of life material must be technically suitable for a given recycling process. There may be cases where if recycling is not initially economically viable, it is still carried out to avoid penalties or to gain access to subsidies.

Composites made with thermo-plastic matrices can be recycled directly by melting and remoulding into new material [25], however those made with thermo-set matrices are much more difficult to recycle as they cannot be remoulded [26]. It is therefore necessary to separate the reinforcement and matrix phases for material recovery in a recycling process for thermo-set based composites. There are 2 main categories of recycling process for this, mechanical processes and thermal processes. In mechanical processes, the size of the scrap material is reduced to produce the recyclate which can be used as a particulate reinforcement or filler. However these functions differ from that of the original material and so there is a reduction in value [27]. In thermal processes the phases are separated out using heat, either through combustion with energy recovery, pyrolysis or a fluidised bed process. A review of the current recycling technologies has been given by Pickering [28].

2.2.1 Fluidised Bed Process

Fluidised bed technology is an established technique widely used in process and combustion engineering, for example gas-solid reactions and combustion of solid fuels [29]. The process has been adapted for recycling of composites of thermo-set matrices at the University of Nottingham [30]. The principle of the technology is to recover fibres by removal of the polymer matrix phase. Fluidising air (pre-heated to 450-550 $^{\circ}$C depending on the matrix phase) is introduced into a bed of silica sand. Scrap composite is fed into the bed and rapid decomposition of the matrix occurs. The fibres are then released and elutriated into an air stream where they are separated from the air by a cyclone. The decomposed polymer is carried out in a gas stream and can also be isolated by a cyclone.

The recyclate is in the form of short, single filaments where the bulk has a 'fluffy' texture (Fig 2.4). One advantage of this process is the lack of surface contamination, organics are fully decomposed on the fluidised bed and any metal contaminants fall to the bottom of the bed where they can be later collected.

The fibre length distribution of the recyclate depends on the length distribution of the input scrap (30 mm is the practical limit, longer lengths result in agglomeration issues). The resulting fibres are clean, however due to the operating temperatures of the process some fibre oxidation is inevitable, even though it has been shown to happen quite slowly [31]. The mechanical properties of the recovered fibres varies depending on their type, though generally their elastic modulus remains the same but their tensile strength decreases significantly [32].

Fig 2.4 – Reyclate form after thermal recycling process

2.2.2 Pyrolysis

Pyrolysis is defined as "chemical decomposition occurring as a result of high temperature" [33]. More specifically it is a thermally initiated chemical process that decomposes organic matter in an inert atmosphere [34]. In terms of composites recycling it is still in the development phase and is not yet widely used in industry. However the fibres used in this work were recycled by pyrolysis.

One advantage of this method is that the matrix phase decomposes into valuable feedstock/fine chemicals which evaporate and can therefore be recovered along with the reinforcement phase, which is recovered as a solid residue [34]. However optimising the pyrolysis conditions for obtaining high quality recyclates of both phases is not yet possible and some compromises have to be made, particularly with respect to the reinforcing phase which has the highest value.

Generally the process involves feeding the scrap composite into a pyrolyser. Hot gases carry away the decomposed matrix phase to a condenser where hydrocarbon products (both solid and liquid) can be recovered. This leaves behind the reinforcement phase as

a solid residue. In some cases catalysts can be employed to reduce the required temperature for resin decomposition.

As with the fluidised bed process, the reinforcement recyclate is in the form of short, single filaments (Fig 2.4). Their properties again depend on the grade of the original fibre, but also on the type of pyrolyser used as these vary widely in this techniques' developmental stage as an application for composites recycling. Research in Japan showed that the tensile strength of carbon fibre recycled by pyrolysis at 500 ^{o}C was similar to that of the virgin equivalent, yet at 600 ^{o}C there was a drop of over 30 % [35].

2.2.3 Applications of the Recyclate

The short, single filaments that are extracted from the thermal recycling processes described above can be used in several applications, some directly and others that require further material processing.

The recyclate in its pure form (Fig 2.4) is suitable for use in BMCs as the 'fluffy' fibre can be blended with the resin in the same way that virgin fibre is used. It can also be used in compounding with thermo-plastics prior to injection moulding [36]. SMCs are more challenging as they generally have a 2D structure and the fibre in its fluffy form is not suitable for manufacture of 2D composite sheets.

Non-woven veils can be produced from the fibre recyclate in a wet processing method similar to paper making. The industrial partner in this work (Technical Fibre Products Ltd. [TFP]) processed the material in such a way as to manufacture a non-woven veil

that has a degree of fibre alignment. However the nature of the process means that fibre alignment decreases with increasing veil density. Such non-woven veils are applicable for SMC manufacture and also for wet lay-up (as in this work) and as a starting material for pre-impregnation with resin. Such veils can also utilise the electrical conductivity of carbon fibre for electromagnetic (EMI) shielding [37].

There are numerous examples of applications for recycled carbon fibre, although further research to improve fibre alignment is being conducted. This will enable higher fibre volume fractions to be achieved, which will result in further potential applications as the material moves towards achieving properties worthy of it being used as a structural material.

2.3 The Interface and Interphase

An interface is defined as the boundary between 2 distinct phases. In a composite the interface is at the boundary of the fibre phase and the matrix phase. The properties of a composite are critically dependent on the structure and bonding at the interface region, as it is here that stresses are transferred from the matrix phase to the fibre phase and vice versa. As a result commercial fibres are generally treated in some way to give them a coating or 'size' to aid interfacial bonding (see section 2.3.1).

Early models of interface micromechanics such as those by Cox [18] and Kelly-Tyson [38] imply a discrete change in material properties at the interface between the fibre and matrix phases. However it is unrealistic to view the interface as a discrete boundary

between two phases for several reasons. Firstly, there are chemical reactions between the resin and fibre sizing during curing. Secondly, it cannot be assumed that the interface is consistent throughout. Irregularities created by voids and contaminants are likely to be present. Also, the surface properties of carbon fibres are different from the bulk properties. For these reasons it is more accurate to consider the region between the fibre and matrix phases as an 'interphase'. An interphase is a region where the fibre and matrix phases are chemically and/or mechanically combined or otherwise indistinct [39]. In this way the separation of bulk fibre and bulk matrix is a gradual change across the interphase, not a discrete one as is implied by the term 'interface'. A schematic of a composite interphase is depicted in Figure 2.5 [40].
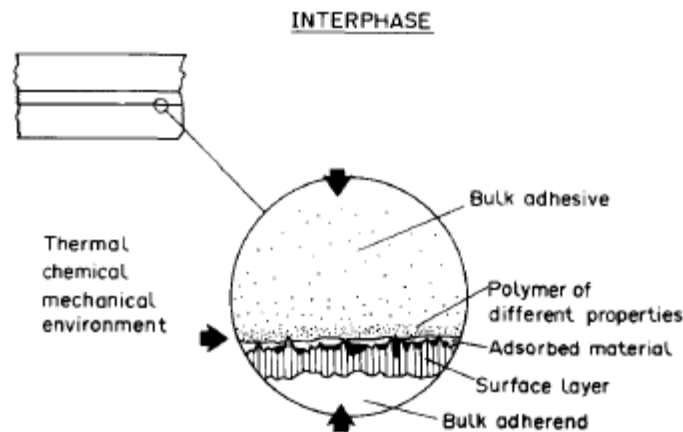
Fig 2.5 – Interphase region as illustrated by Drzal [40] (reproduced with permission from Elsevier).

The relationship between interface quality and composite performance is demonstrated by Drzal and Madhukar [41], who showed that optimal performance is achieved at an optimal level of interfacial adhesion, implying that an overly strong interface can inhibit mechanical properties. This demonstrates the degree of control required when surface

treating fibres for interface optimisation, as the relationship between interfacial adhesion and composite performance is by no means linear.

2.3.1 Carbon Fibre Surface Treatment

After manufacture, carbon fibres are usually treated or 'sized' to provide a protective coating for their processing into complex weaves and/or composites [42]. Untreated carbon fibres generally have poor adhesion to epoxy resins. This is largely due to graphitic carbon being chemically inert, and the graphitic basal planes aligned with the fibre axis provide few sites for chemical bonding [43]. It follows that high modulus fibres exhibit poorer adhesion to matrices than high strength fibres. The higher final graphitisation temperature in the manufacture of high modulus fibres leads to better alignment of the basal planes.

The most common way of treating carbon fibres is oxidative in an anodic electrolytic surface treatment. This results in oxygen functionalisation at the edges of the basal planes. This phenomenon has been extensively characterised for both high modulus and high strength fibres by Kozlowski and Sherwood [44]. There are several mechanisms by which fibre treatments can improve interfacial adhesion. For electrolytic oxidative treatments these are as follows; it has been shown that electrolytic oxidation roughens the surface of carbon fibres [45] which may promote mechanical interlocking at the interface. Covalent bonding between the polar oxygen groups on the surface and the resin is another possibility [46]. Drzal proposes that in addition to imparting oxygen functionality the electrolytic treatment removes the weak surface layer of the fibre, allowing the resin to bond to a stronger layer underneath [40]. In reality it is likely that a

combination of all three mechanisms contribute to interfacial bonding, of which chemical bonding is the most important [42].

Non-oxidative techniques are also used. These include vapour phase deposition, polymer grafting and pyrolitic carbon deposition. Plasma treatments can be oxidative or non-oxidative and this is explored in the next section.

2.4 Plasma Treatment of Fibres

A plasma is a partially or fully ionised gas, and is sometimes referred to as the fourth state of matter. Plasma induction by microwaves or radio-frequency (RF) generation has found increasing use in the treatment of fibre surfaces. The reactive species present in the plasma and the reactions and collisions that occur within it are utilised to introduce functional groups and/or clean and etch fibre surfaces to promote interfacial bonding. The nature of the treatment can be gaseous (oxygen and nitrogen plasmas) or a polymerisation using carefully selected monomers.

2.4.1 Plasma Polymerisation

Plasma polymerisation has been used extensively in the treatment of carbon and glass fibres and there are numerous examples of it enhancing the mechanical properties of the resulting composites.

Swait [47] observed an increase in tensile strength as a result of plasma polymerisation using an optimal ratio of functional monomer to non-functional monomer. He found

that an overly strong interface (from higher functional monomer/non-functional monomer ratios) led to a reduction in strength; this implies that plasma conditions must be highly controlled to obtain better properties (as was the case with Drzal and Madhukar [41]) and despite good interfacial bonding being important for composite performance, such a bond can be too strong and inhibit the properties of the material. The process can be applied to improve other properties too as a similar treatment system was used by Liu et al [48] that resulted in improved inter-laminar shear strength (ILSS) of the composites. In this case the highest values for ILSS were obtained from the highest functionality coatings. This is in contrast to Swait [47] and demonstrates how optimal treatments differ for different mechanical properties.

Plasma polymerisation has also been used in the treatment of carbon fibres. Kettle et al [49] also varied the ratio of functional/non-functional monomer and attributed improvements in the level of interfacial adhesion to oxygen and nitrogen containing functionalities. This is backed up by Loppatananon et al [50] who also observed increased adhesion (attributed to covalent bonding) when increasing concentrations of functional monomer were plasma polymerised. The technique has also been shown to improve the tensile strength of carbon fibres. Dilsiz et al [51] observed an increase in fibre tensile strength along with interfacial adhesion between fibre/epoxy when using dioxane and xylene in the plasma. It is notable that xylene is non-functional (it is a hydrocarbon), and so an increase in interfacial adhesion is in contrast to Swait [47] who found adhesion to be poorest on fibres coated with plasma polymerised hydrocarbon. Dagli and Sung [52] also observed increased fibre tensile strength after plasma polymerisation and proposed that this was due to the coating healing flaws on the fibre surface.

2.4.2 Gas Plasma Treatment

An alternative to plasma polymerisation is a plasma treatment using a flow of gas. In this method bottled gases such as oxygen, nitrogen and argon form the plasma rather than monomer(s). In this work oxygen plasma was used and is discussed in this section. Oxygen plasma treatment results in oxygen functionality on the fibre surface, which can be confirmed by X-Ray Photoelectron Spectroscopy XPS [53]. As stated previously, such functionality can improve fibre/matrix adhesion through covalent bonding at the interface [46]. It also improves the wetting properties of the fibres, permitting a more intimate fibre/matrix contact [54]. In addition the treatment alters the physical properties of the fibre surface; most significantly the level of surface roughness is increased [54].

These positive effects are demonstrated by Mujin et al [53], who observed an increase in ILSS in CFRPs where the fibres were treated by oxygen plasma. He observed an increase in oxygen functionality (confirmed by XPS); better wetting properties (confirmed by contact angle measurements) and an increase in surface roughness (confirmed by scanning electron microscopy [SEM]). Chang [55] observed an increase in transverse tensile strength of CFRPs after oxygen plasma treatment. Interestingly there was a steady increase in strength along with treatment time. However the longer treatment times (10 minutes and over) reduced the fibre strength by up to 20%, which would impact on the longitudinal tensile strength negatively. The increase in surface roughness (shown by SEM) explains these findings. XPS analysis showed that oxygen functionality was significantly increased by the treatment.

In contrast Bismarck et al [56] found that although wetting properties were improved (confirmed by contact angle measurements) there was almost no change in surface

morphology (confirmed by SEM) after oxygen plasma treatment. Yet other studies also show surface roughening occurring after oxygen plasma treatment, for example Huang et al [57] found that post-treatment the fibre surfaces had been etched as well as functionalised. These conflicts in surface roughness findings demonstrate the diversity of different plasma treatment processes. Different systems yield different results, and even in similar systems gas flow rate and plasma power can be varied. The origin of the fibres (and thus their surface chemistry) also plays an important role.

So far the effect of oxygen plasma treatment has been evaluated according to 3 main mechanisms; a) increase in fibre surface oxygen functionality, b) increase in fibre surface wettability and c) increase in fibre surface roughness. A fourth possible mechanism is that oxygen plasma treatment removes contaminants from the fibre surface. This ties in with Drzal's theory [40] that electrolytically oxidising treatments remove a weak boundary layer on the fibre surface. Montes-Moran et al [58] found that after oxygen plasma treatment fibre surfaces were 'cleaned' of carbonaceous contaminants (observed through scanning tunnelling microscopy [STM]).

In comparison plasma treatment (PT) and plasma polymerisation (PP) are similar in that they both impart functionality to the fibre surface. With PP a more controlled interface can be engineered through careful selection of monomers. In some cases PT has been shown to damage the fibres, reducing their mechanical properties, although this does not happen in every case, the consensus being that overtreatment (for example long treatment times and high plasma powers) is most likely to lead to this. PP in contrast has been shown to 'heal' fibre surface flaws. Overall it is difficult to conclude which is a better treatment as there are so many variables across both. In PT there are many species

that can be used as gaseous plasma, and in PP there are many monomers that can be chosen. The nature of the starting fibres will also affect how well the treatment process works, and plasma parameters such as power, treatment time and reactant flow rate can all be varied. In total this makes for many thousands of possible plasma treatment conditions. An oxygen plasma treatment system was chosen for this work as it has been shown to improve interface properties in literature, is simple to set up with an existing plasma reactor and has good potential for industrial scale-up.

2.5 Characterisation of Interface Properties

Characterisation of the interface is generally split into two types of analysis: a) analysis of the fibre surface; surface chemistry, topography, wettability and b) mechanical testing; tests on composite specimens that measure interface performance in treated specimens versus untreated controls. Mechanical data is then correlated with fibre surface analysis to determine how changes to the fibre surface have affected mechanical performance.

2.5.1 Surface Analysis

The principal technique for analysing fibre surface chemistry is XPS. In this technique the fibre sample is bombarded by X-rays under vacuum [59]. The incident X-ray photons have energy hv (where h is Planck's constant and v the X-ray frequency) which, when directed at the sample surface, result in emission of core electrons with kinetic energy E_K. E_K is the experimental quantity measured by the spectrometer, however its value is dependent on the energy of the incident X-ray photons. The electron binding

energy E_B is the parameter used in XPS to give chemical state information, and is calculated using equation 2.7:

$$E_B = hv - E_K - W \qquad\qquad [2.7]$$

where W is the work function of the spectrometer. The binding energy E_B is plotted graphically versus intensity (expressed as counts per second [CPS]). This gives chemical state information of species present within the sample as well as compositional information of the elements present. XPS has been used to quantify surface chemistry of many different carbon fibre types (see below). The technique is particularly useful for quantifying oxygen functionality, as different carbon oxidation states have their own characteristic binding energies. Proctor and Sherwood [59] used a relaxation potential model to predict chemical shifts associated with carbon functionality which had excellent agreement with experimental spectra.

Although carbon is the main constituent of carbon fibre surfaces, other species, mainly oxygen and nitrogen as well as in some cases silicon, sulphur and sodium are also present. XPS analysis of many different fibre types have shown that oxygen is always present (generally at 10-20% composition), nitrogen is present in most cases (2-7%) with silicon only present in one fibre type (5%) and sulphur and sodium being detected in some cases (at trace levels) [60, 61]. Oxygen is present as oxidised carbon in the form of carboxyl, phenolic and various other functionalities [62]. Nitrogen is present in the form of amine groups. It was commonly accepted that the nitrogen was residual, leftover from PAN after carbonisation however Alexander and Jones [63] showed that it arose from NH_3 in the NH_4HCO_3 electrolyte in the sizing process.

Time of Flight Secondary Ion Mass Spectrometry (ToF-SIMS) can also be used to analyse the chemistry of carbon fibre surfaces [64]. As with conventional mass spectrometry, ionic fragments are detected according to their mass/charge ratio and assigned to specific atomic or molecular fragments. The process involves the pulsing of primary ions onto the sample surface. The ToF analyser utilises an electric field to accelerate the ejected secondary ions to the detector. As all the secondary ions are accelerated to the same kinetic energy in this technique, the time of flight to the detector of each fragment varies only as the square root of their mass [64]. ToF-SIMS combines extremely low detection limits with high surface specificity unrealised by other techniques, and is an ideal tool for adsorption and contamination studies of carbon fibre surfaces. Vickers et al [65] used the high sensitivity and specificity of ToF-SIMS to distinguish adsorbate from substrate in studying the adsorption of organic polymers on carbon fibre surfaces.

SEM has been used extensively in the analysis of fibre surface topography (for example in [55-57]). Whilst providing detailed pictures at high resolution, deductions about topography are qualitative and changes in topography are difficult to conclude except in cases where the micrograph shows an obvious change in the roughness of the fibre surface.Contact angle measurements are widely used for measuring fibre surface wettability. The contact angle is determined by Young's equation [66]:

$$\gamma_{SV} = \gamma_{SL} + \gamma_{LV} cos\theta \hspace{4cm} [2.8]$$

where γ_{SV} is the surface energy of the solid/vapour phase, γ_{SL} that of the solid/liquid phase and γ_{LV} that of the liquid/vapour phase. θ is the contact angle. It can also be measured manually using a goniometer, which captures the profile of a liquid on a solid

substrate. Complete wetting occurs when θ = 0°, although a contact angle of 90° or less usually indicates favourable wetting [67]. In the case of very fine monofilaments such as carbon fibres, measuring θ accurately is very difficult compared to plane surface analysis [68].

This gives rise to other techniques of measuring θ; for example the Wilhelmy plate technique [69] which measures the contact force M (μg) between a single fibre of circumference C and a liquid of surface tension r_{lv}. θ can then be determined from the following equation:

$$Cos\theta=Mg/Pr_{lv}$$
[2.9]

where g is the gravitational constant.

Adaptations of this method can be made for measuring wettability of powders and of fibrous sheets using derivations of the Washburn Equation [70, 71].

2.5.2 Mechanical Testing

There are many different types of test that can be conducted to measure interface properties in a composite. The adequacy of them for different systems is varied, but in general in a test configuration, stress distribution must be similar to that in a real composite [72]. The micro-bond test can be used where interfacial de-bonding occurs where there is relatively little matrix deformation near the fibre. The micro-bond test gives a direct measurement of interfacial shear strength (IFSS) according to the equation [73]:

$$IFSS=F_{(max)}/(\pi d_f l_e) \hspace{4cm} [2.10]$$

Where $F_{(max)}$ is the peak load, d_f the fibre diameter and l_e the embedded length. Although this method gives a value for IFSS it does not separate the contributions of friction (mechanical interlocking) and chemical bonding, although there are examples of them being indirectly estimated [74]. Another problem is that there is a large amount of scatter associated with this test, many samples have to be tested to give a meaningful data set. For CFRPs where $\varepsilon_m >> \varepsilon_f$ the single fibre fragmentation test appears the most valid. In this test load is transferred from matrix to fibre through shear across the interface. The load applied results in a fibre break, and as the load increases further fibre breaks occur until a 'saturation point' [75], where the fragments are too short to undergo further breaks. However Piggott [76] states that single fibre tests for measurement of interface properties are fundamentally flawed. He states that the centro-symmetry of the specimens forces a shear failure which is not necessarily representative of interface failure in an actual composite and proposes that off-axis tensile testing of a composite specimen is more accurate. Another drawback of single fibre tests is that it is assumed that at saturation all fragments are de-bonded from the interface, and that the fibre strength of the fragments is extrapolated from the fibre strength of much longer fibres [75]. One way of overcoming these drawbacks is to couple single fibre fragmentation testing with Raman spectroscopy. This technique has the advantage of being able to directly measure the fibre stress or strain [77]. When carbon fibres deform under tension, there are characteristic shifts in their Raman spectra, therefore stress and strain distributions can be measured along embedded fibres.

Chapter 3

Experimental

3.1 Materials

3.1.1 Fibre

The carbon fibres used throughout this work were supplied by Technical Fibre Products Ltd (TFP) in the form of an aligned non-woven veil approximately 400 m long and 0.5 m wide (Fig 3.1). The veil density was 10 gm^{-2}. Fibres were reclaimed from bulk composites by pyrolysis and sent to TFP for further processing. The veil was manufactured in a wet processing technique similar to paper making. The fibres were coated with a water-dispersible polyester binder to hold the sheet together (in situ with the veil manufacture). The tensile strength of the sheet was approximately 90 times greater at 0$^{\mathbf{o}}$ to the fibre alignment axis than at 90$^{\mathbf{o}}$ (Fig 3.1). The number average fibre length = 10.8 mm and the weight average fibre length = 12.6 mm. Originally the fibres were high strength carbon fibres manufacture by Toho Tenax Europe.
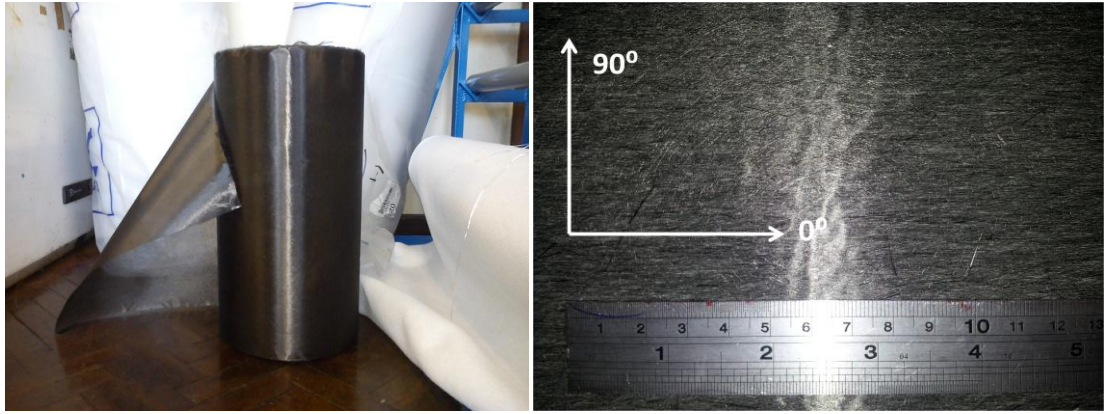
Fig 3.1 – Supplied carbon fibre veil

3.1.2 Matrix

The resin used as the matrix phase in this work was an epoxy-based system CY 2188, mixed with its hardener HY 2188, both supplied by Delta Resins Ltd. Chemical compositions of each are subject to their intellectual property. The components were mixed at a ratio of 10 parts by mass of epoxy with 3 parts by mass of hardener. The components were weighed out into a cup and mixed by hand using a tongue depressor for 5 minutes to ensure thorough mixing. Once mixed, degassing was performed in a vacuum oven at 80 $^{\circ}$C and 1 atm of vacuum pressure for approximately 15 minutes. See section 3.2.3 for cure schedule. Tensile properties of the cured resin system were tested and are summarised in Table 3.1 N.B. properties are test method dependant, figures are given as a guide only.

Table 3.1 – Tensile properties of the cured resin.

Tensile Strength (MPa)	Elastic Modulus (GPa)	Failure Strain (%)
47	2.4	3.3

3.2 Material Characterisation

Standard tests (tensile, 3-point bend and short beam shear) were carried out under conditions according to their appropriate international standards to determine the material properties for this recycled carbon fibre/epoxy resin matrix system. This section details the experimental procedure of their manufacture and testing.

3.2.1 Pre-Form Manufacture

The roll of fibre used in this work had a veil density of 10 gm^{-2}. This is extremely light compared to conventional woven carbon fibre fabrics, which are normally of the order of 200 gm^{-2}. It was therefore necessary to manufacture some 100 gm^{-2} 'pre-forms' to save time in preparing samples of the required thickness for testing.

This was done by cutting 10 sections of fibre 300 x 300 mm and stacking them together onto a polytetrafluoroethylene (PTFE) covered lay-up plate, with the bottom 5 being concave to the normal and the top 5 convex, to balance out the curvature of the roll and ensure a flat 100 gm^{-2} sheet (Fig 3.2). All veils were stacked unidirectional. Multiple pre-forms could be made simultaneously by inserting a sheet of PTFE between the stacks. The plate was then envelope vacuum bagged (akin to Fig 3.3) and left under vacuum for 2 hours.
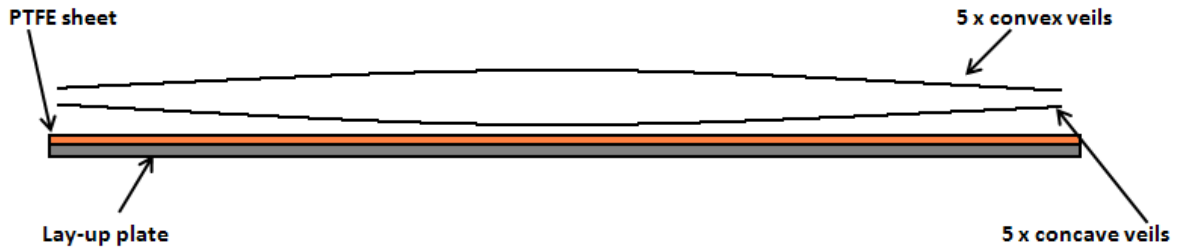
Fig 3.2 – Schematic of pre-form preparation prior to vacuum bagging

3.2.2 Lay-Up Procedure

The method used to manufacture composites was hand lay-up. Firstly, a steel lay-up plate was covered in a PTFE sheet. Steel does not warp under vacuum and PTFE is an excellent releasing agent for removal of the sample after curing. A thin layer of the resin system was applied to the plate using a paint brush, with similar dimensions to the sample being made. The first layer of fibre (in this case a 100 gm^{-2} pre-form) was applied to the coated surface. The brush was used to stick the sheet in place, apply further resin and ensure complete wetting out of the layer. A finned roller was used to aid this process and squeeze out excess resin and remove air bubbles. In this way V_f was maximised and void content minimised. The process was then repeated for all subsequent layers until the desired thickness was achieved. Each layer was laid up unidirectional (0°) with respect to the first layer so that a unidirectional composite sample was manufactured. See Table 3.2 below for detailed lay-up specifications. The subscript ($_{10}$) indicates a ten layer pre-form stack.

Table 3.2 – Specifications of manufactured panels, tests performed and sample sizes

Panel Size (mm)	Lay-Up	Tests Performed	Sample Size (mm)
300 x 300	$(0^o{}_{10})_3$	Tensile	250 x 15 x 1
300 x 300	$(0^o{}_{10})_6$	3 Point Bend	100 x 15 x 2
		Short Beam Shear	20 x 10 x 2

3.2.3 Curing

Upon completion of the lay-up a PTFE-covered caul plate was placed on top of the sample to provide a consistent finish on both sides. Breather fabric was placed onto the caul plate, this had the dual purpose of soaking up any excess resin and facilitating the removal of air from the system. The system was vacuum bagged (Fig 3.3) for curing.
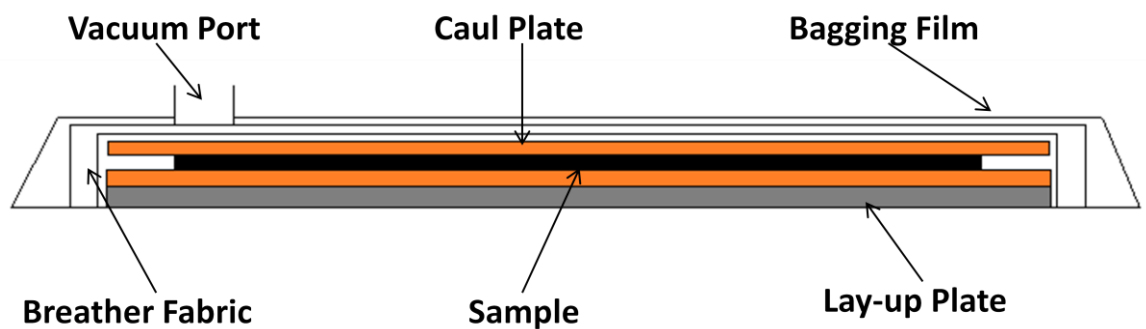

Fig 3.3 – Schematic of envelope vacuum bag curing system

The bag was placed into the oven and left to cure at 25 $^{\circ}$C for 24 hours. Upon completion the sample was removed from the vacuum bag and placed into the oven for a second time for post-curing, the cycle of which is 40 $^{\circ}$C for 2 hours, 60 $^{\circ}$C for 2 hours, 80 $^{\circ}$C for 2 hours, 100 $^{\circ}$C for 2 hours and 120 $^{\circ}$C for 12 hours, followed by slow cooling back to room temperature. All ramp rates were set to 2 $^{\circ}$C per minute.

3.2.4 Test Specimen Preparation

Upon completion of the sample manufacture, it was necessary to cut the panels into appropriately sized test pieces. Initially the edges were trimmed so that the panels were of consistent thickness throughout. One side of the panel was covered with masking tape, measured and marked for cutting into test specimens of dimensions given in Table 3.2.

A circular diamond saw with water cooling was used to cut the test specimens. For samples tested in bending and shear, no further preparation was necessary, however for tensile testing end-tabs were adhered to the test specimens at a given gauge length (150 mm). The end-tabs protected the test specimens from the machine grips.

The end-tabs were made from a woven fibre-glass/polyester composite, with the fibres running at +/-45° to the direction of testing. The faces of them were sanded down to assist adhesion to the end of the test specimens. Araldite curing adhesive was applied to the end tabs and the sample ends sandwiched between them and held in place with bulldog clips whilst the Araldite cured. See Figure 3.4 for end-tab dimensions and test specimen schematics. The dimensions of the test specimens were measured using Vernier calipers.
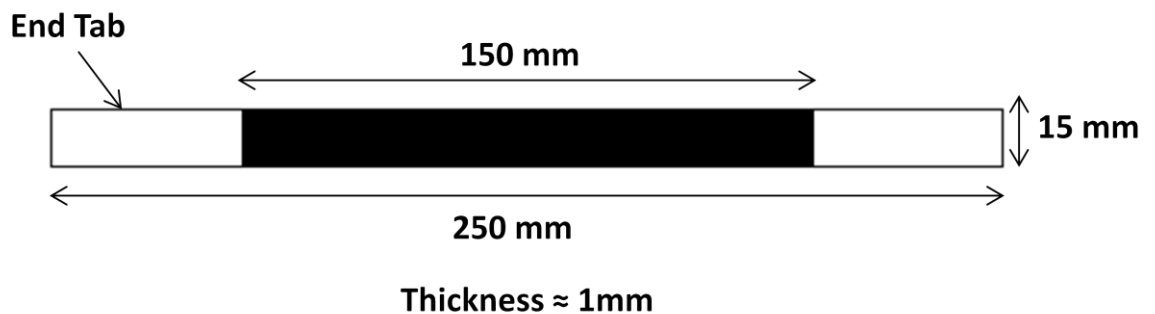

Fig 3.4 – Schematic of composite tensile test specimen

3.2.5 Volume Fraction of Fibres (V_f)

Fibre volume fraction was determined using Method B of ISO 14127[78]. This involved taking 10 measurements of thickness uniformly across a trimmed sample and recording the average. Fibre volume fraction was then given by the following equation:

$$V_f = \frac{N \times \rho_{A,p}}{d \times \rho_f} \times 10^{-1} \qquad\qquad [3.1]$$

Where N is the number of plies in the composite, $\rho_{A,p}$ is the mass per unit area of the fibre in the plies (10 gm^{-2}), d is the average measured thickness of the sample (mm) and ρ_f is the density of the fibre (1.75 gcm^{-3}).

3.2.6 Tensile Testing

Tests were performed and analysed according to the conditions outlined in ISO 527-1 [79] and ISO 527-5 [80] on a Hounsfield Universal Testing Machine with a 10 kN load cell. 5 specimens were tested. Load was applied at 0⁰ to the fibre alignment axis of the unidirectional samples. The samples were clamped using self-tightening grips. The test speed was 2 mm/min. A spread-sheet of load/extension was obtained for each test. The parameters obtained from the tests were as follows:

- Tensile strength, σ_u
- Elastic Modulus, E
- Failure Strain, ε_u

3.2.6.1 Calculating Modulus (E)

The elastic modulus (E) was calculated by plotting the linear portion of the stress/strain curve separately, adding a linear trend line and taking the gradient. Strain is plotted as a decimal and not a percentage. As $E = \sigma/\varepsilon$, this corresponds to gradient $(m) = dy/dx$. As the linear portion of the curve is a straight line, the $y = mx + c$ equation is obtained where $y = \sigma$, $x = \varepsilon$ and $m = E$. Figure 3.5 illustrates the example of E calculation of sample 4 of the unidirectional recycled CFRP.
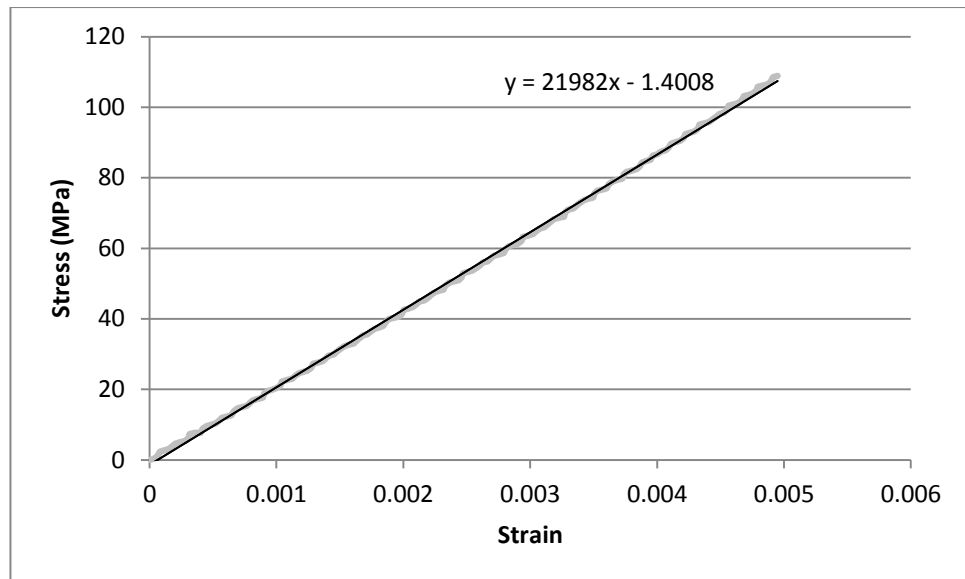
Figure 3.5 – Linear portion of stress/strain curve for sample 4 of UD recycled CFRP

Figure 3.5 shows that the $y = mx + c$ equation for the trend line is $y = 21982x – 1.4008$.

Therefore E = 21982 MPa = 21.982 GPa.

3.2.6.2 Calculating Strain (ε)

According to ISO 527-1, failure strain is calculated by equation 3.2 below:

$$\varepsilon_u(\%) = 100 \times \Delta L_0/L_0 \qquad\qquad [3.2]$$

where L_0 is the gauge length of the specimen (mm) and ΔL_0 is the increase in specimen length between the gauge marks (mm). In the absence of an extensometer (as there were none compliant with the test machine used) this equation does not take into account machine compliance, i.e. the movement of the machine which contributes to the extension measurement. To account for this a tensile test was performed on a steel bar of dimensions 68.5 mm x 25.25 mm x 6.3 mm. It can be assumed that in the force/extension plot that results, extension is purely due to machine movement as such a

thick specimen will not deflect (extend). From this data the average compliance *(C)* of the machine can be calculated in mm N^{-1}. Therefore equation 3.2 can be modified for compliance to give a more accurate failure strain value for the composite samples:

$$\varepsilon_u(\%) = 100 \times (\Delta L_0 - FC)/L_0 \qquad\qquad [3.3]$$

where *F* is the load at failure of the sample. The same principle can be applied when calculating the strain at any stress. This is important for calculating the elastic modulus (E), defined as stress (σ) / strain (ε), as if compliance is not accounted for false low values would be obtained for E. It must be noted however that the assumption of machine movement being wholly responsible for the extension measurement in the compliance test is false. There will inevitably be some deflection of the steel bar contributing to the extension measurement, although these values would be very small compared to the deflection of the composite test specimens at similar load. Extensometers are more accurate as they give a direct measurement of the sample extension, whereas compliance testing eliminates most (but not all) of machine movement from the extension measurement. The strain values calculated for the composite specimens are still valid for comparison to each other but not necessarily for comparison to other materials. See Appendix A for the compliance test data.

3.2.7 Three Point Bend Testing

Flexural properties were determined by tests performed and analysed according to the conditions outlined in ISO 14125 [81] on a Hounsfield Universal Testing Machine with a 10 kN load cell. 5 specimens were tested. The test speed was 5 mm/min. A spread-sheet of load/extension was obtained for each test. The parameters obtained from the tests were as follows:

- Flexural strength, σ_F

- Flexural modulus of elasticity, E_F

3.2.8 Short Beam Shear Testing

The inter-laminar shear strength was determined under a three point bending load. The tests were performed and analysed according to the conditions specified in ISO 14130 [82]. Tests were performed on a Hounsfield Universal Testing Machine with a 10 kN load cell. 5 specimens were tested. The test speed was 1 mm/min. A spread-sheet of load/extension was obtained for each test. The parameters obtained from the tests were as follows:

- Inter-laminar shear strength, ILSS

3.3 Plasma Treatment

3.3.1 Apparatus

The reactor apparatus consisted of a glass tubular vessel of volume 3.93 dm^3 connected to a vacuum pump at one end and a pressure gauge and pin valve at the other. The plasma was induced by a radio frequency (13.56 MHz) generator (supplied by Coaxial Power Systems) coupled to the reactor by a 3 turn wound coil. Reflected power was minimised using a matching unit also supplied by Coaxial Power Systems. A diagram of the reactor is shown in Figure 3.6 below.
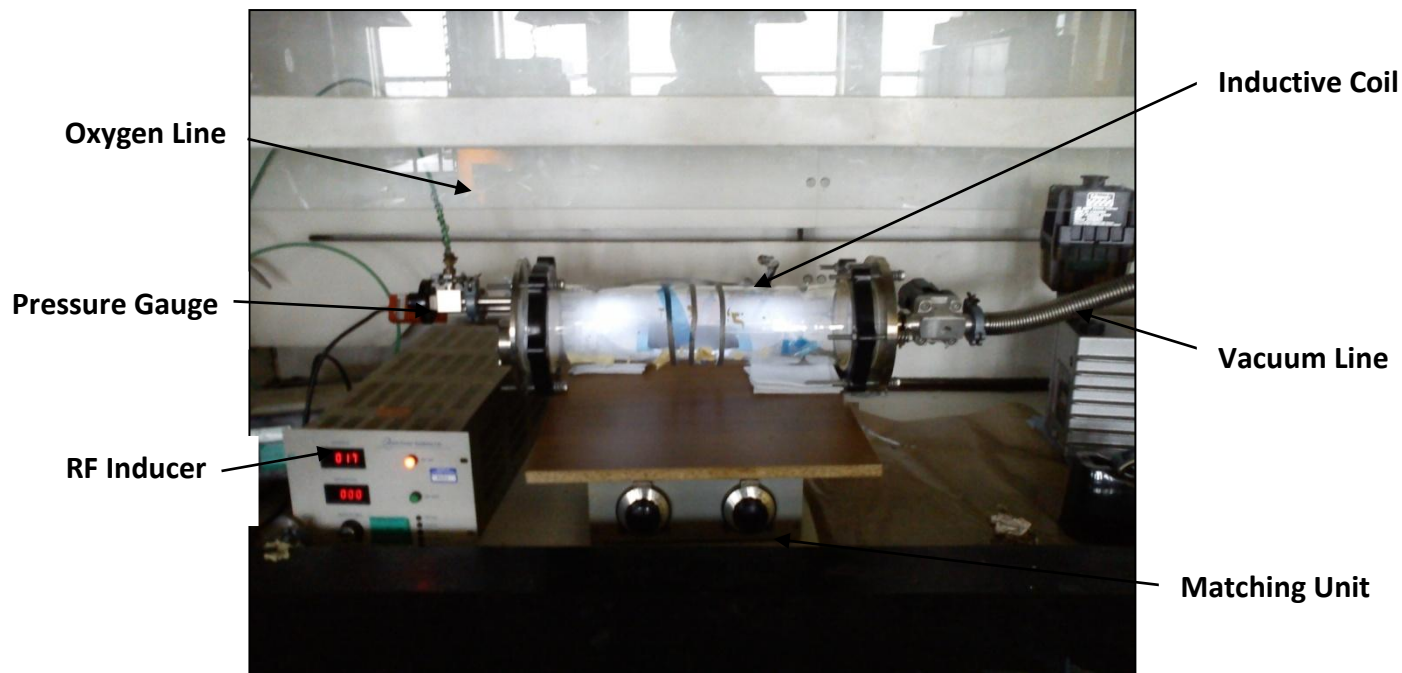
Fig 3.6 – Plasma Reactor

3.3.2 Treatment Process

A section of fibre measuring 120 x 70 mm was cut with a scalpel and affixed with tape at each end to microscope slides (with a 5 mm overlap) so that they sat centrally in the chamber. The reactor was first evacuated to a pressure of approximately $6x10^{-3}$ mbar. At this point oxygen was fed into the chamber via the pin valve, taking care to keep the flow rate as constant as possible across treatments (see section 3.3.3 for flow rate determination).

Once the desired flow rate was achieved the plasma was struck using the radio frequency generator and adjusted to achieve the desired power (in Watts [W]). Once stable the treatment was left to run for its allotted time. Upon completion of the treatment the plasma was extinguished and the oxygen pin valve left open for 15 minutes to terminate any reactive groups.

3.3.3 Reactant Flow Rate

The chamber was isolated from the vacuum using the shut-off valve between it and the pump. At this point the chamber becomes a fixed volume of gas where the pressure is steadily increasing due to the flow of oxygen (assuming there is no contribution from leaks). The rate of the pressure increase could then be calculated through manipulation of the ideal gas law (equation 3.4). This approach is valid for oxygen as it obeys the ideal gas law quite well particularly at low pressure.

$$pV = nRT \qquad\qquad [3.4]$$

p is the pressure in atm, V the volume in dm^3, n the number of moles of gas, R the ideal gas constant (8.314 J K^{-1} mol^{-1}) and T the temperature in K. Differentiating with respect to time for the flow of gas into a constant volume at constant temperature gives Equation 3.5:

$$\frac{dp}{dt}V = \frac{dn}{dt}RT \qquad\qquad [3.5]$$

where dp/dt is the change in pressure over time in atm s^{-1} and dn/dt is the number of moles of gas passing through the chamber per second with units of mol s^{-1}. Re-arranging Equation 3.5 for dn/dt then allows a calculation of flow rate to be made, in moles per second (mol s^{-1}):

$$\frac{dn}{dt} = (\frac{dp}{dt}V)/RT \qquad\qquad [3.6]$$

so it follows that flow rate (F), represented by dn/dt, is equal to dp/dt multiplied by a constant:

$$F = (p_2 - p_1) \times C \qquad\qquad [3.7]$$

The constant C was determined experimentally. Oxygen flow was stabilised at $p_1 = 0.06$ mbar, the shut-off valve was closed for $t = 30$ s and p_2 was recorded as 0.6 mbar. Therefore:

$$dp = 0.54\ mbar = 5.33 \times 10^{-4}\ atm \qquad [3.8]$$

Therefore:

$$\frac{dp}{t} = 1.78 \times 10^{-5}\ atm\ s^{-1} \qquad [3.9]$$

Multiplying by 60 s gives:

$$\frac{dp}{dt} \times 60s = 1.07 \times 10^{-3}\ atm\ min^{-1} \qquad [3.10]$$

Equation 3.6 is now:

$$\frac{dn}{dt} = 1.07 \times 10^{-3}\ atm\ min^{-1} \times V/RT \qquad [3.11]$$

where the chamber volume $V = 3.93$ dm^3 and $T = 293$ K:

$$\frac{V}{RT} = 1.61 \times 10^{-3}\ dm^3\ J^{-1}\ mol \qquad [3.12]$$

and so dn/dt is now:

$$\frac{dn}{dt} = 1.07 \times 10^{-3} \times 1.61 \times 10^{-3} = 1.72 \times 10^{-6}\ mol\ min^{-1} \qquad [3.13]$$

To convert mol min^{-1} to the more convenient units of standard cubic centimetres per minute (sccm), i.e. the volume of gas passing through the chamber if it were at standard temperature and pressure (STP), the following arrangement of the ideal gas law applies:

$$V = \frac{nRT}{p} \tag{3.14}$$

$$V(dm^3) = \frac{1.72 \times 10^{-6} \, mol \times 8.314 \, J \, K^{-1} \, mol^{-1} \times 273 \, K}{1 \, atm} = 3.9 \times 10^{-3} \, dm^{-3} = 3.9 \, cm^3 \tag{3.15}$$

and so the flow rate of oxygen in this experiment = 3.9sccm. The constant C is therefore:

$$C = \frac{F}{dp} = \frac{3.9 \, sccm}{0.54 \, mbar} = 7.22 \tag{3.16}$$

In future flow rate calculations the following equation was therefore used:

$$F(sccm) = (p_2 - p_1) \times 7.22 \tag{3.17}$$

In all plasma treatments a flow rate of 3.9 sccm was used as the plasma would readily strike at this flow rate using any power from 10-50 W.

3.4 Analysis of Plasma Treated Samples

This section details the manufacture and testing of samples produced from plasma treated fibres.

3.4.1 Samples Manufactured from Pre-forms

Samples were laid up using 2 pre-form stacks, whose manufacture is described in section 3.2.1, and plasma treated as in section 3.3. The lay-up procedure is described in section 3.2.2. See Table 3.3 below for the specification summary of the samples. Curing

of the samples is described in section 3.2.3. V_f determination is described in Section 3.2.5.

Table 3.3 – Specifications of manufactured panels, plasma treatment conditions, tests performed and sample sizes

Panel Size (mm)	Plasma Power (W)	Treatment Time (mins)	Lay-up	Tensile Test	Sample Size (mm)
120 x 70	Untreated	Untreated	$(0^o_{10})_2$	10° off-axis	100 x 5 x 0.7
120 x 70	10	20	$(0^o_{10})_2$	10° off-axis	100 x 5 x 0.7
120 x 70	20	20	$(0^o_{10})_2$	10° off-axis	100 x 5 x 0.7
120 x 70	28	20	$(0^o_{10})_2$	10° off-axis	100 x 5 x 0.7
120 x 70	35	20	$(0^o_{10})_2$	10° off-axis	100 x 5 x 0.7
120 x 70	50	20	$(0^o_{10})_2$	10° off-axis	100 x 5 x 0.7

Test specimens were prepared in the same way as in section 3.2.4 except for 2 key differences:

- Specimens were marked and cut on the diamond saw at *10° off-axis* to the fibre alignment axis.
- End tabs were adhered to give a 70 mm gauge length.

Tests were performed on a Hounsfield Universal Testing Machine with a 10 kN load cell and a test speed of 2 mm/min. Load was applied parallel to the sample length which as they were cut 10° off-axis resulted in a 10° off-axis tensile test. The samples were clamped using self-tightening grips. A spreadsheet of load/extension was obtained for each test. The parameters obtained from the tests were as follows:

- Tensile strength, σ^{10}_u
- Elastic Modulus, E^{10}

- Failure Strain, $\varepsilon^{10}{}_{u}$

When calculating strain (ε) and failure strain ($\varepsilon^{10}{}_{u}$) the same adjustments were made as in Section 3.2.6.2 to account for machine compliance. The mean values of each data set were calculated and are summarised in Table 4.2 of Section 4.2.1. They were then normalised for V_f by dividing the mean value of V_f for that data set and then multiplying by the mean V_f of all samples manufactured from pre-forms.

3.4.2 Comparison of Treated Samples

Samples were manufactured from individual veils as well as from pre-forms to remove the variable of 'shadowing' during the treatment process. It is possible that plasma treatment of the pre-forms only treated the outer veils, and so samples were made from 2 treated veils so as to test composites with uniform plasma treatments applied to each fibre layer.

3.4.3 Samples Manufactured from Individual Veils

Samples were laid up using 2 individual veils. The plasma treatment process is described in Section 3.3. The lay-up procedure is described in section 3.2.2. See Table 3.4 below for the specification summary of the samples. Curing of the samples is described in Section 3.2.3. V_f determination is described in Section 3.2.5.

Table 3.4 – Specifications of manufactured panels, plasma treatment conditions, tests performed and sample sizes

Panel Size (mm)	Plasma Power (W)	Treatment Time (mins)	Lay-up	Tensile Test	Sample Size (mm)
120 x 70	Untreated	Untreated	0^o_2	10° off-axis	100 x 5 x 0.1
120 x 70	10	20	0^o_2	10° off-axis	100 x 5 x 0.1
120 x 70	20	20	0^o_2	10° off-axis	100 x 5 x 0.1
120 x 70	30	20	0^o_2	10° off-axis	100 x 5 x 0.1
120 x 70	40	20	0^o_2	10° off-axis	100 x 5 x 0.1
120 x 70	50	20	0^o_2	10° off-axis	100 x 5 x 0.1

Samples were marked and cut at 10° off-axis and end tabs adhered to give a 70 mm gauge length in the same way as those in Section 3.4.1. Tests were performed on a Lloyd Instruments TA500 with a 500 N load cell and a test speed of 1 mm/min. As with the samples in section 3.4.1, the samples were clamped using self-tightening grips and a spreadsheet of load/extension was obtained for each test. The parameters obtained from the tests were as follows:

- Tensile strength, σ^{10}_u

- Elastic Modulus, E^{10}

- Failure Strain, ε^{10}_u

When calculating strain (ε) and failure strain (ε^{10}_u) no adjustments were made for compliance as the load required to fracture such thin samples was significantly lower than the samples made from pre-forms as to make adjustments to the value of extension negligible. The mean values of each data set were calculated and are summarised in Table 4.4 of Section 4.2.2. They were then normalised for V_f by dividing the mean value by the mean V_f for that data set and then multiplying by the mean V_f of all samples manufactured from individual veils.

3.5 Surface Analysis

3.5.1 X-Ray Photoelectron Spectroscopy (XPS)

The surface chemistry of the as-received and plasma treated veils (as well as that of the polyester binder) were analysed by XPS. The spectra were acquired using a Kratos Axis Ultra spectrometer, with a monochromated Al-Kα X-ray source. The beam had a take-off angle of 30° relative to the sample surface. The fibres were inserted into the sample holder directly whereas the binder was first dried onto a glass plate before mounting in the sample holder. In the case of the fibres the X-ray beam was parallel to the fibre alignment axis.

In addition to the survey scans high-resolution Carbon 1s (C1s) and Silicon 2p (Si2p) scans were performed on untreated samples and plasma treated samples at 10 W, 20 W and 35 W plasma power, all having had treatment times of 20 minutes. In the case of treated veils the analyses were performed immediately after treatment to minimise surface contamination. Survey and narrow scans were also performed on the polyester binder. The pass energy of the survey scans was 160 eV, and for the narrow scans was 20 eV.

Curve fitting was performed using CasaXPS Software. Curve fitting involved adding peaks to the spectrum until the residual peak fit the shape of the experimental peak. In the C1s spectra, peak line widths were set at 1.5 eV, and all peak full-width half maximums (FWHM) were set equal to that of the graphitic carbon peak. The only exception to this was the case of the shakeup satellite (π-π*) peak, the line width and FWHM of which varied across the spectra. The number of peaks added in the first stage

of curve fitting was according to the expected number of chemical states present for that given element. For example, in the C1s peak of the polyester binder, 3 peaks were added on the basis that there was expected to be peaks associated with C-C, C-OH(R) and C-OOH(R) bonds (Figure 4.13). The experimental peak curve showed a small peak at approximately 291.5 eV and so a 4th peak was added corresponding to π-π*. The FWHM of the first 3 peaks was set to 1.5 eV as the peak position in C1s spectra varies by 1.5 eV per each additional oxygen bonded to carbon. The peaks assigned by the user form a curve on the spectra (brown), and a correct assignment can be assumed should this curve match the experimental peak (red). See section 5.9.5 for a discussion of the errors associated with curve fitting. In the case of the plasma treated veil samples, the peaks mentioned above were not sufficient to speciate the experimental peak, and required the addition of a 5th peak (C=O).

In the Si2p peaks it is difficult to separate the Si2p$_{1/2}$ and Si2p$_{3/2}$ components (which arise because the p energy level is split by spin-orbital interaction). This is because the Si2p peak is a doublet of these components with very small variations in binding energy (usually a few tenths of an eV).

3.5.2 Time-of-Flight Secondary Ion Mass Spectrometry (ToF-SIMS)

Surface silicon was analysed by ToF-SIMS. The spectra were acquired using an Ion-Tof GmbH Tof-SIMS 5, with a Bi$_3^{2+}$ primary ion source. Analyses were carried out on the polyester binder (dried onto a film) and on the surface of the carbon fibre veil. Both positive and negative spectra were obtained, with peak position determined by the mass/charge ratio. For the polyester binder a primary ion dose of 6.63x10^7 ions/cm^2 was rastered over an area 500 μm^2 for both the positive and negative spectra. For the fibre

veil the primary ion dose was $2.35x10^8$ ions/cm^2 for the positive spectra and $5.88x10^7$ ions/cm^2 for the negative. In both cases the dose was rastered over an area 300 μm^2.

Peak intensity was not quantitatively indicative of relative amount of species present, only that the ions of species resulting in high intensity peaks travelled to the detector more readily. SurfaceLab 6 (Ion-Tof Gmbh) software was used for the analysis of the spectra.

3.5.3 Wicking Test

Surface wettability was measured by calculating the rate of uptake of ethanol and isopropanol onto the veils in a process known as the Wicking Test. 25 mm^2 sheets were cut and affixed to a rod attached to a 4-place balance. A stand was placed over the balance so that a petri dish could be placed on it without affecting the weight of the system. A cardboard lid was placed over the whole system to minimise the effect of air on the weight measurement. This petri dish was then slowly filled with solvent via a pipette until touching the bottom of the veil. Software (known as a DENVER spreadsheet) recorded the weight every second so that a rate of uptake could be established. The test is illustrated schematically in Figure 3.7 below:
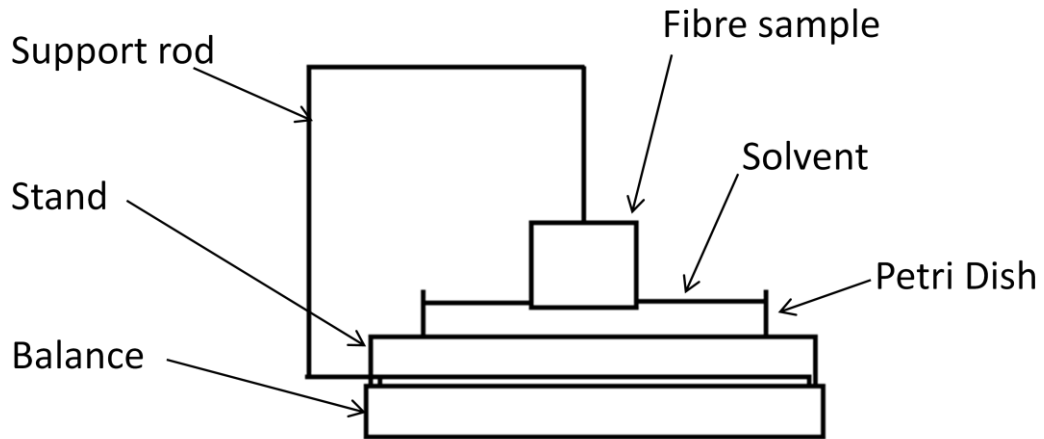
Fig 3.7 – Schematic representation of the Wicking Test

The rate of uptake measurement was related to the contact angle according to Equation 3.18, which is a derivative of the Washburn equation [70].

$$m^2 = \frac{C\rho^2\gamma cos\theta}{\eta} t \qquad\qquad [3.18]$$

Where *m* is the samples mass once 'Wicked' (change in weight stabilised), *C* the material Washburn constant, ρ the material density, θ the contact angle, η the liquid viscosity and *t* the time taken for wicking to occur.

Chapter 4

Results

4.1 Mechanical Characterisation

This section details the results of standard tests carried out on unidirectional composites of the recycled carbon fibre/epoxy resin matrix system. The aim of the tests was to assess the mechanical properties of the material system manufactured by wet lay-up and vacuum bag cured. All samples were unidirectional and bore load in the direction of the fibre alignment in order to achieve the maximum mechanical properties for this material system. The manufacturing details and sample dimensions are given in Section 3.2. Table 4.1 below summarises the data.

Table 4.1 – Mechanical Properties of Unidirectional (0°) Recycled CFRPs

Test	Property	Mean Value	St. Dev.	V_f (%)
Tensile	Strength (MPa)	364.5	10.5	15.7
	Modulus (GPa)	22.16	0.5	
	Failure Strain (%)	2.52	0.27	
3-Point Bend	Strength (MPa)	405.6	10.2	16.6
	Modulus (GPa)	27.07	0.6	
Short Beam Shear	ILSS (MPa)	30.67	1.51	

The stress/strain plots of the tensile specimens are presented in Figures 4.1 The load/extension plots of the 3-point bend specimens are presented in Figure 4.2. The load/extension plots of the short beam shear specimens are presented in Figure 4.3.
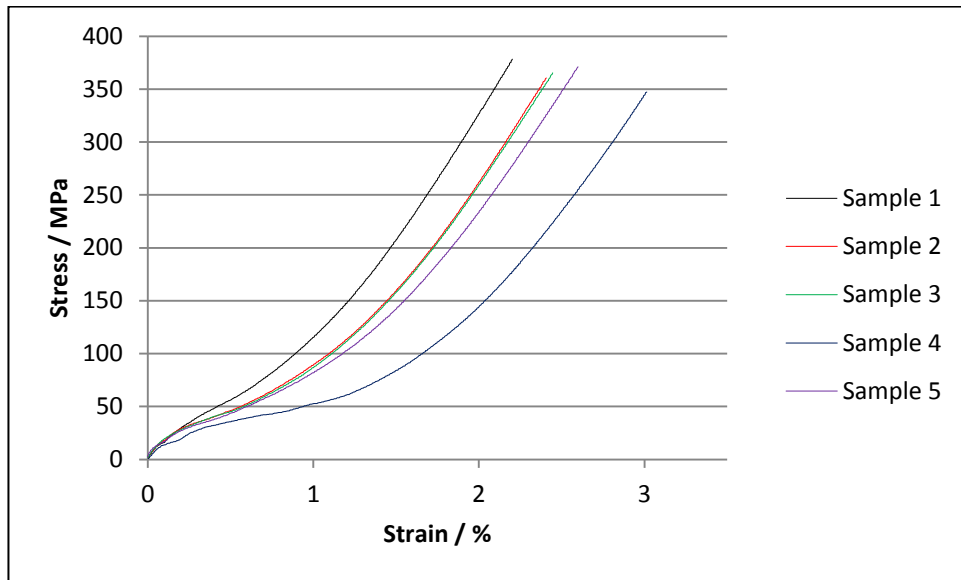

**Fig 4.1** – Stress/strain plot of 0° tensile test specimens
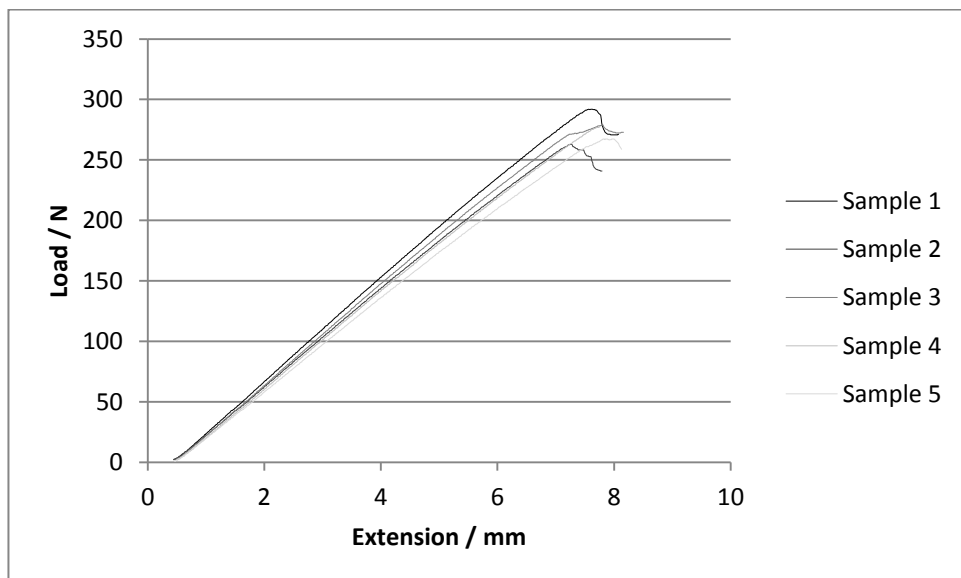
**Fig 4.2** – Load/extension plot of the 0^{0} three point bend test specimens
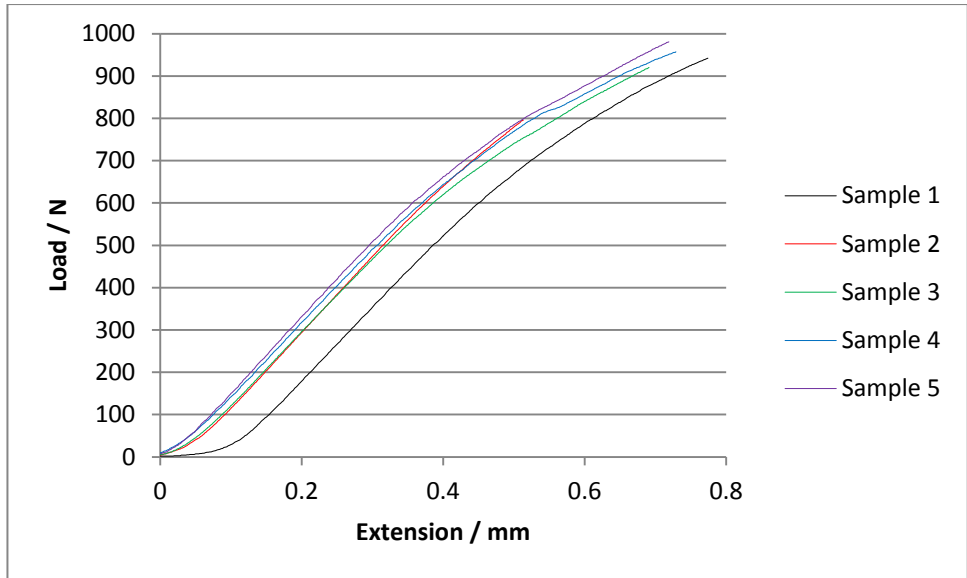
Fig 4.3 – Load/extension plot of the 0° short beam shear test specimens

4.2 Mechanical Testing – Plasma Treated Samples

This section details the results obtained from 10° off-axis tensile testing of plasma treated samples and an untreated control.

4.2.1 Samples Manufactured from Pre-forms

The results obtained from the 10° off-axis tensile tests of plasma treated samples manufactured from pre-forms are summarised in Table 4.2. The results normalised for V_f are summarised in Table 4.3. Figures quoted are the calculated mean values, and the figures in parentheses denote one standard deviation from the mean. Stress/strain plots are presented for each data set in Figure 4.4. See Appendix B for the individual sample data of each set. The data summarised in Tables 4.2 and 4.3 are presented graphically in Figures 4.5 (tensile strength), 4.6 (elastic modulus) and 4.7 (failure strain). The dashed lines represent the mean and the mean +/- 1 standard deviation of the untreated control (as received). The mean V_f across all specimens was 15.05 % and the standard deviation 0.31 %.

Figure 4.4 shows that all specimens failed abruptly at σ^{10}_u, which therefore corresponds to ε^{10}_u, and that all specimens exhibited a degree of plastic deformation past approximately 1 % strain. General trends in mechanical properties were observed for the various treatment conditions. Figure 4.5 shows that σ^{10}_u is maximised at an intermediate level of treatment (20 W) and that overtreatment at 35 and 50 W leads to a significant reduction in σ^{10}_u compared to the untreated control. Treatment at 10 W and 28 W yielded similar values of σ^{10}_u to the untreated control. When normalised for V_f (σ^{10}_{uN}) the pattern in the data is very similar. Figure 4.6 shows that E^{10} is fairly constant across all samples, and when normalised all E^{10}_N values for treated samples fall within

the E^{10}_N value +/- 1 standard deviation of the untreated control except for the 35 W treated samples. It was expected that E^{10}_N would be consistent across all samples as E is a function of V_f, as $E_f \gg E_m$. Figure 4.7 shows that ε_u was consistent from untreated through to 28 W treated samples however was reduced significantly for the 35 and 50 W treated samples. The same pattern was apparent for values of ε_{uN}.

Table 4.2 – Effect of plasma treatment of pre-forms on 10° off-axis tensile properties

| Sample	Tensile Strength σ^{10}_u / MPa	Elastic Modulus E^{10} / GPa	Failure Strain ε^{10}_u / %	V_f (%)
Untreated	230.8 (20)	15.63 (0.52)	2.77 (0.42)	15.58 (0.45)
10W Treated	248.2 (21.7)	14.78 (2.20)	2.69 (0.27)	14.52 (0.85)
20W Treated	267.0 (17.4)	14.87 (1.97)	2.63 (0.56)	14.98 (0.70)
28W Treated	239.7 (14.8)	14.61 (0.75)	2.76 (0.41)	15.00 (0.51)
35W Treated	151.2 (16.5)	13.84 (1.14)	1.57 (0.12)	15.04 (0.23)
50W Treated	172.9 (13.8)	15.42 (0.72)	1.88 (0.16)	15.18 (0.72)

Table 4.3 – Data summary of 10° off-axis tensile testing of samples manufactured from plasma treated pre-forms normalised for V_f

| Sample	σ^{10}_{uN} / MPa	E^{10}_N / GPa	ε^{10}_{uN} / %
Untreated	222.9 (19.3)	15.10 (0.50)	2.68 (0.41)
10W Treated	257.3 (22.5)	15.32 (2.13)	2.79 (0.28)
20W Treated	268.2 (17.5)	14.94 (1.98)	2.64 (0.56)
28W Treated	240.5 (14.8)	14.66 (0.75)	2.77 (0.41)
35W Treated	151.3 (16.5)	13.85 (1.14)	1.57 (0.12)
50W Treated	171.4 (13.7)	15.29 (0.71)	1.86 (0.16)
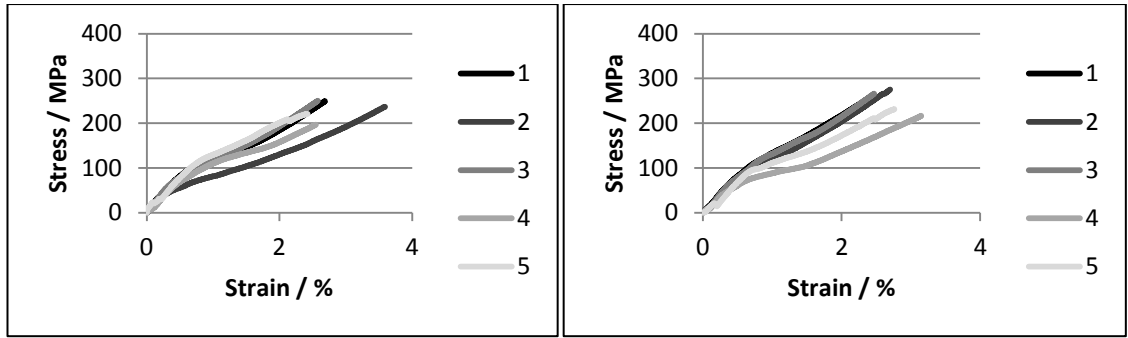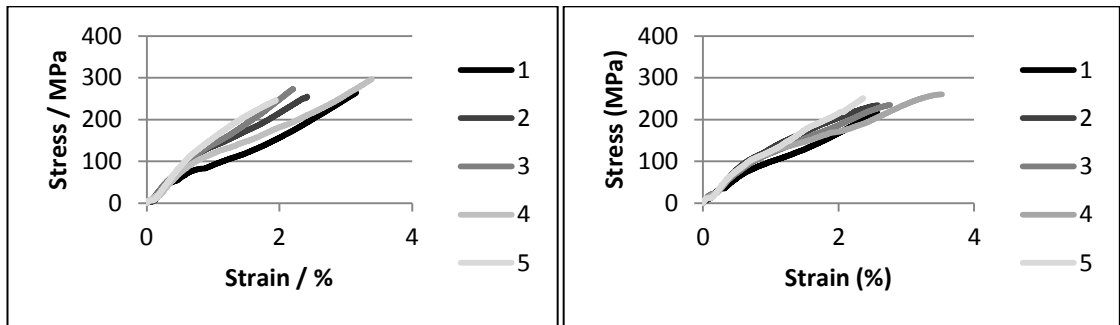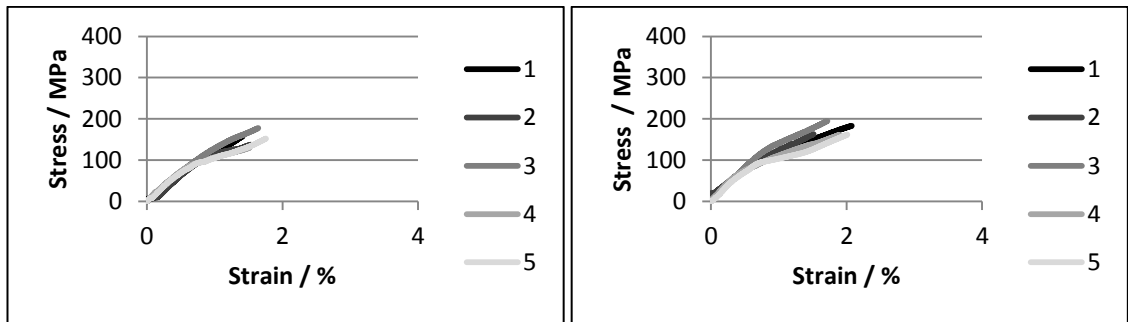
**Fig 4.4** – Stress/strain plots of samples manufactured from $(10^{o}{}_{10})_2$ pre-forms of (a) as received veil, (b) 10 W treated, (c) 20 W treated, (d) 28 W treated, (e) 35 W treated and (f) 50 W treated fibres.
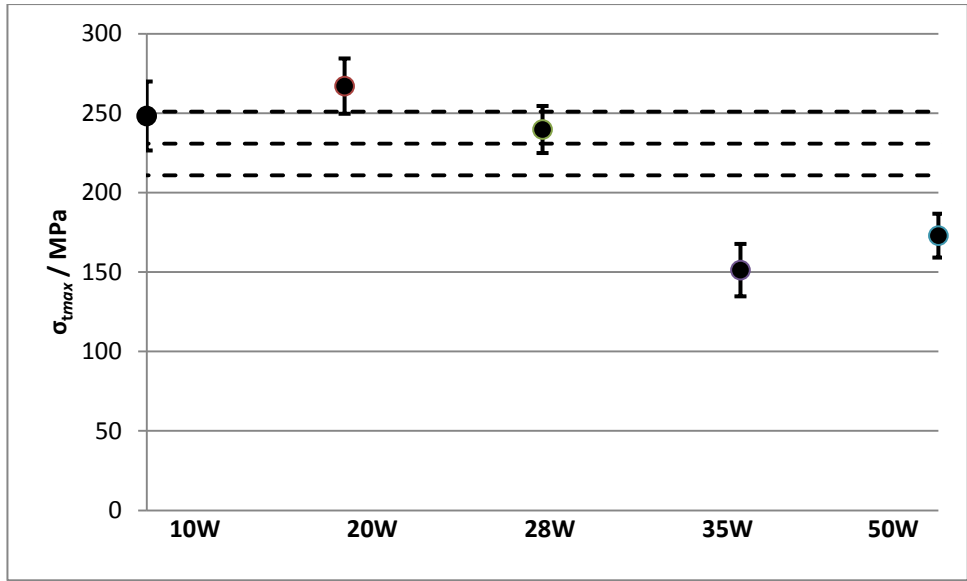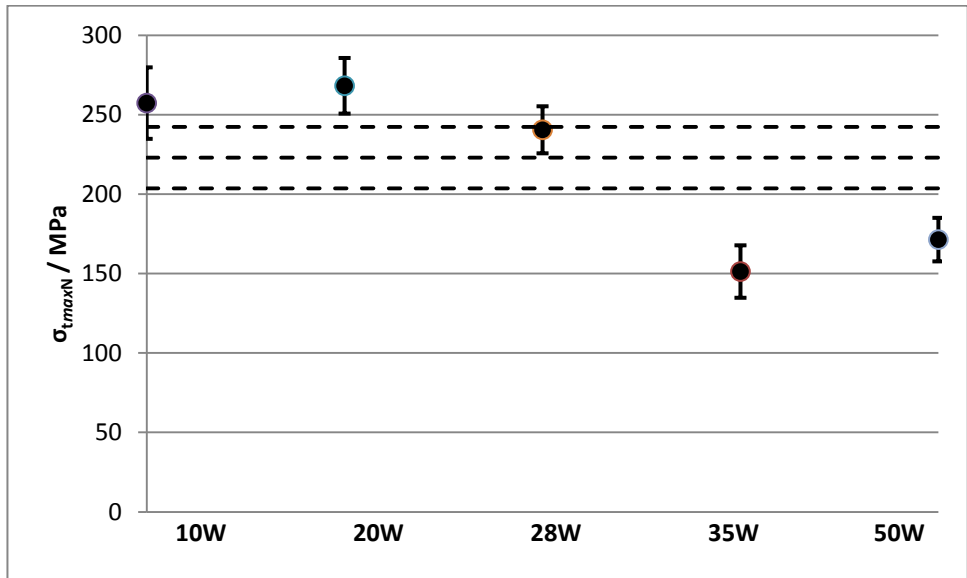
(a)

(b)

Fig 4.5 – (a) σ^{10}_{u} and (b) σ^{10}_{uN} of plasma treated composites manufactured from $(10^{o}_{10})_2$ pre-forms compared to as received veil.
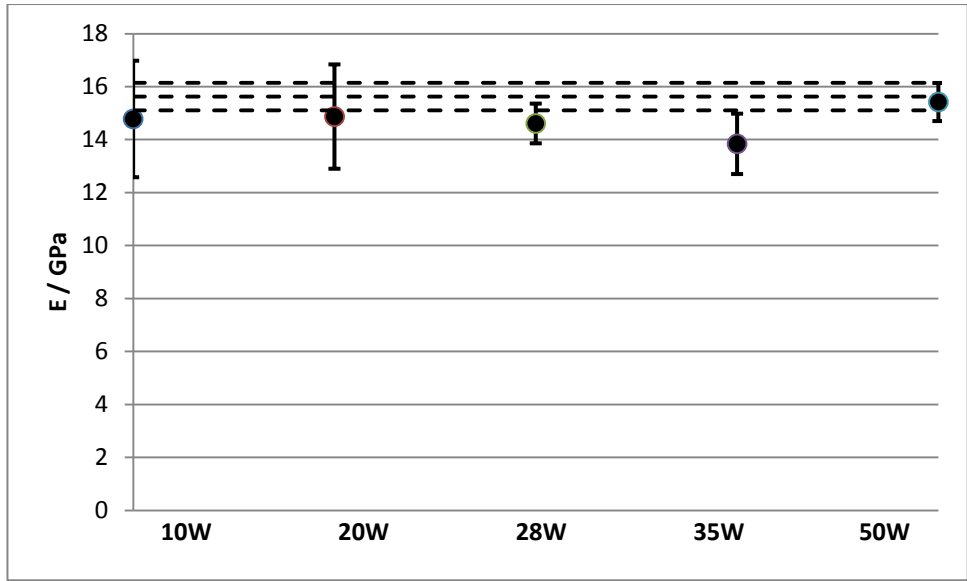
(a)

(b)
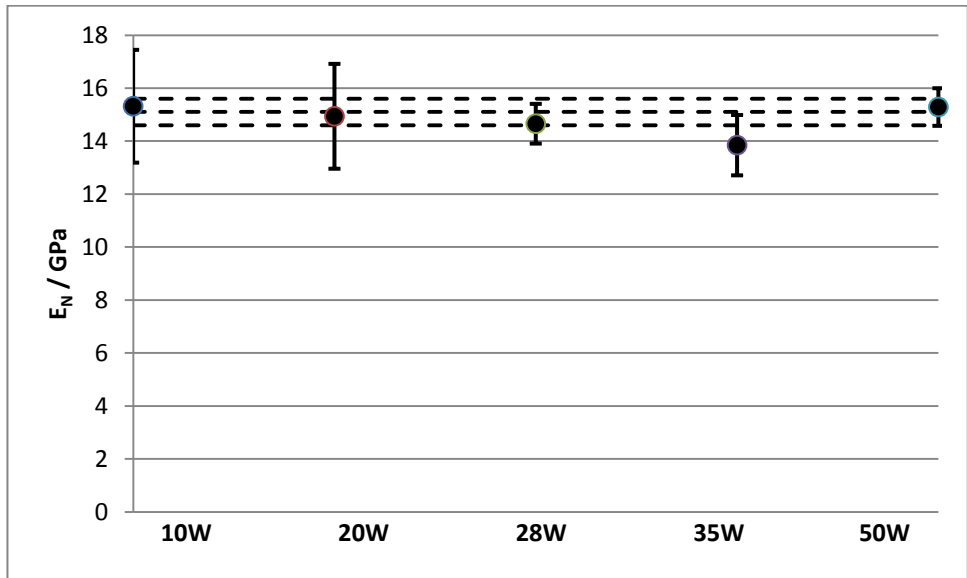
Fig 4.6 – (a) E^{10} and (b) E^{10}_N of plasma treated composites manufactured from $(10^o_{10})_2$ pre-

forms compared to as received veil.

(a)

(b)
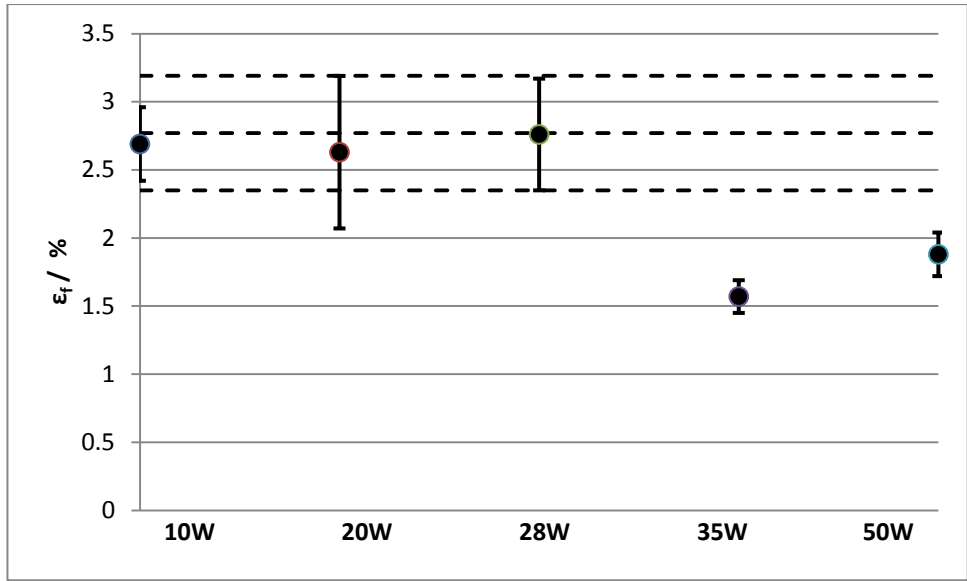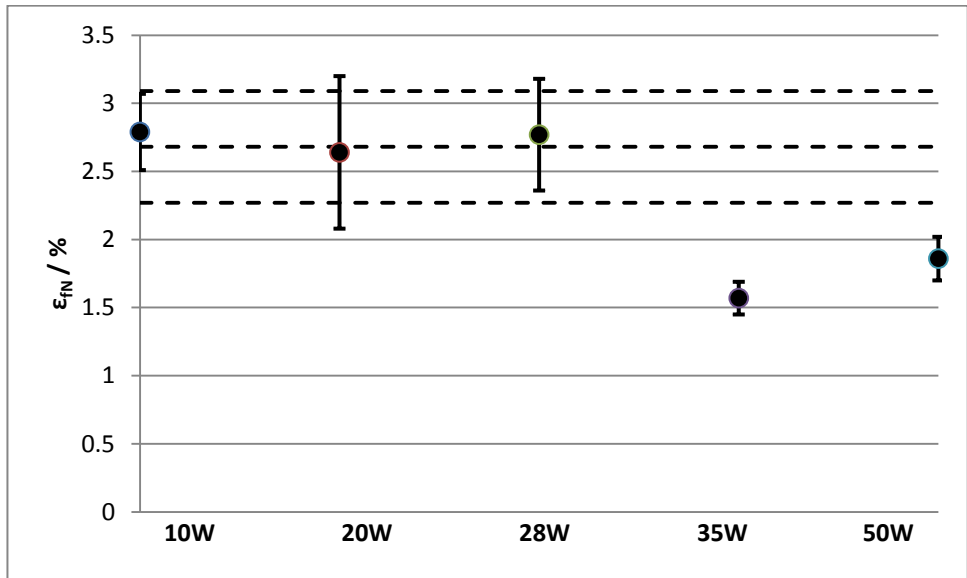
Fig 4.7 – (a) ε^{10}_u and (b) ε^{10}_{uN} of plasma treated composites manufactured from $(10^o{}_{10})_2$ pre-forms compared to as received veil.

4.2.2 Samples Manufactured from Individual Veils

The results obtained from the 10° off-axis tensile tests of plasma treated samples manufactured from individual veils are summarised in Table 4.4. The results normalised for V_f are summarised in Table 4.5. Figures quoted are the calculated mean values, and the figures in parentheses denote one standard deviation from the mean. Stress/strain plots for each data set are presented in Figure 4.8. See Appendix C for the individual sample data of each set. The data summarised in Tables 4.4 and 4.5 is presented graphically in Figures 4.9 (tensile strength), 4.10 (elastic modulus) and 4.11 (failure strain). The dashed lines represent the mean and the mean +/- 1 standard deviation of the untreated control. The mean V_f across all specimens was 9.0 % and the standard deviation 0.65 %.

General trends in mechanical properties were observed for the various treatment conditions. Figure 3.9 shows that σ^{10}_u is maximised at an intermediate level of treatment (20 W) and that overtreatment at 40 and 50 W leads to a significant reduction in σ^{10}_u compared to the untreated control. Treatment at 10 W and 30 W yielded similar values of σ^{10}_u to the untreated control. When normalised for V_f (σ^{10}_{uN}) treatment at 20 W shows a greater improvement over the untreated control, and there is general downward trend in σ^{10}_u and σ^{10}_{uN} from 20 W to 50 W treatment. Figure 4.10 shows that E^{10} is fairly constant across all samples except for the 40 W treated samples which is low. However when normalised all E^{10}_N values for treated samples fall within the E^{10}_N value +/- 1 standard deviation of the untreated control. Figure 4.11 shows that ε^{10}_u follows a similar pattern with respect to treatment as σ^{10}_u. This is to be expected as E^{10} is fairly constant across all samples. The highest values of ε^{10}_u and ε^{10}_{uN} are from the 20 W treated

samples. When normalised ε^{10}_{uN} follows a downward trend from 20 W to 50 W, where at 50 W ε^{10}_{uN} is well below the untreated control value.

Table 4.4 – Data summary of $10^{\mathbf{o}}$ off-axis tensile testing of samples manufactured from plasma treated individual veils.

Sample	Tensile Strength σ^{10}_u / MPa	Elastic Modulus E^{10} / GPa	Failure Strain ε^{10}_u / %	V_f (%)
Untreated	116.8 (8.5)	4.34 (0.74)	4.54 (0.44)	9.55 (0.34)
10W Treated	119.7 (11.0)	4.28 (0.57)	4.40 (0.54)	8.78 (0.56}
20W Treated	136.2 (11.9)	4.13 (0.23)	4.65 (0.26)	8.65 (0.53)
30W Treated	114.9 (9.2)	3.97 (0.38)	4.18 (0.41)	8.25 (0.40)
40W Treated	96.5 (9.9)	3.53 (0.51)	3.91 (0.35)	8.60 (0.42)
50W Treated	88.6 (7.8)	4.24 (0.46)	2.90 (0.18)	10.15 (0.23)

Table 4.5 – Data summary of $10^{\mathbf{o}}$ off-axis tensile testing of samples manufactured from plasma treated individual veils normalised for V_f

Sample	σ^{10}_{uN} / MPa	E^{10}_N / GPa	ε^{10}_{uN} / %
Untreated	110.1 (8.0)	4.10 (0.70)	4.28 (0.41)
10W Treated	122.7 (11.3)	4.39 (0.58)	4.51 (0.55)
20W Treated	141.7 (12.4)	4.30 (0.24)	4.84 (0.27)
30W Treated	125.3 (10.0)	4.33 (0.41)	4.56 (0.45)
40W Treated	101.0 (10.4)	3.69 (0.53)	4.09 (0.37)
50W Treated	78.6 (6.9)	3.76 (0.41)	2.57 (0.16)
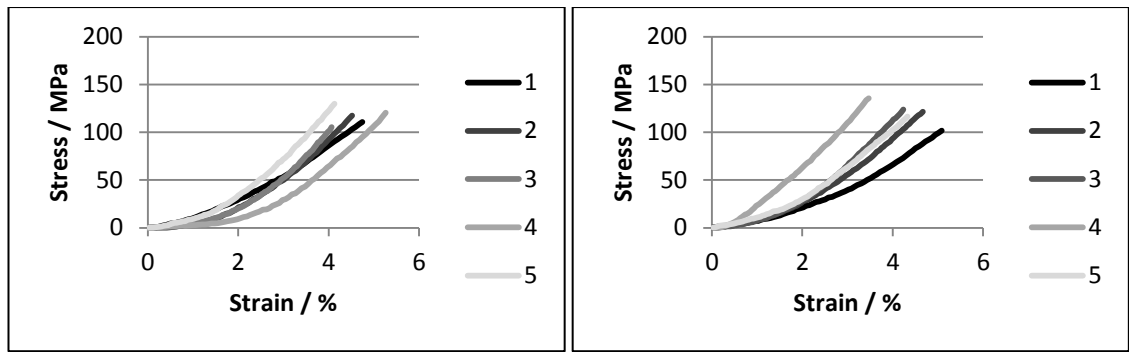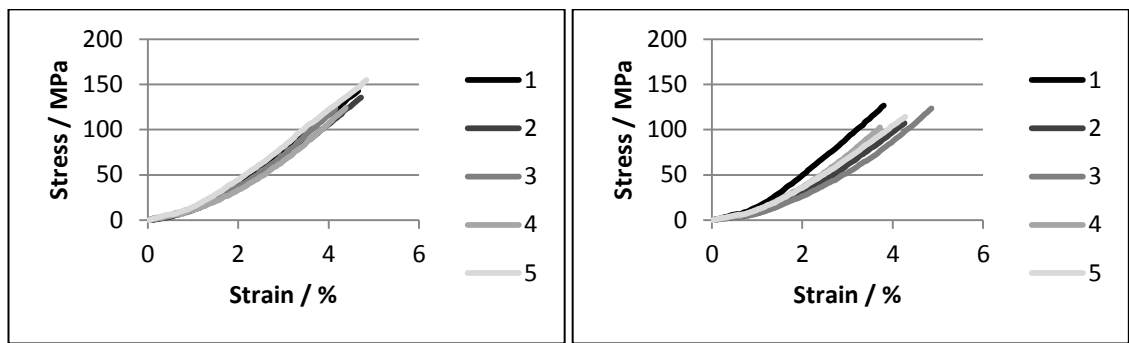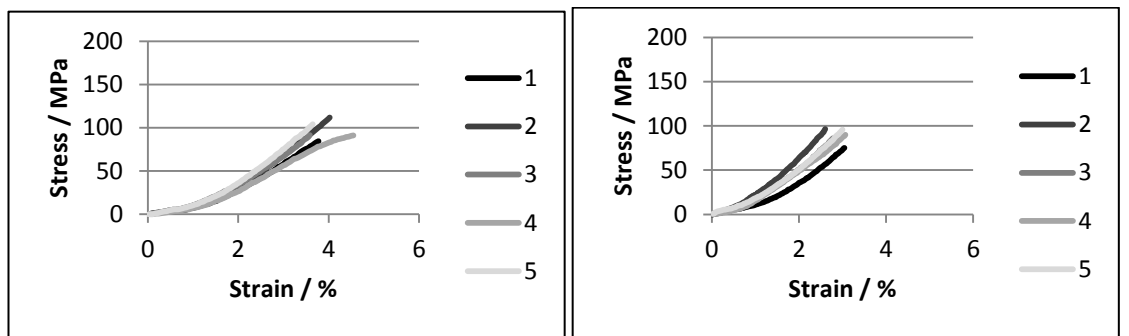
Fig 4.8 – Stress/strain plots of samples manufactured from 10^o_2 veils of (a) as received veil, (b) 10 W treated, (c) 20 W treated, (d) 30 W treated, (e) 40 W treated and (f) 50 W treated fibres.
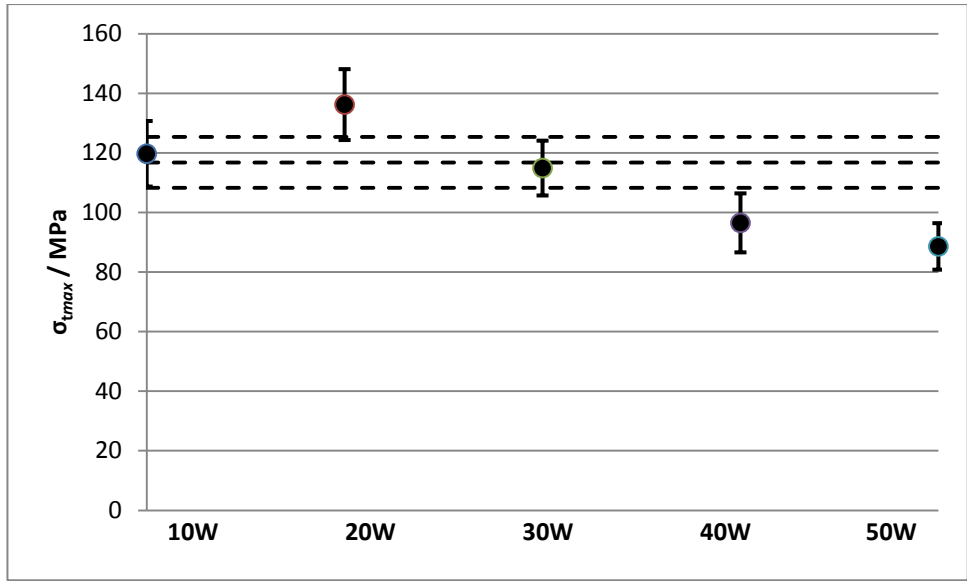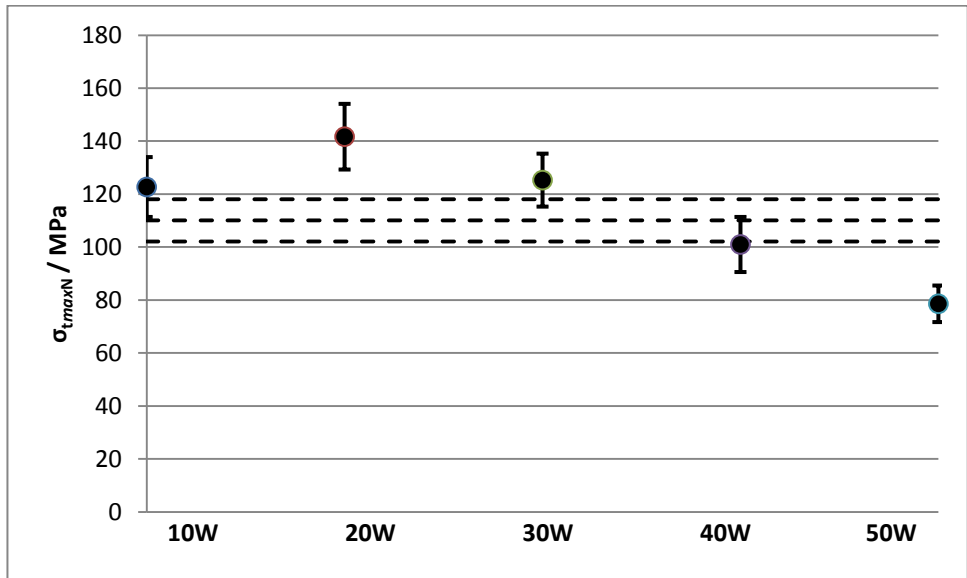
(a)

(b)

Fig 4.9 – (a) σ^{10}_{u} and (b) σ^{10}_{uN} of plasma treated composites manufactured from 10^{o}_{2} veils compared to as received veil.
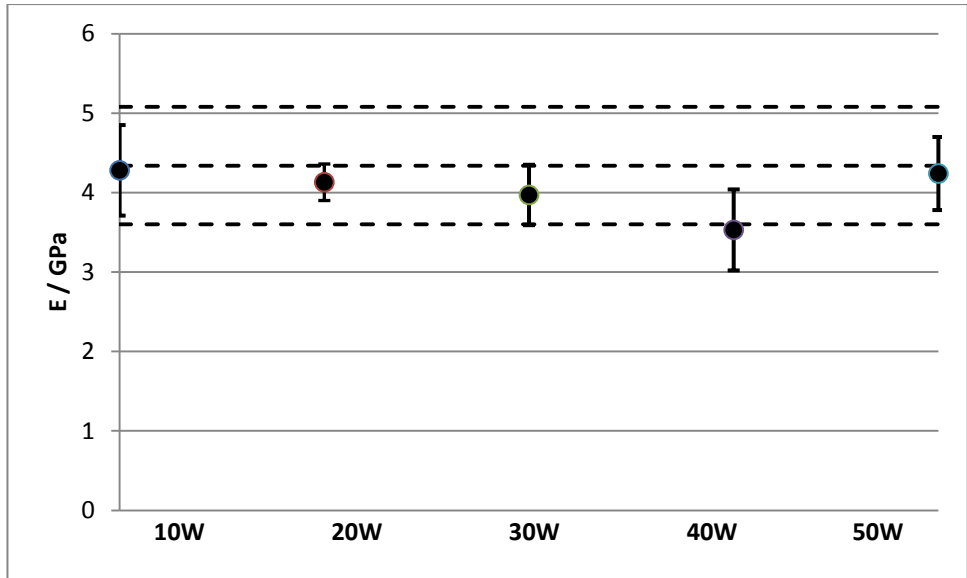
(a)
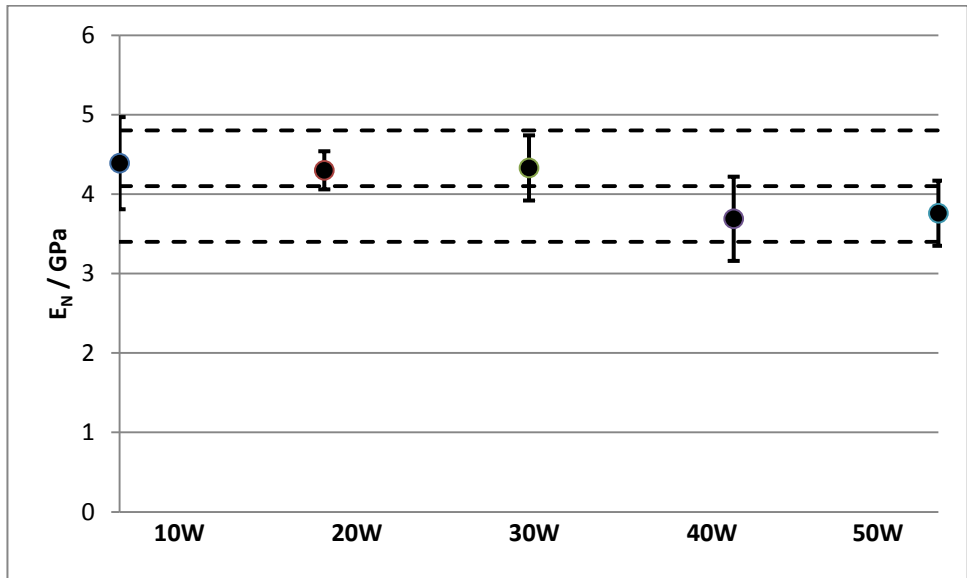
(b)

Fig 4.10 – (a) E^{10} and (b) E^{10}_N of plasma treated composites manufactured from 10^o_2 veils compared to as received veil.

(a)

(b)
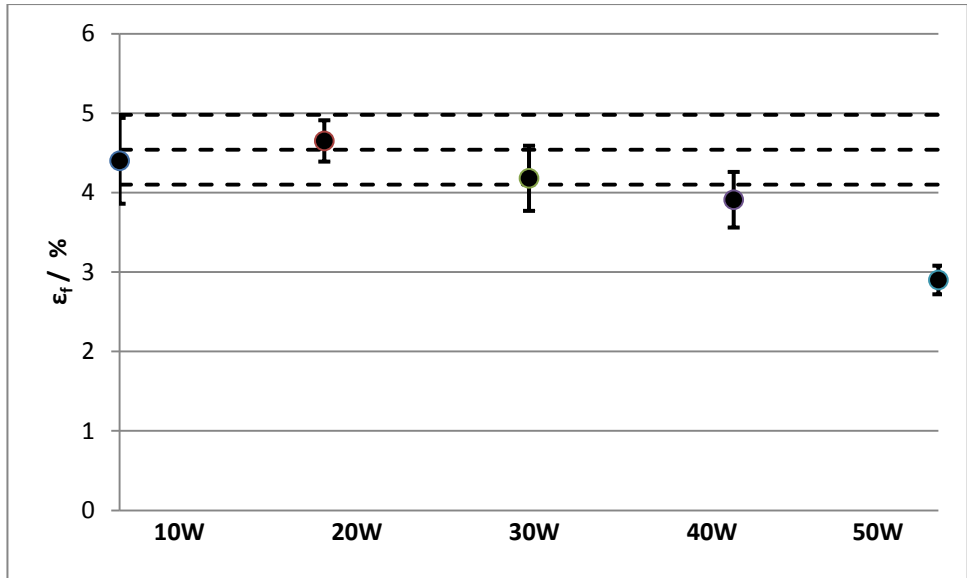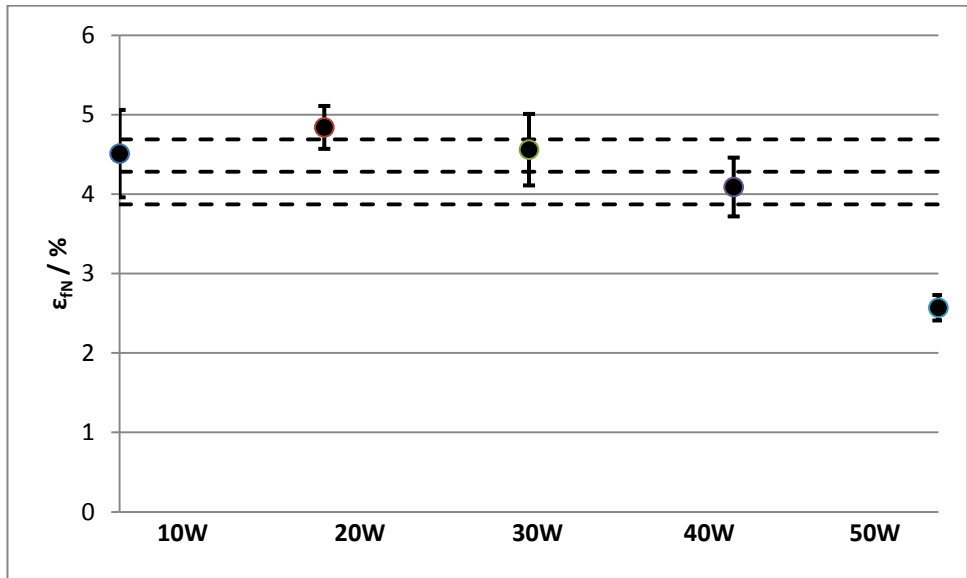
Fig 4.11 – (a) ε^{10}_{u} and (b) ε^{10}_{uN} of plasma treated composites manufactured from 10^{o}_{2} veils compared to as received veil.

4.3 Fibre Surface Wettability

This section details the results of Wicking tests performed on the carbon fibre veils to establish contact angles with standard fluids ethanol and isopropanol (IPA). The mean ethanol contact angle and mean ethanol/IPA contact angle ratio results are detailed in Table 4.6, and illustrated graphically in Figure 4.12. Figures in parentheses represent one standard deviation from the mean.

It can be seen from Figure 4.12 that the 10 W treated sample had the most readily wettable surface. The 20 W treated sample is more wettable than the untreated control, however treatment at 35 W left the veil less wettable than when untreated.

Table 4.6 – Mean EtOH contact angle and mean EtOH/IPA ratio results of Wicking test on as received veil, 10W, 20W and 35W plasma treated samples.

Result/Sample	Untreated	10W	20W	35W
EtOH Contact Angle (°)	47.64 (1.4)	17.97 (0.61)	38.65 (7.48)	54.92 (3.35)
EtOH (°) /IPA (°) Ratio	0.63 (0.034)	1.25 (0.009)	0.84 (0.175)	0.46 (0.076)
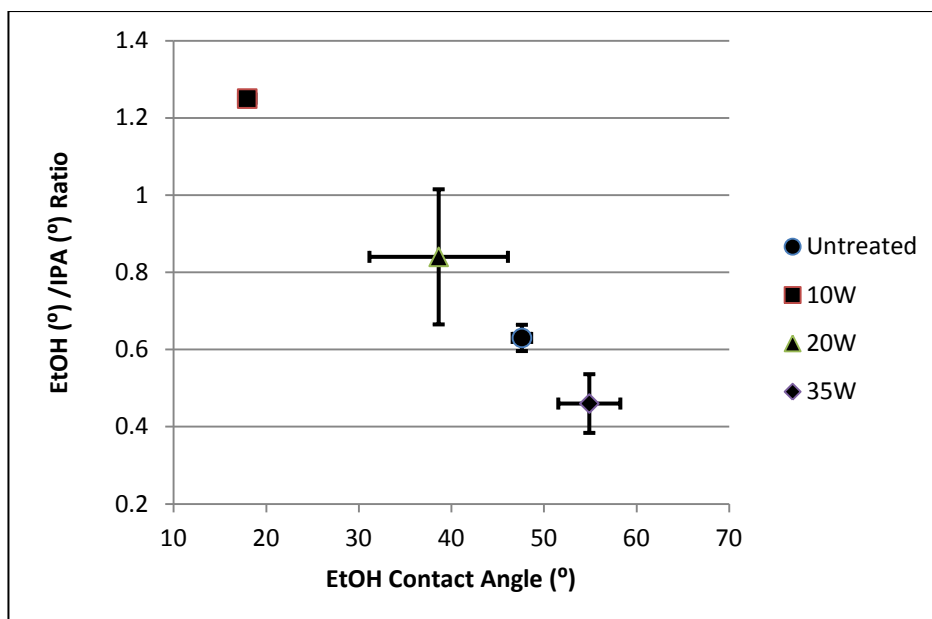
Fig 4.12 – Relationship between EtOH contact angle and EtOH/IPA ratio for untreated, 10W, 20W and 35W plasma treated fibre veils.

4.4 Surface Analysis by XPS

4.4.1 Chemistry of the Binder

The veil used in this work is held together by a water-dispersible polyester binder introduced as part of the wet-processing technique used to make the veil from recycled carbon fibre. Manufactured by Eastmans of Tennssee, USA, its trade name is 'WD30' meaning 'water-dispersible' with '30% solids'. Its general structure is illustrated in Figure 4.13 below [83]:
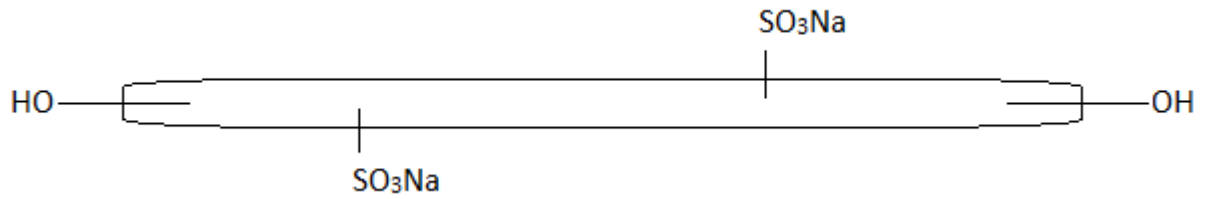
Fig 4.13 – Generalised structure of WD30 binder

Most of the end groups are primary hydroxyl groups and there are sodiosulpho groups located at random intervals along the polyester chain. The results of the XPS survey scan are summarised in Table 4.7 below:

Table 4.7 – Relative concentration of elements (in atomic % [At %]) on the surface of the binder analysed by XPS.

Peak	Abundance (%)
C1s	77.08
O1s	22.03
S2p	0.38
Si2p	0.33
Na1s	0.17

All elements present in the binder were detected by the XPS survey scan. Unlike in the case of the fibre veils no Nitrogen 1s peak was present. In addition silicon was also detected, and its presence is discussed in Section 5.6. The spectrum of the C1s narrow scan is displayed in Figure 4.14 below, and the peak speciation is detailed in Table 4.8:
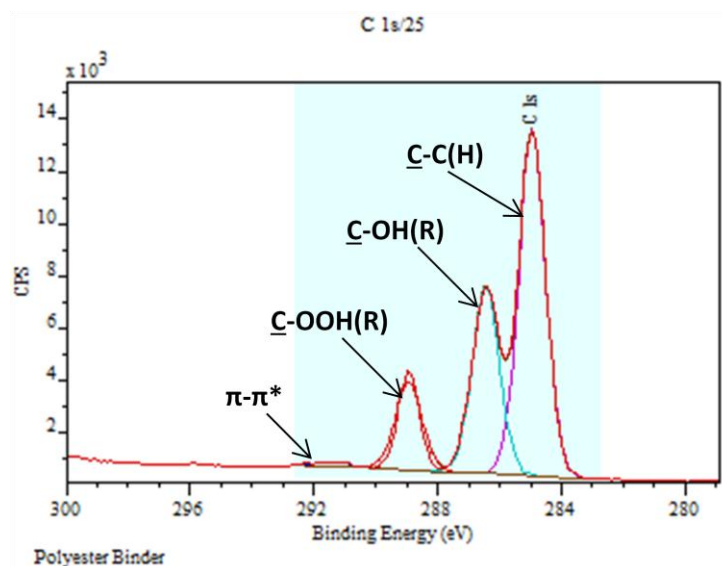
Fig 4.14 – C1s narrow scan of the polyester binder

Table 4.8 – Speciation of C1s peak of polyester binder showing peak position, peak assignment and relative abundance.

Peak Position (eV)	Assignment	Abundance (%)
285	C-C(H)	55.3
286.5	C-OH(R)	29.4
289	C-OOR(H)	14.0
291.5	π-π*	1.3

4.4.2 Fibre Surface Characterisation

The results of the XPS survey scans on the as received veil as well as those treated at 10W, 20W and 35W (all for 20mins) are summarised in Table 4.9.

Table 4.9 – Change in elemental concentration after plasma treatment at 10, 20 and 35 W compared to as received veil analysed by XPS.

Sample/Composition	O/C ratio	N (%)	Na (%)	S (%)	Si (%)
Untreated	0.29	1.35	1.01	0.56	/
10W Treated	0.33	1.18	2.18	1.41	0.61
20W Treated	0.41	1.46	2.81	1.36	0.72
35W Treated	0.32	0.99	3.9	1.52	1.37

It can be seen from Table 4.9 that the O/C ratio increases slightly after treatment at 10 W, followed by a significant increase after treatment at 20 W. However after treatment at 35 W the O/C ratio is similar to that of the 10 W treated sample, only slightly above that of the untreated sample. Relative content of Na increases gradually with treatment, as does relative Si content of which there was none detected in the untreated sample. N content fluctuates across the treatments, there is no discernible pattern in its relative content. S content is fairly constant in all treated samples, where it is approximately 2.5 times more prevalent than in the untreated sample. The C1s narrow scans are displayed in Figure 4.15 below, and the peak speciation is detailed in Table 4.10:

(a)

Untreated

b) 10W Treated

(b)

C 1s/45

b) 20W Treated

(c)

C 1s/49
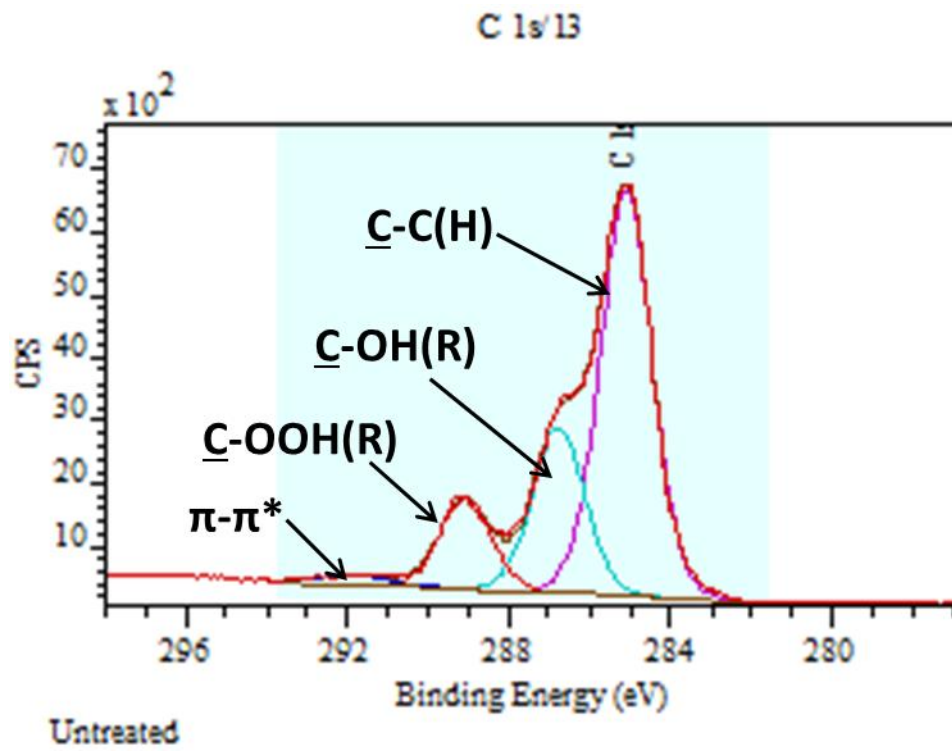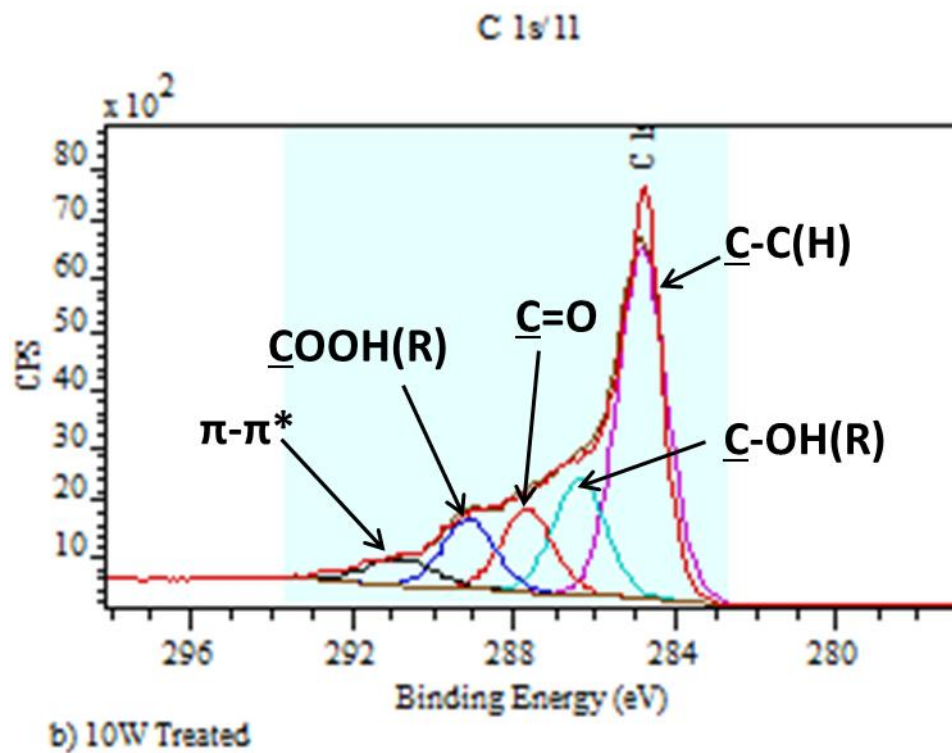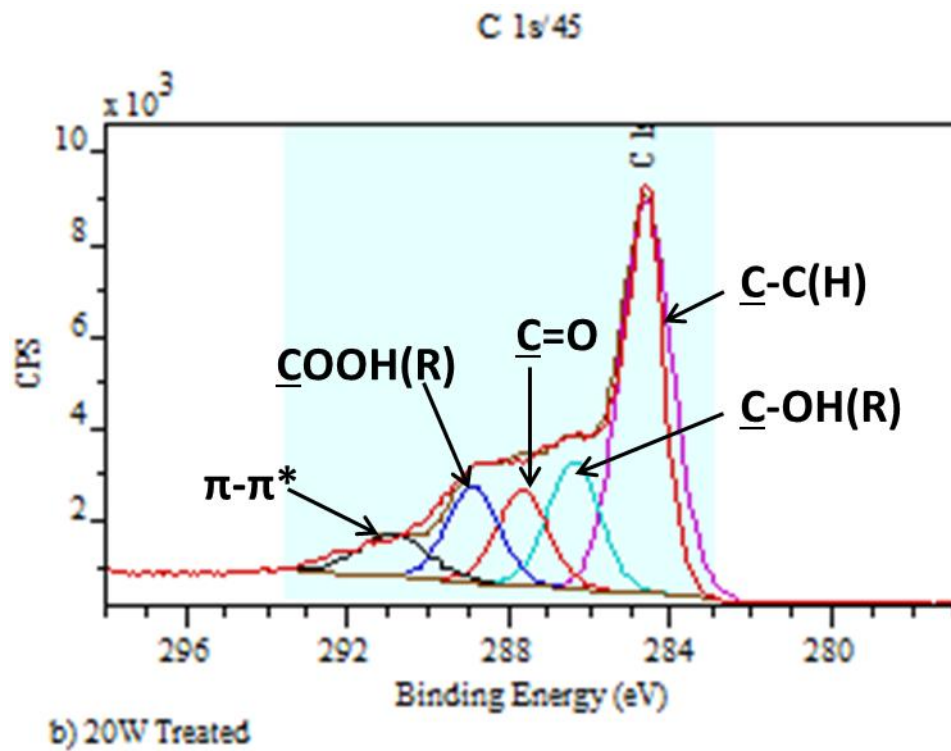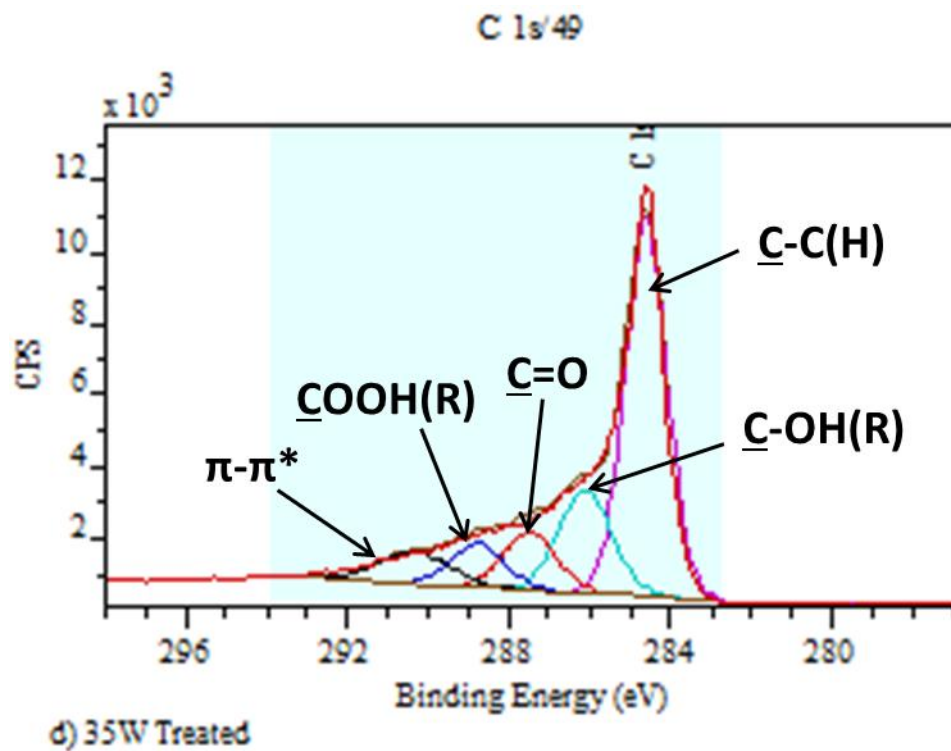
d) 35W Treated

(d)

Fig 4.15 – C1s curve fitting of a) as received, b) 10W treated, c) 20W treated and d) 35W treated carbon fibre veils

Table 4.10 - Speciation of C1s peak of untreated, 10W, 20W and 35W plasma treated fibre samples showing peak position, peak assignment and relative abundance.

Peak Position (eV)	Assignment	Relative Abundance (%)			
		Untreated	10W	20W	35W
≈ 285.0	C̲-C(H)	60.2	50.8	51.2	54.9
≈ + 1.5	C̲-OH(R)	24.6	18.6	16.5	18.8
≈ + 3.0	C̲=O, O-C-O	No peak	13.0	12.4	10.7
≈ + 4.5	C̲OOR(H)	13.4	11.5	12.5	7.8
≈ + 6	π-π*	1.8	6.1	7.4	7.8

It can be seen from Figure 4.15 and Table 4.10 that the plasma treatment of the fibre changes the surface chemistry. On the untreated fibre, the same functionality is present as in the binder, although the peaks are slightly less defined. The main difference on the plasma treated fibres is the presence of a carbonyl (C=O) peak which is not present on the binder or the untreated fibre. There was a corresponding reduction in the relative abundance of the aliphatic (C-C(H)) peak on the treated fibres. The shake-up satellite peak intensity is also increased on the treated fibres. Hydroxyl/ether functionality (C-OH(R)) is decreased on the treated fibres. The Si2p narrow scans are discussed in Section 5.6.

4.5 Surface Analysis by ToF-SIMS

This section details the results obtained from Tof-SIMS analysis of the untreated fibre veil and the polyester binder. Figure 4.16 illustrates the spectra obtained from the polyester binder and Figure 4.17 those from the untreated carbon fibre veil. Each figure contains 2 spectra of that particular sample, except for the positive spectra of the binder (Fig 4.16 (a)) which contains 3. Assignment of peaks is not definitive as many chemical

78

species (fragments) can be responsible for each peak, thus their assignment is discussed in Section 5.6. However some general observations can be made. There are many more peaks in the negative spectra than the positive for both the binder and the fibre veil. In the positive spectra the most intense peak is at 23D representing Na^+, which is a component of the binder.
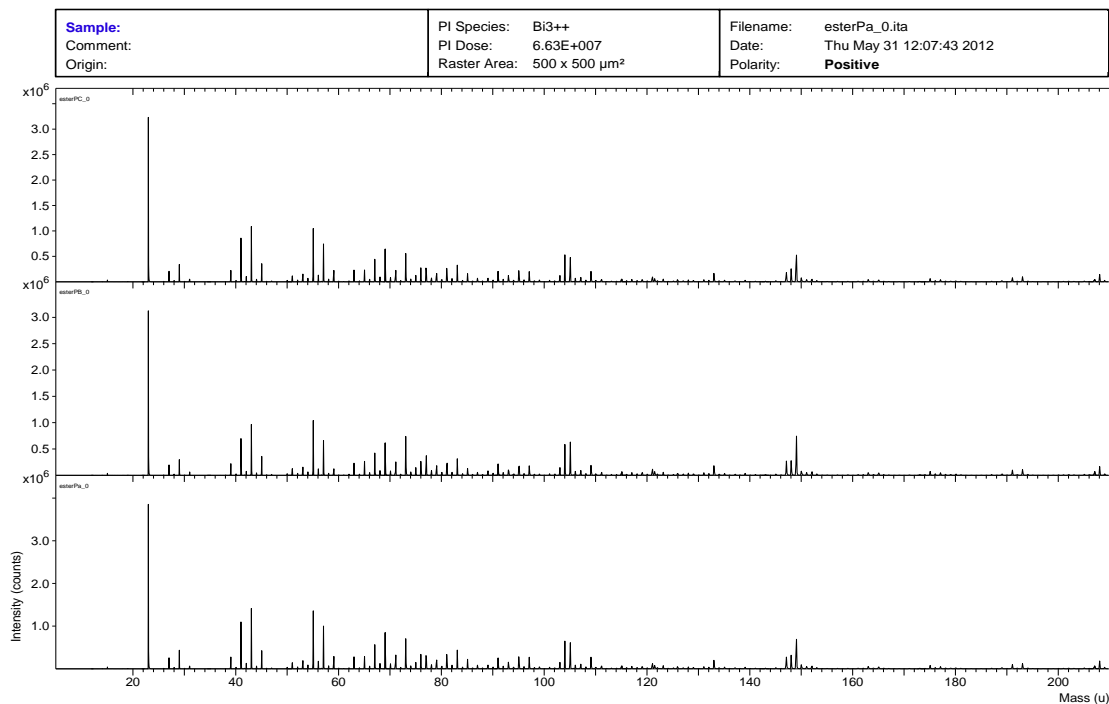
(a)
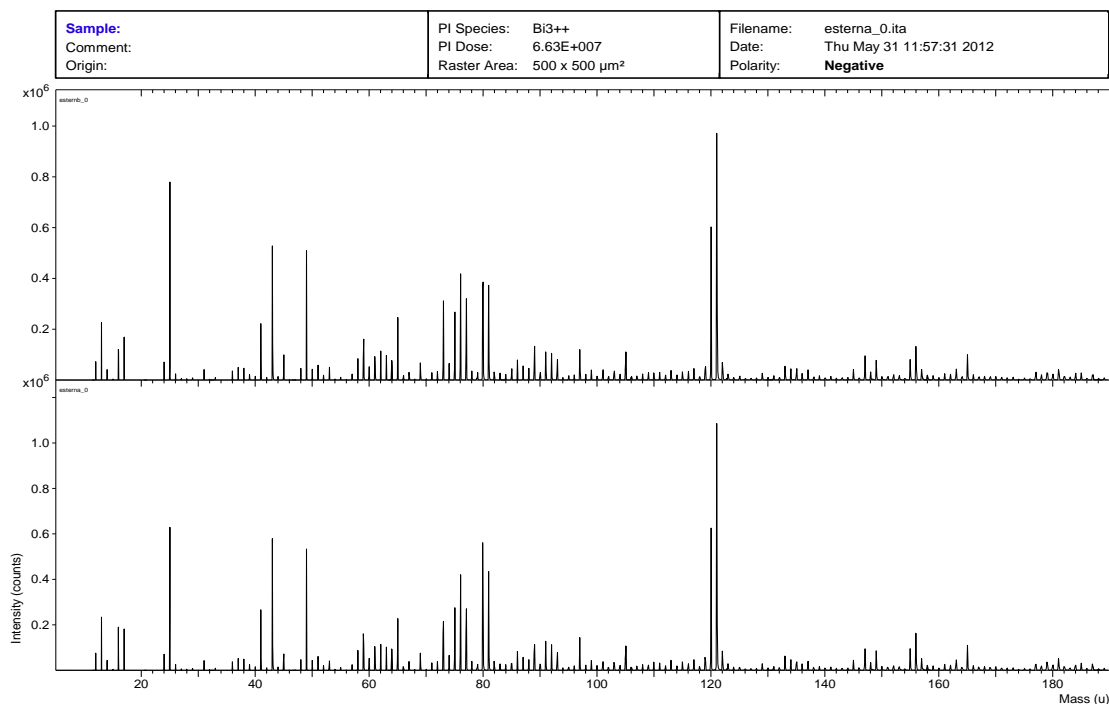
(b)

Fig 4.16 – (a) positive and (b) negative Tof-SIMS spectra of the polyester binder
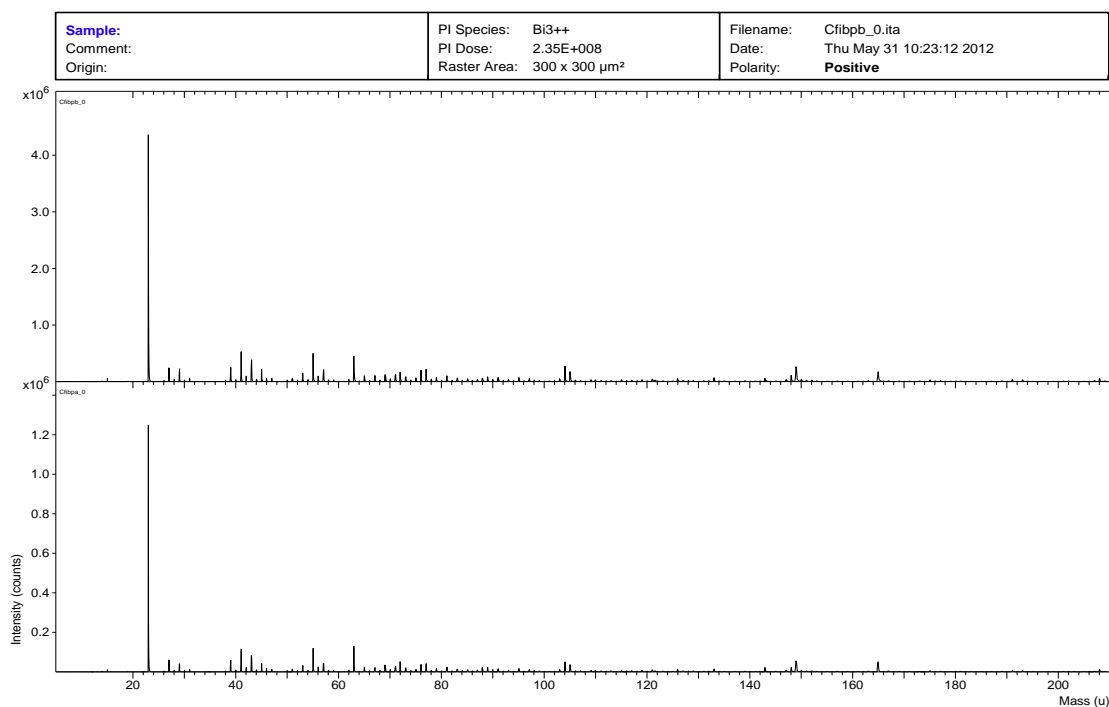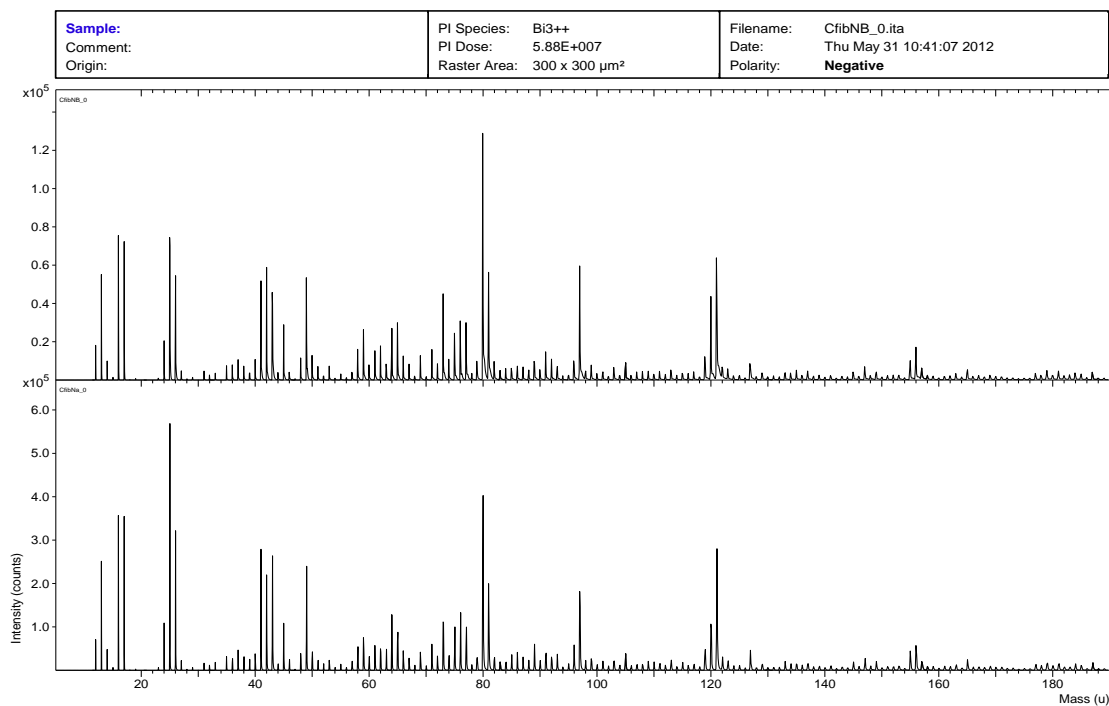
Fig 4.17 – (a) positive and (b) negative Tof-SIMS spectra of the untreated carbon fibre veil.

Chapter 5

Discussion

5.1 Mechanical Characterisation

The results of mechanical testing performed on the recycled carbon fibre/epoxy resin matrix system yielded consistent results, each parameter tested had a low standard deviation from the mean value. With this in mind it is possible to compare the recycled carbon fibre system with other common commercially available composite materials. Table 5.1 compares the properties of this material system to that of a woven virgin carbon fibre/epoxy resin matrix system and that of a unidirectional (UD) carbon fibre/epoxy resin pre-preg. The data for the woven system is taken from Thibault [84] and the data for the pre-preg system from the product data sheet of HexPly 8552 (manufactured by Hexcel) [85].

Table 5.1 – Mechanical properties comparison of recycled carbon fibre system with virgin woven carbon and UD pre-preg systems.

Property	Recycled CF System	Woven CF System	UD CF Pre-preg
Tensile Strength (MPa)	364.5 (10.5)	443.4 (34.3)	2207 (320)
Elastic Modulus (GPa)	22.16 (0.50)	35.47 (5.58)	141 (20.5)
Failure Strain (%)	2.52 (0.27)	2.01 (0.21)	-
ILSS (MPa)	30.67 (1.51)	61.12 (2.18)	128 (18.6)
V_f	15.7	~40	57

It can be seen from Table 5.1 that the recycled fibre composite has approximately 80% of the tensile strength, 60% of the Young's modulus and 80% of the strain to failure of the virgin woven fabric system. Although lower, this is offset against the recycled system having a V_f of 15.7 %, whereas the woven systems' V_f was approximately 40%. This suggests that the recycled system performs better in tension when normalised for V_f, however this does not account for the fact that in the woven system only 50% of the fibres are making a significant contribution to the tensile properties, as the other 50% are at 90° to the load direction during testing. Although the fibre alignment in the recycled veil is imperfect, it is highly significant and these composites are essentially unidirectional with respect to fibre orientation. Also, the recycled system is a discontinuous fibre reinforcement whereas the woven system is a continuous fibre reinforcement.

A similar pattern was observed for ILSS, the recycled system having 50% of the ILSS of the woven system. These differences are again explained by the variation in V_f and degree of fibre alignment. Although the properties of the current system are less than that of a conventional carbon fibre hand lay-up composite, its potential as a workable material is clear in that if V_f (which can be achieved with better fibre alignment) can be enhanced significantly, then so can the mechanical properties in order it for it to compete in performance.

Table 5.1 shows that the UD pre-preg vastly outperforms the recycled system. UD pre-pregs represent the ultimate in mechanical performance of CFRPs, combining high V_f with continuously aligned fibres making them suitable for structural applications in the aerospace and automotive industries. The recycled system is not intended to compete with this material, and although it has the potential to compete with hand laid up woven

fabrics, it is currently more appropriate to compare the recycled system with other short fibre reinforced composites. Table 5.2 below compares the mechanical properties of the recycled fibre system with another discontinuously reinforced carbon/epoxy composite [86] and with chopped strand mat (discontinuous random fibreglass/unsaturated polyester resin).

Table 5.2 – Mechanical properties comparison of recycled carbon fibre system with discontinuous carbon fibre and chopped strand mat systems

Property	Recycled CF System	Short CF System	Chopped St'd Mat
Tensile Strength (MPa)	364.5 (10.5)	1100	88.0
Elastic Modulus (GPa)	22.16 (0.50)	-	6.18
Failure Strain (%)	2.52 (0.27)	-	-
ILSS (MPa)	30.67 (1.51)	-	-
V_f	15.7	50	17.3

It can be seen from Table 5.2 that the recycled system has a comparable tensile strength per unit volume of fibre (V_f) to the short carbon/epoxy literature value. This indicates that the recycled system can compete with currently available short-carbon fibre reinforcements, and of course have the added advantage of being recycled. It can also be seen the recycled fibre system vastly outperforms the chopped strand mat. This is to be expected as chopped strand mat is of random fibre orientation. However this data and the UD pre-preg data in Table 5.1 demonstrate that the recycled fibre system is of intermediate properties between the cheapest available FRP and ultimate (in terms of performance) FRP. It is highly possible therefore that a market exists for a material of this type with mechanical properties intermediate between the current high and low end of what is available.

5.1.1 Non-linearity of stress/strain curves

It can be seen from Figure 4.1 that the stress/strain curves for the UD composite samples are non-linear. Figure 5.1 depicts Figure 4.1 with an added stress/strain curve for the pure matrix material:
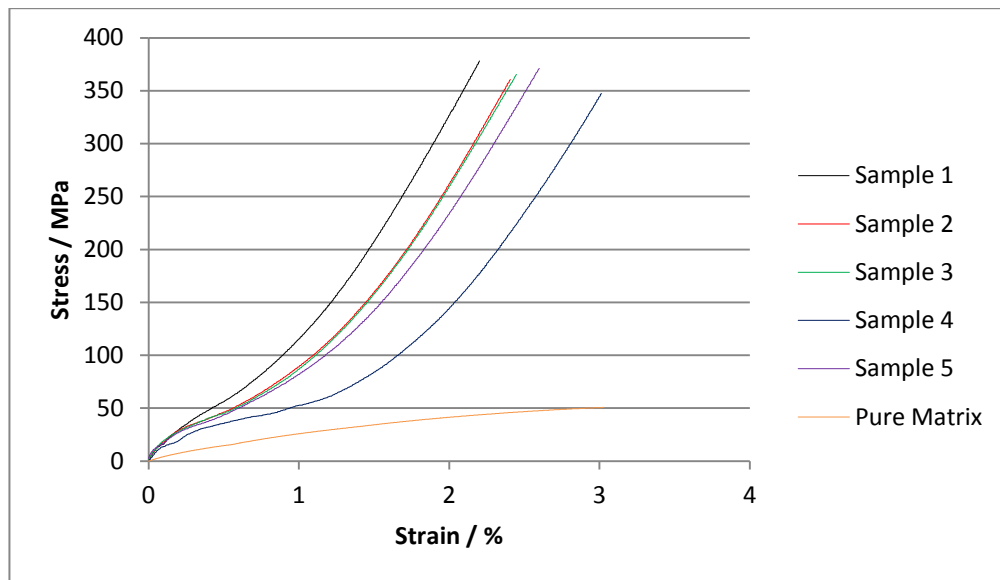
Fig 5.1 – Stress/strain plot of 0° tensile test on composite specimens and pure matrix material

It is possible that the sum of the stress/strain curves of the pure matrix and the fibre veil would result in the composite stress/strain curves displayed in Figure 4.1 (accounting for V_f and V_m). The non-linearity may be a result of the fibres aligning (orienting) as a result of the load. This would explain the increased gradients of the curves at higher loads.

5.2 Theoretical Calculations

Composite strength and stiffness can be predicted using the rule of mixtures (Section 2.1.4). Thus, for a continuously aligned fibre/matrix composite, the elastic modulus can be predicted according to:

$$E_c = E_f V_f + E_m(1 - V_f)$$ [5.1]

Assuming that the recycled fibre/epoxy system is continuously aligned, E_f would be 238 GPa (from the product data sheet of Tenax HTA fibres [87], and E_m would be 2.4 GPa (Table 3.1). $V_f = 0.157$ (Table 4.1) and $1-V_f = 0.843$. Thus equation 5.1 gives a theoretical composite modulus E_c of 39.39 GPa. The results of the tensile test on the system showed that the actual composite modulus $E_c = 22.16$ GPa. The discrepancy between the theoretical and actual values is due to the system being reinforced with discontinuous fibres with a high degree of alignment as opposed to continuous fibres that are perfectly aligned. To account for fibre length and orientation a fibre length factor η_l and fibre orientation factor (Krenchel factor) η_0 are incorporated into the rule of mixtures:

$$E_c = \eta_0 \eta_1 E_f V_f + E_m(1 - V_f)$$ [5.2]

The contribution of the fibre phase to actual composite stiffness E_c is:

$$\eta_0 \eta_1 E_f V_f = E_c - E_m(1 - V_f) = 20.14 \, GPa$$ [5.3]

The contribution of the fibre phase to theoretical composite stiffness = 37.37 GPa. Thus the product of $\eta_0 \eta_1$, the effect of the fibre length and orientation distributions = 20.14 GPa / 37.37 GPa = 0.54. Thus the discontinuous, highly aligned nature of the non-

woven veil contributes 54 % of the stiffness imparted by continuously aligned fibres of the same type.

A similar analysis can be applied to composite strength σ_c. The modified rule of mixtures for composite strength is given below:

$$\sigma_c = \eta_0 \eta_l \sigma_f V_f + \sigma_m (1 - V_f) \qquad\qquad [5.4]$$

Again, assuming continuous alignment, σ_f would be 3950 MPa [87], and $\sigma_m = 47$ MPa (Table 3.1). Thus theoretical composite strength $\sigma_c = 659.8$ MPa. The results of the tensile test on the system showed that the actual composite strength $\sigma_c = 364.5$ MPa. Applying the same process as for modulus above, the product of $\eta_0 \eta_l = 0.56$.

There is close agreement in the calculations on the efficiency of the reinforcement compared to continuously aligned fibres in an ideal composite where $V_f = 15.7$ %. The key implication of this analysis is that through improvement of the fibre alignment in the veil making process, an improvement in strength and stiffness would result as the product of $\eta_0 \eta_l$ would increase. This would combine with the improvements in V_f that a higher degree of alignment would allow manufacture to achieve, resulting in an increase in mechanical properties. However fibre length improvements cannot be achieved in the veil making process as fibre length is limited to the chopping of the end of life composite prior to the pyrolysis process. It would therefore be advantageous to separate the contributions of η_0 and η_l, and this is discussed in the next section.

5.2.1 Critical Fibre Length

The critical fibre length l_c is defined as the minimum length at which the centre of the fibre reaches σ_{fu} when the matrix is at maximum shear stress, and fibre length l needs to exceed this to impart reinforcement (Section 2.1.4). l_c is calculated from Equation 2.6. σ_{fu} = 3950 MPa [87], assuming d_f = 7 μm (0.007 mm) and estimating *IFSS* to be equal to ILSS (30.67 MPa) as they often have similar values [88] *l_c = 0.902 mm*. The number average fibre length of the veil is 10.8 mm and the weight average fibre length 12.6 mm (Section 3.1.1). Therefore in composites reinforced with the recycled non-woven veil, *l* >> *l_c*. Significantly, as l > (10l_c) the fibres can be considered as continuous with respect to length. Therefore the value of η_l in the modified rule of mixtures (Equations 5.2 and 5.4) can be considered to be 1. Thus the discrepancy between theoretical and actual values in strength and stiffness is explained by the imperfect fibre orientation. And so η_0 = 0.54 for E_c and 0.56 for σ_c. These values are between the lower (⅜) and upper (1) boundaries for the Krenchel factor as expected. The chopping process prior to pyrolysis does not inhibit the performance of the non-woven veil in composites as l >> l_c. Improvements in fibre alignment will increase the value of η_0 and strength and stiffness would be closer to the theoretical value.

5.3 Fibre Surface Chemistry

This section discusses and quantifies the surface chemistry of the recycled carbon fibre veil. As the veil is coated with the polyester binder during manufacture, it follows that the binder will affect the surface chemistry greatly, and so it is necessary to quantify its chemical composition and assess the degree to which it has coated the fibres. Carbon

fibre surfaces are strongly adsorptive [89] and so it is unlikely that the binder would not fully coat the surface. The processing of the reclaimed 'fluffy' carbon fibre (Fig 2.4) into a veil involves dispersion in water. The concentration of binder is chosen so that it should be deposited at the fibre crossing points to hold the discontinuous fibres into a handleable veil.

Figure 4.13 gives a generalised structure of the polyester binder and depicts the functionalities that are bound to the polyester backbone. The XPS survey scan of the binder confirms the presence of the elements depicted in Figure 4.13 and in addition confirmed the presence of silicon (Table 4.7). As silicon containing species are not present in the binder specification its presence is possibly due to contamination, which is discussed in Section 5.6. Table 5.3 compares the results of the XPS narrow scans on the binder and on the as received fibre veil:

Table 5.3 –Results of XPS survey scans of polyester binder and the as received fibre veil.

Sample/Composition	O/C ratio	N (%)	Na (%)	S (%)	Si (%)
Polyester Binder	0.29	/	0.17	0.38	0.33
As received veil	0.29	1.35	1.01	0.56	/

If the binder completely covered the individual fibres in the veil we would expect that the O/C ratio and relative elemental compositions for each scan would be the same (as the XPS analysis depth is of the order of 10 nm). The O/C ratios were identical, however the relative concentrations of all other detected species were different. This suggests that the binder has covered most of the veil, as similar O/C ratios combine with O and C accounting for over 95% of elemental composition in each scan. The presence of nitrogen on the fibre veil suggests that the X-ray beam can 'see' some of the fibre

surface, it was stated previously that nitrogen is present on carbon fibre surfaces in most cases [60, 61]. Increased content of sodium and sulfur on the fibre is likely due to contamination prior to the veil making process. No silicon is detected in the survey scan of the fibres as it is buried by the binder, its presence is confirmed by further analysis (see section 5.6 for the quantification of silicon contamination). Figure 5.2 below compares the XPS C1s narrow scans of the binder and the untreated fibres and Table 5.4 quantifies the speciation of the assigned peaks:

(a)   (b)
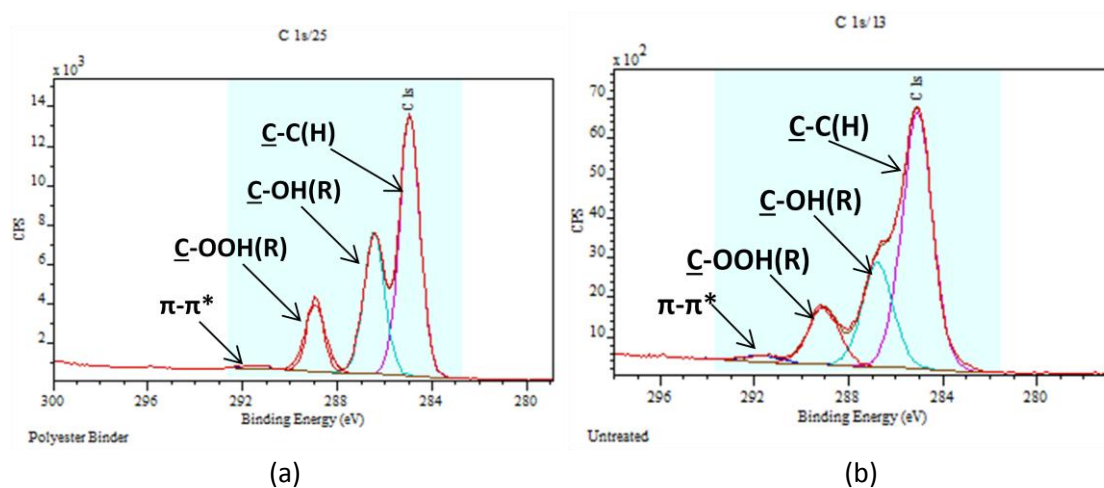
Fig 5.2 – XPS C1s narrow scan spectra comparison of a) polyester binder and b) as received veil

Table 5.4 – C1s narrow scan peak speciation of polyester binder and as received veil

Peak Position (eV)	Assignment	Relative Abundance (%)	
		Polyester Binder	As Received Veil
285	C-C(H)	55.3	60.2
286.5	C-OH(R)	29.4	24.6
289	COOR(H)	14	13.4
291	π-π*	1.3	1.8

Figure 5.2 shows that as well as having a similar O/C ratio the binder and the fibre also contain the same carbon-oxygen functionalities, and have similar concentrations of each functionality as shown in Table 5.4. The peaks are more sharply defined in the binder spectrum. This is due in part to the topography of the analysed surfaces, the binder sample was dried onto a glass surface and was therefore smooth. The increase in relative abundance of the C-C(H) peak on the fibrous surface is possibly due to some fibre underneath the binder being detected. This may indicate that the binder coating is patchy and thinner than the total analysis depth in places, so that the fibrous surface contributes to the spectrum. This was also demonstrated by the presence of nitrogen in the survey scan of the as received veil, and is further confirmed by the increased abundance of the π-π* peak (the presence of a π-π* peak in the binder suggests that there is some aromaticity in its structure). The decrease in abundance of the C-OH(R) peak in the as received veil is larger than expected, an increase in C-C(H) abundance should decrease the relative abundance of the hydroxyl and ester functionalities proportionally. It is therefore likely that the binder coating is uneven on the as received veil. It is also possible that some of the hydroxyl groups adsorbed onto the fibre surface during veil manufacture, or that the peak broadening present in the fibre C1s spectrum has skewed the data somewhat, and there is likely a degree of experimental error that contributed to these different intensities. See Section 5.9.5 for a discussion of errors in XPS analysis. Figure 5.3 presents a Na^+ ToF-SIMS image of the untreated carbon fibre surface:
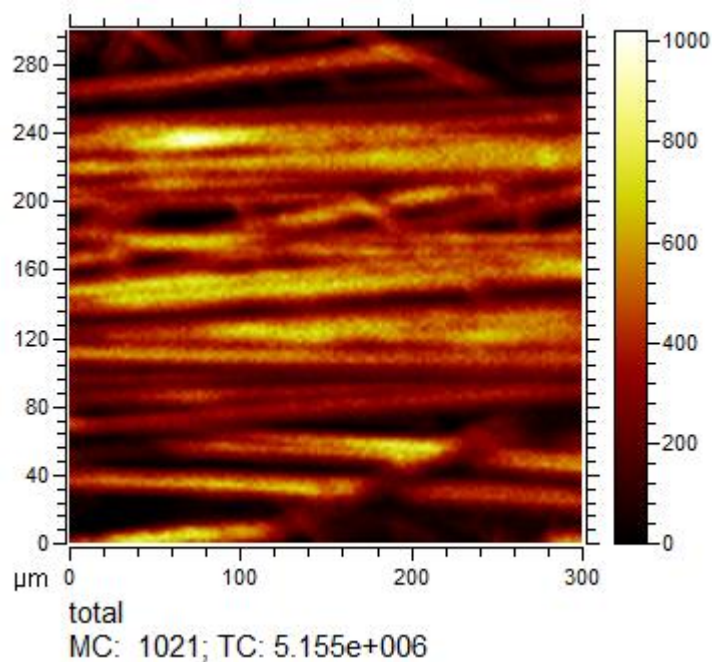
Fig 5.3 – Na$^+$ ToF-SIMS image of untreated carbon fibre surface

Figure 4.13 and Table 4.7 show that sodium is present in the binder in the form of sodiosulfo groups. Figure 5.3 shows that sodium, and therefore the binder, is uniformly distributed on the fibre surface. This in combination with the evidence discussed above is a strong indication that the fibre surface is almost completely covered by the binder, and thus the fibre surface chemistry is very similar.

5.4 Plasma Treated Fibre Surface Chemistry – Survey Scans

Table 4.9 shows that as the plasma power increases the relative concentration of Na, S and Si increases. Na and S are present in the binder as SO$_3$Na (Figure 4.13) and Si is present in the binder as a contaminant (Table 5.3). This suggests that the plasma treatment is removing the organic species of the binder and leaving behind the inorganic species. The removal of organic species from the surface explains the pattern of O/C

ratios. O/C ratio is increased in the 10W sample compared to the untreated control and is increased further after treatment at 20 W. The removal of the organic species in the binder is exposing the oxygen functionality already present on the fibre surface. Previous characterisation has shown that oxygen is present on the surface of all carbon fibre types [60, 61]. The decrease in O/C ratio after treatment at 35 W suggests that oxygen is also removed from the surface at sufficiently high powers.

S concentration increases significantly after treatment at 10 W and then varies only slightly from this value after treatment at 20 and 35 W. It can be assumed that all the S in the binder has been exposed after treatment at 10 W, and thus similar S content is observed after treatment at 20 and 35 W as there is no more to expose and the treatment is not removing S from the surface. In contrast Na content increases as plasma power increases, this suggests that as well as being present in the binder Na is a contaminant of the fibre surface as more and more is exposed as treatment becomes more aggressive.

Si content also increases with increasing plasma power. Si was observed in the survey scan of the binder, but not in the survey scan of the untreated fibre. It is possible that the binder is shielding the Si species when coated onto the fibre, and thus as more organic species are removed Si becomes more visible. It is also possible that Si is a contaminant of the fibre as well as the binder. Si contamination is discussed in more detail in Section 5.6.

5.5 Plasma Treated Fibre Surface Chemistry – C1s Narrow Scans

It can be seen from Figure 4.15 that the plasma treatment alters the fibre surface chemistry. The shape of the C1s peak is different in each case. Although much of the

same functionality is present, the relative amounts of these species is different, as shown by the peak speciation. The most obvious difference is the presence of a carbonyl (C=O) peak in the treated samples that is not present in the untreated sample. It can be concluded that the plasma treatment is responsible for the exposure of carbonyl functionality to the fibre surface. The presence of this peak is complemented by an accompanying reduction in the relative abundance of the aliphatic carbon peak [C-C(H)] and of the hydroxyl peak (C-OH), as shown by Table 4.10. Figure 5.4 below graphically illustrates the data from Table 4.10.
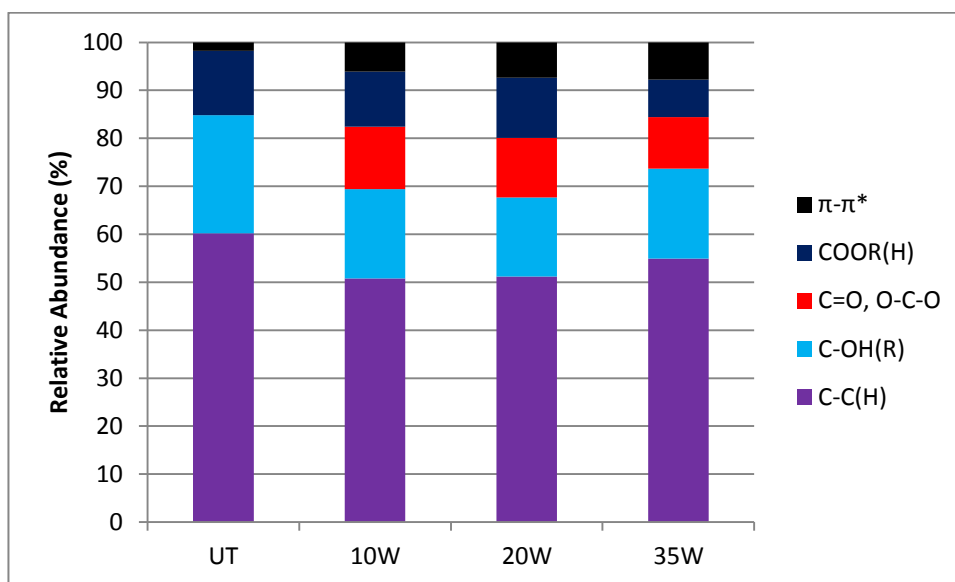
Fig 5.4 – Relative abundance of each C/O functional group and π-π* peak of plasma treated samples and untreated control

The π-π* peak is significantly increased in the plasma treated samples. This concurs with the theory discussed in Section 5.4 above that the treatment is removing the organic binder and exposing the fibres underneath. Thus the appearance of the carbonyl peak in the treated sample spectra implies that this functionality was present on the fibre surface and has been exposed by removal of the binder. The ester peak at ≈289.5 eV in

the 10 and 20 W treated spectra is slightly reduced compared to the untreated control implying its relative content on the fibre surface compared to <u>C</u>-C(H) is slightly less than in the binder. This peak is significantly reduced after treatment at 35 W, and is due to desorption of oxygen from the surface at sufficiently high powers. The carbonyl peak is also at its lowest relative abundance after treatment at 35 W. Interestingly the relative abundance of the <u>C</u>-OH(R) peak remains fairly consistent across all treated samples, and thus removal of oxygen at higher powers may be selective according to the functionality. It is also possible that some oxygen is being deposited from the surface as well as removed and thus maintaining the level of hydroxyl functionality on the surface. In summary the plasma treatment facilitates removal of the organic components of the binder thus performing its purpose of exposing the oxygen functionality underneath. Such functionality is changed by the plasma depending on the power resulting in the appearance of a carbonyl peak in the C1s narrow scans and differing relative amounts of hydroxyl and ester peaks (through surface exposure and possibly oxidation and/or deposition). How these treatments and the resulting surface chemistry affect the interfacial properties in mechanical testing is discussed in Section 5.7.

5.6 Analysis of Silicon Contamination

This section discusses the nature and characterisation of silicon present on the recycled fibre veil. It can be seen from Table 4.7 that there is silicon present in the binder, even though it is not in the generalised structure (Fig 4.13). It is therefore a contaminant of the binder, possibly in the form of polydimethylsiloxane (PDMS) as it is often

ubiquitous in industrial water. No silicon is detected in the XPS survey scan of the as received veil (Table 4.9), however it is present in the survey scans of all plasma treated fibre samples, suggesting that there is contamination on the fibre too, despite it not being detected on the survey scan. However in the Si2p narrow scan of the untreated fibre a poorly defined peak is present (Figure 5.9). Therefore Si could be associated with SiO_2 deposits on the fibre surface, which is covered by the binder and later exposed by plasma desorption. It has previously been confirmed that the plasma treatment is desorbing the organic elements of the binder. It was noted in Section 3.5.1 that speciation of the Si2p peak is difficult due to p-orbital splitting. This gives rise to a doublet peak ($Si2p_{1/2}$ and $Si2p_{3/2}$), the components of which are separated by very small variations in binding energy, making quantitative assignment difficult. Table 5.5 below details some literature values of Si2p component peak assignments [90]:

Table 5.5 – Binding energies of Si2p component peaks [90]

Core Line	Reference BE (eV)	Assignment
$Si2p_{3/2}$	102.4	Siloxane bond
$Si2p_{1/2}$	103.1	Si-O-Si
$Si2p_{3/2}$	103.5	Doublet ass. with SiO_2
$Si2p_{1/2}$	104.2	and SiOH

It can be seen from Table 5.5 that differences in binding energy between peaks are small, and care must be taken when curve fitting. A list of silicon species binding energies by Briggs and Seah [91] shows that PDMS has a BE value of 102.4 eV. As PDMS is a polymeric siloxane there is agreement with Table 5.5 however their list does not account for or mention p-orbital splitting. Choudhury [90] also states that an additive shift of 0.6 eV can be applied to silicones on introduction of an oxygen, thus

BEs range from 101.2 eV for SiC_4 to 103.6 eV for SiO_4. Thus Si_2O_2 (as in PDMS) would occur at 102.4 eV, which matches Table 5.5 and [91]. However this means that the $Si2p_{3/2}$ peak at 103.5 eV (SiO_2 and SiOH) is easily confused with the BE of 103.6 eV for SiO_4. Figure 5.5 below shows the Si2p narrow scan of the polyester binder:
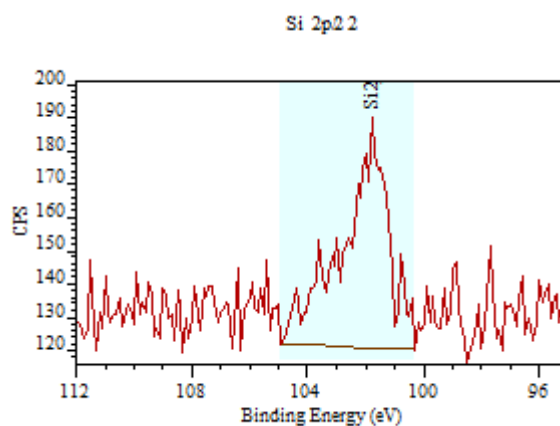
Fig 5.5 – Si2p narrow scan of polyester binder

The resolution of the Si2p peak is poor, this is likely because Si is only present in the binder at 0.33 % relative to the other elements. The region created ranges from 100.3 to 104.9 eV, thus any combination of peaks in Table 5.7 are possible. It is clear that there is more than one component peak contributing to the spectrum, however due to the poor resolution, no combinations of 2 or more peaks satisfied the software's requirements for a match to the obtained spectral peak. From the shape of the peak it is possible that there is a contribution from PDMS at lower binding energy and a smaller contribution from silica species at higher binding energy, though this is impossible to conclude from this spectrum. However PDMS is a very likely contaminant of the binder as characteristic peaks were present in the ToF-SIMS spectra. Figure 5.6 below details characteristic peak positions of linear and cyclic PDMS in ToF-SIMS positive ion

spectra, and Table 5.6 characteristic PDMS fragments in negative ion spectra. Spectra of pure PDMS assigned with these characteristic peaks are present in literature [92, 93].

n value	Peak Position (D)
0	73
1	147
2	221
3	295

n value	Peak Position (D)
0	133
1	207
2	281
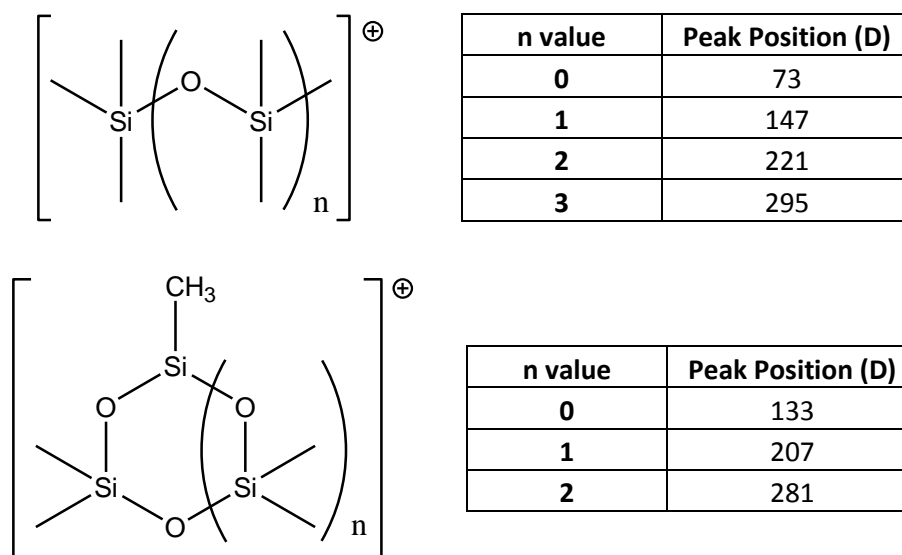
Fig 5.6 – Structure and characteristic ToF-SIMS positive spectra peak positions of linear and cyclic PDMS

Table 5.6 – Characteristic ToF-SIMS negative spectra peak positions of PDMS.

Fragment	Peak Position (D)
CH_3SiO^-	59
SiO_2^-	60
$CH_3SiO_2^-$	75
$CH_3Si\text{-}O\text{-}SiO_2^-$	119
$(CH_3)_3Si\text{-}O\text{-}SiO_2^-$	149
$(CH_3)_3Si\text{-}O\text{-}Si(CH_3)_2O\text{-}SiO_2^-$	223

The annotated ToF-SIMS spectra of the polyester binder are presented in Figure 5.7 (a) positive ion spectra and (b) negative ion spectra. It can be seen from Figure 5.6 that the characteristic peaks for PDMS are present in both the positive and negative spectra, and it is thus likely the (or at least partly) source of silicon contamination in the binder. The

presence of the sodiosulfo groups is also confirmed with an intense Na^+ peak at 23D in the positive ion spectrum and the SO_3^- peak at 80D in the negative ion spectrum. Figure 5.8 shows the annotated (a) positive ion and (b) negative ion ToF-SIMS spectra of the as received carbon fibre surface. It is difficult to correlate the positive ion spectra of the veil with that of the binder as the peaks in the veil spectrum were of much lower intensity with the exception of the Na^+ peak at 23D. However the negative ion spectrum of the fibre showed strong evidence for the presence of PDMS as similar characteristic peaks were present as in the binder spectrum. An SO_3^- peak was also present in the spectrum of the fibre further confirming the deposition of the binder in the veil making process.
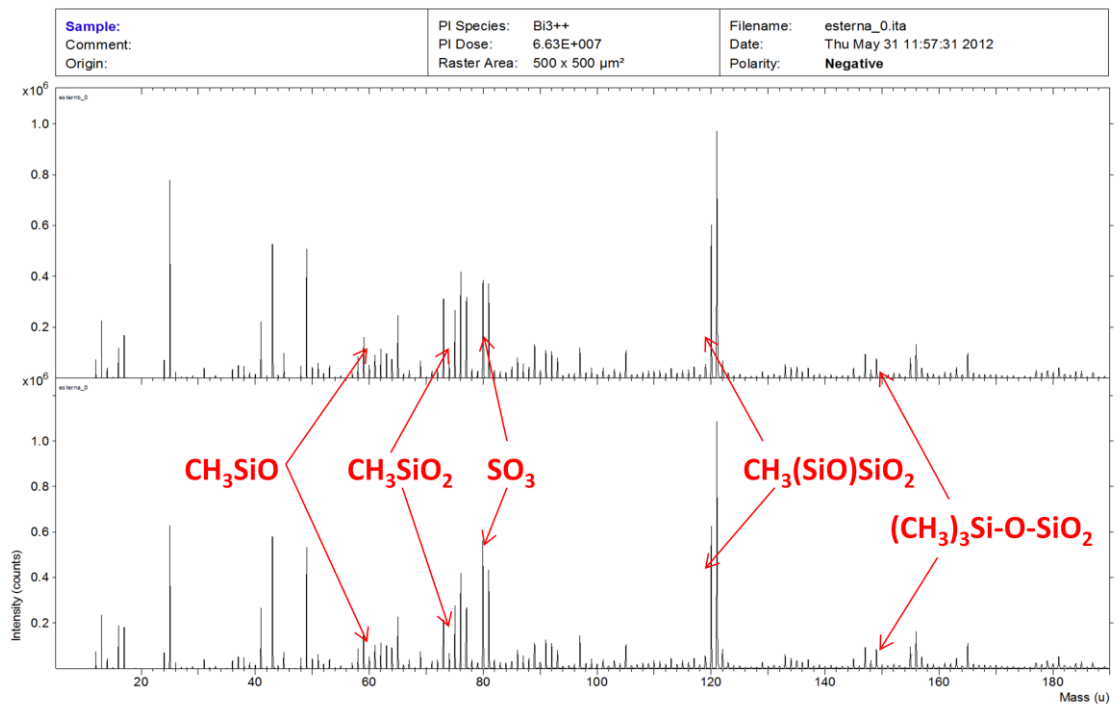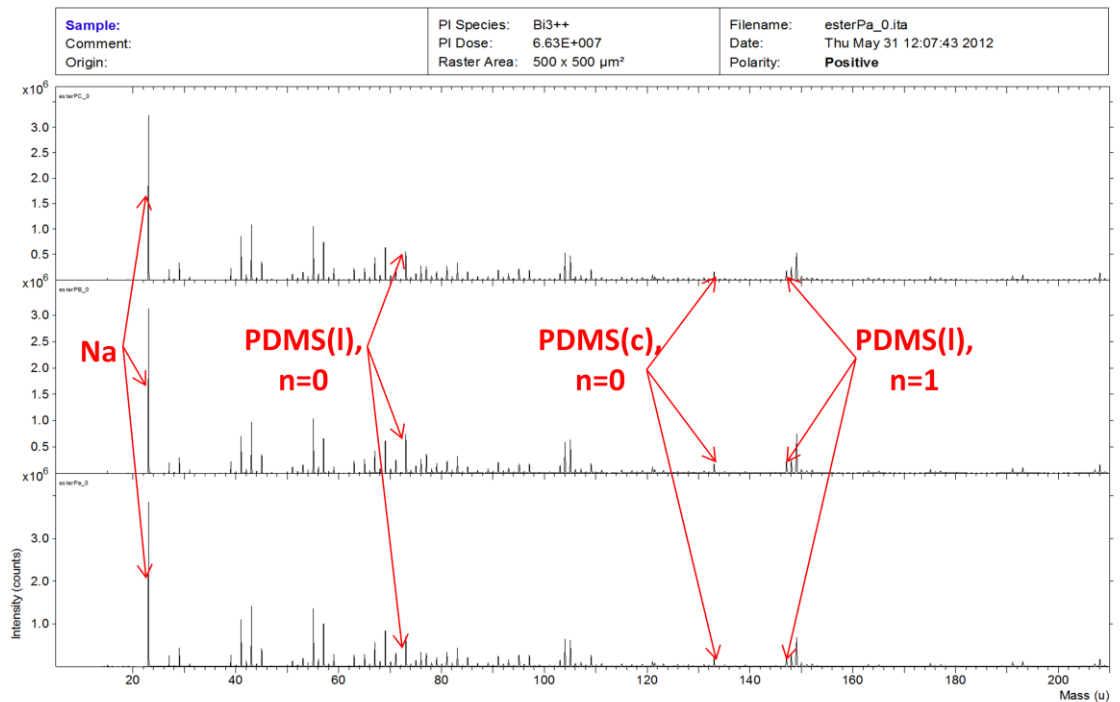
Fig 5.7 – (a) positive and (b) negative assigned ToF-SIMS spectra of polyester binder
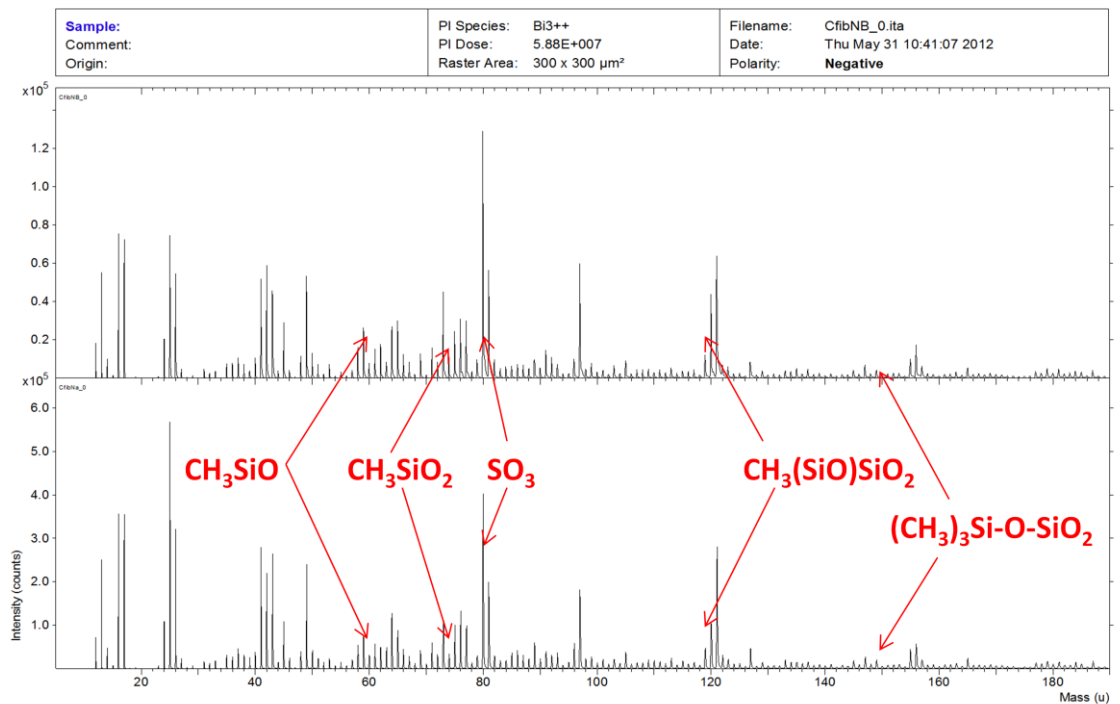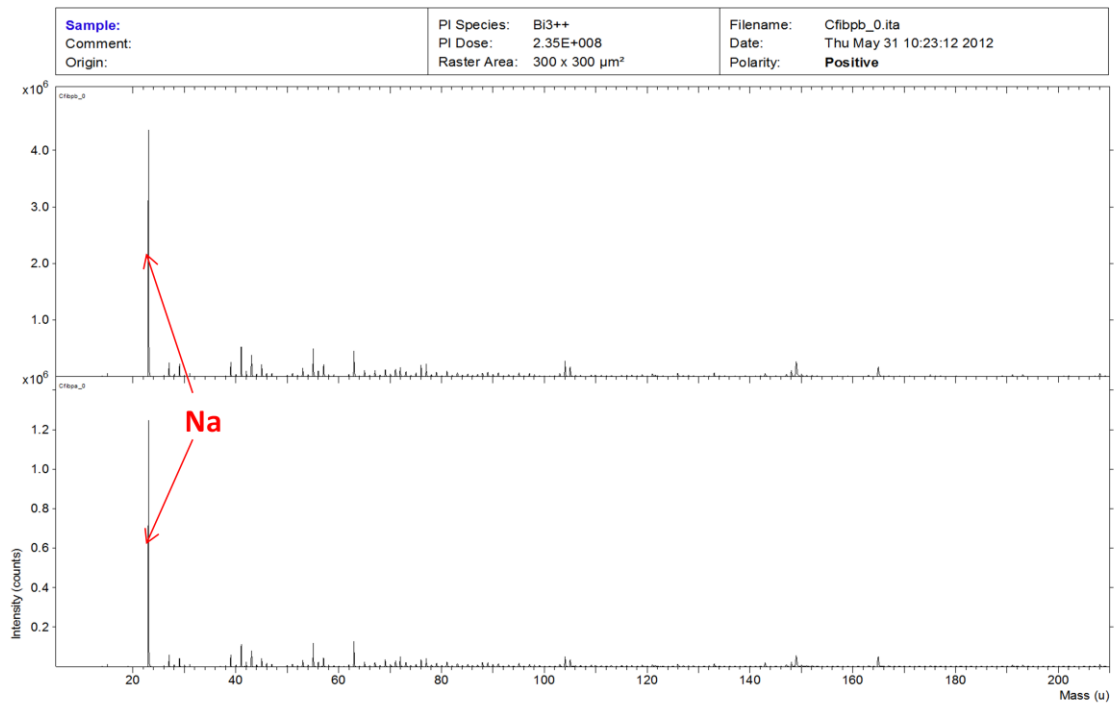
Fig 5.8 – (a) positive and (b) negative assigned ToF-SIMS spectra of untreated carbon fibre

Figure 5.9 below presents the Si2p narrow scans of (a) as received, (b) 10 W, (c) 20 W and (d) 35 W plasma treated carbon fibre veils:

(a)

(b)

(c)

(d)
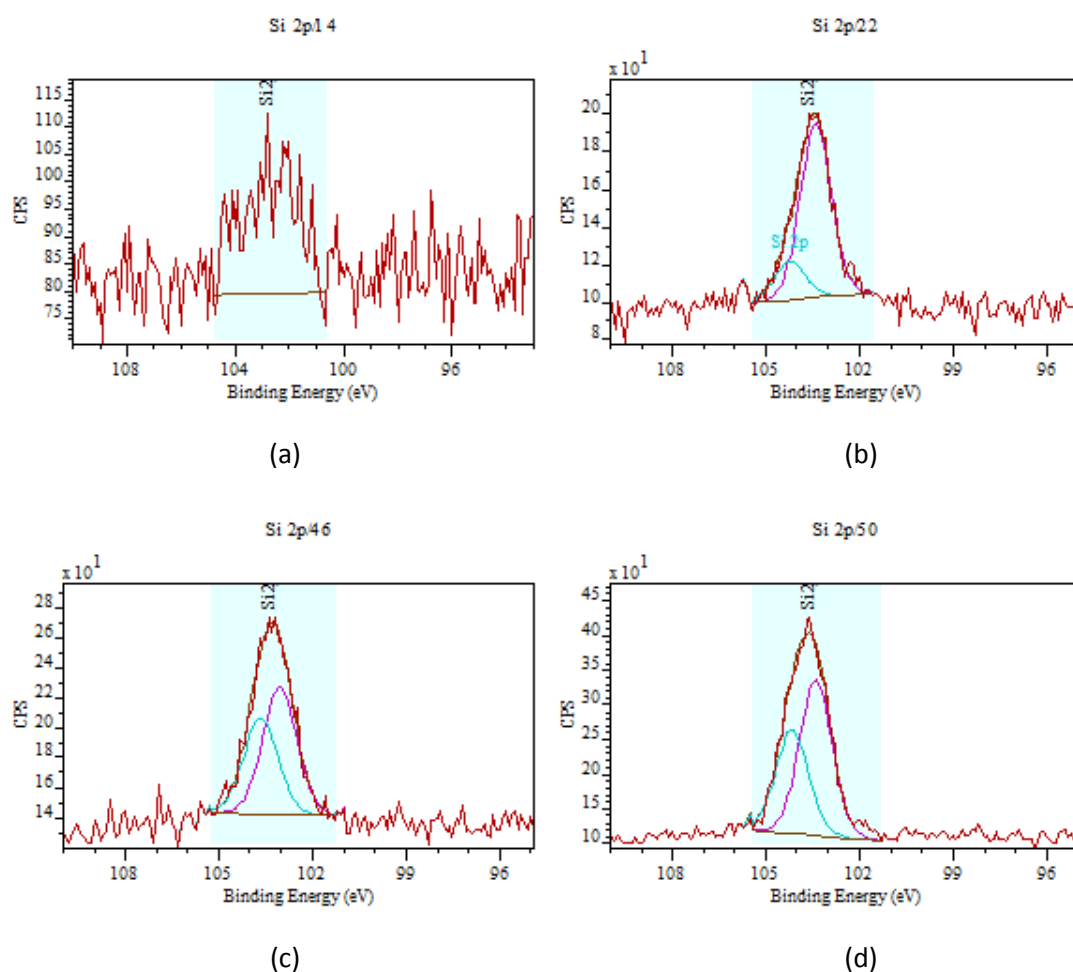
Fig 5.9 – Si2p narrow scans of (a) as received, (b) 10W treated, (c) 20W treated and (d) 35W treated carbon fibre veils

It can be seen from Figure 5.9 that the Si2p peak becomes better defined after plasma treatment. The peak lines are clearer and the CPS count becomes progressively higher. For the as received veil, the Si2p peak is insufficiently strong for curve fitting. The peak is so ill-defined that it does not stand out from the background on the survey scan. The speciation of the peaks for the plasma treated samples are detailed in Table 5.7 below:

Table 5.7 - Speciation of Si2p peaks of 10W, 20W and 35W plasma treated samples showing peak position, core line and peak assignment.

Sample	Peak Positions (eV)	Core Line	Assignment
10W Treated	103.4	Si2p$_{3/2}$	SiO$_2$ and SiOH
	104.2	Si2p$_{1/2}$	
20W Treated	103.0	-	SiO$_3$C
	103.6	-	SiO$_4$
35W Treated	103.4	Si2p$_{3/2}$	SiO$_2$ and SiOH
	104.2	Si2p$_{1/2}$	

The data suggests that the silicon on the treated fibre is present in the form of silica species (SiO$_2$ and SiOH). There were no peaks to indicate PDMS presence on the fibre surface. This is likely due to the plasma treatment processes removing it along with other organic components of the binder. The doublets associated with silica species are clearly present in the scans of the fibre treated at 10 W and 35 W. However the sample treated at 20 W does not follow this pattern, with peaks at 103.0 and 103.6 eV that correspond to SiO$_3$C and SiO$_4$ respectively. There are 2 possible explanations for this. One is that there was an error in the scan and these peaks should appear at approximately 0.5 eV higher binding energy. This would make them fit the same assignment as those for the 10 W and 35 W treated samples. Another explanation is that these peaks correspond to SiO$_3$C and SiO$_4$. Examining the full nature of the silicon contamination can explain this.

Although the XPS survey scan of the untreated fibre did not detect any silicon, there is a weak Si2p peak in the narrow scan that confirms its presence. ToF-SIMS analysis shows that this is due (at the very least partly) to PDMS contamination of the binder. A definitive speciation of the silicon contamination on the fibre cannot be concluded without XPS spectra of the untreated fibre prior to conversion into a veil. This is not practical as the fibre at this point is in its pure recyclate 'fluffy' form (Figure 2.4). There

will also be varying degrees of contamination (and indeed all surface chemistry) both across and within batches of the recyclate. The XPS survey scans show that relative silicon content increases from the as received veil to 10 W treated fibre, and continues to increase as plasma power is increased (Table 4.9). Thus the contamination is being exposed as the plasma removes the organic components of the binder. However it cannot be ruled out that the plasma is changing the chemical composition of the silicon-containing species on the fibre surface, and that 20 W plasma power is optimal for oxidation of these species to SiO_3C and SiO_4. It is likely that silicon is present on the fibre surface, and that the plasma treatment can desorb PDMS from the surface, or oxidise it to SiO_2, and also expose SiO_2 on the fibre itself, and in the case of treatment at 20 W, oxidising the silica to SiO_3C and SiO_4. Therefore the 2 possible sources of SiO_2 on the fibre surface are a) a result of the pyrolysis process and b) oxidation of PDMS by the plasma.

5.7 10° Off-axis Tensile Testing of Plasma Treated Samples

This section discusses the results obtained from 10° off-axis tensile testing of plasma treated samples compared to the as received veil. These tests were selected as although single filament extraction from the veil was possible, to do this without contaminating the fibre surface was extremely difficult. An off-axis tensile test was chosen to better facilitate an interfacial response from the composites, as tensile tests at 0° are fibre-dominated.

5.7.1 Sample Design, Treatment Selection and Test Conditions

The samples tested to assess the effect of plasma treatment were not prepared or tested according to the ISO standard for fibre-reinforced plastics [79, 80]. Such samples are rather large (250 x 15 mm) and to treat enough samples under each power to lay-up enough panels to produce the required number of test specimens would be extremely time-consuming. Thus smaller samples of approximate dimensions 100 x 5 mm were chosen. In this way a panel large enough to produce the required number of test pieces could be laid up after just 2 treatment cycles. Although comparisons to other materials would not be valid, this is irrelevant as the data obtained is used to compare like-for-like samples under different treatment conditions only.

Initially samples were treated and manufactured from pre-forms, as this was the case when performing the standard material tests. Later samples were treated and manufactured from individual veils so as to remove the possibility of 'shadowing'. Shadowing is a potential problem with plasma treating pre-forms as it is possible that the treatment only affects the outermost layers of the fibre. By treating individual veils, all of the reinforcement has been subjected to plasma treatment in the resulting composite.

The pre-forms were initially treated at 10, 20 and 35 W. From the data it was apparent that 20 W treatment enhanced the mechanical properties and 35 W treatment reduced them, and so treatment at 28 W was carried out to fill the gap in information and treatment at 50 W was carried out to confirm the overtreatment at higher powers. Tests performed on the 50 W treated samples confirmed overtreatment. Thus for surface analysis (XPS and Wicking tests) samples were analysed after treatments at 10 W to represent initial treatment, 20 W (optimal treatment) and 35 W (overtreatment). When

moving on to individual veils, plasma powers from 10 to 50 W were again chosen but this time in increments of 10 W for consistency.

5.7.2 Samples Manufactured from Pre-forms

The results summarised in Table 4.2 show that the plasma treatment affected the mechanical properties of the samples. This is seen by plotting each mechanical property against the plasma power used in the treatment process as shown in Figures 4.5-4.7. The results are described in Section 4.2.1. A statistical 't-test' was carried out on each data set (normalised for V_f, Table 4.3) to determine where significant changes occurred as a result of plasma treatment compared to the untreated control. A probability of 0.05 was chosen so that there was 95% confidence in the significant changes indicated by the t-test (as opposed to occurring by chance). The number of degrees of freedom = 8 (total number of specimens in both data sets minus 2). The critical t-value for these parameters is 2.31, thus a t-value > 2.31 represents a significant change. The results of these tests are depicted in Table 5.8, where t-values in bold indicate a significant change. See Appendix D for an example t-test calculation.

Table 5.8 – Results of t-tests on mean values of normalised data from Table 4.3. Bold figures indicate a significant change.

Sample Comparison	$t\,(\sigma^{10}_{uN})$	$t\,(E^{10}_{N})$	$t\,(\varepsilon^{10}_{uN})$
UT to 10W	**2.59**	0.225	0.495
UT to 20W	**3.88**	0.913	0.129
UT to 28W	1.62	1.09	0.347
UT to 35W	**6.3**	2.24	**5.81**
UT to 50W	**4.87**	1.26	**4.17**

The main points of the results analysis are summarised below:

a) Tensile strength (σ^{10}_{uN}) was maximised after plasma treatment of the fibres at an intermediate power of 20 W.

b) According to the t-test, plasma treatment at 28 W had no significant effect on σ^{10}_{uN} whereas treatment at 10 W did.

c) Plasma treatment at 35 and 50 W led to a significant reduction in σ^{10}_{uN}, it can be said they had been 'overtreated'.

d) According to the t-test, it can be said that the plasma treatment had no effect on the normalised elastic modulus E^{10}_{N}.

e) Plasma treatment at 10, 20 and 28 W had no effect on failure strain ε^{10}_{uN} however overtreatment at 35 and 50 W led to a significant reduction.

f) The 50 W treated samples had higher σ^{10}_{uN} and ε^{10}_{uN} than the 35 W treated samples.

Explanations for each of these points are given below:

a) Plasma treatment at 20 W provided the optimal level of interfacial adhesion for this material system and test method. Table 4.9 shows that samples treated at 20W had the highest O/C ratio (0.41), and it was stated previously that oxygen functionality on the fibre can provide sights for chemical bonding with the matrix [46].

b) Treatment at 10 W increased the O/C ratio (Table 4.9) from 0.29 to 0.33. XPS was not performed on 28 W treated samples (see Section 5.7.1 for XPS sample selection). However assuming that treatment led to an O/C ratio intermediate between that of 20 W treated (0.41) and 35 W treated (0.32) it would still be

elevated compared to the as received veil. Therefore an improvement in tensile strength would be expected as high surface oxygen content improved σ^{10}_{uN} after treatment at 20 W. As this was not the case it is possible that the treatment damaged the fibres in some way. This has been demonstrated previously [55]. It is also possible that fibre damage would occur after plasma treatment at 20 W, but as this led to a significant improvement in σ^{10}_{uN} this effect must be of less significance than the introduction of functionality to the surface, which was much higher for treatment at 20 W than at 10 W (and probably at 28W).

c) The reduction in σ^{10}_{uN} for the over-treated samples can be explained by the theory of fibre damage. The 35 W treated samples had an O/C ratio significantly lower than samples treated at 20 W (0.41) but slightly higher than the as received veil (0.29). This has not resulted in σ^{10}_{uN} greater than that of the as received veil. If the integrity of the fibres is damaged by overtreatment, it is likely to be more severe in the case of higher plasma powers.

d) Although there are small variations in E^{10}_{N} these are insignificant as composite stiffness is a function of V_f as $E_f \gg E_m$. Thus normalising for V_f should and does result in similar values. Any differences are due to errors inherent in the treatment and/or manufacturing process and/or test procedure, which are discussed in Section 5.9. The t-test concluded that there were no significant changes in E^{10}_{N} as a result of plasma treatment.

e) The significantly low values of ε^{10}_{uN} for the 35 and 50 W treated samples are consistent with their tensile strength. As E^{10}_{N} is fairly constant, their low values of $\sigma^{10}_{u}N$ result in a correspondingly low ε^{10}_{uN} as $\varepsilon = \sigma/E$.

f) This does not follow the general downward trend in σ^{10}_{uN} and ε^{10}_{uN} between 20 W and 35 W. It is possible that the 50 W treated samples have a significantly

higher O/C ratio on the fibre surface, and/or increased adhesion caused by a greater degree of surface roughening by the high power plasma.

Overall the trend in data of σ^{10}_{uN} is explained by the relative contributions of enhanced interface performance through introduction of oxygen functionality and either increased adhesion or damage to fibre integrity by the plasma resulting in a loss of strength. It can be assumed that the higher the plasma power, the greater the number of reactive species in the plasma and thus available for reaction with the fibre surface. Interestingly this does not result in a linear relationship between power and level of oxygen functionality, as the highest O/C ratio is found in samples treated at 20W.

5.7.3 Samples Manufactured from Individual Veils

The results summarised in Table 4.4 show that the plasma treatment affected the mechanical properties of the samples. This is seen by plotting each mechanical property against the plasma power used in the treatment process as shown in Figures 4.9-4.11. The results are described in Section 4.2.2. A statistical 't-test' was carried out on each data set (normalised for V_f, Table 4.5) to determine where significant changes occurred as a result of plasma treatment compared to the untreated control. A probability of 0.05 was chosen so that there was 95% confidence in the significant changes indicated by the t-test (as opposed to occurring by chance). The number of degrees of freedom = 8 (total number of specimens in both data sets minus 2). The critical t-value for these parameters is 2.31, thus a t-value > 2.31 represents a significant change. The results of these tests are depicted in Table 5.19, where t-values in bold indicate a significant change. See Appendix D for an example t-test calculation.

Table 5.9 – Results of t-tests on mean values of normalised data from Table 4.3. Bold figures indicate a significant change.

Sample Comparison	t (σ^{10}_{uN})	t (E^{10}_{N})	t (ε^{10}_{uN})
UT to 10W	2.03	0.713	0.75
UT to 20W	**4.79**	0.604	**2.55**
UT to 30W	**2.65**	0.634	1.03
UT to 40W	1.55	1.04	0.77
UT to 50W	**6.67**	0.937	**8.69**

The main points of the results analysis are summarised below:

a) Tensile strength (σ^{10}_{uN}) was maximised after plasma treatment of the fibres at an intermediate power of 20 W (as was the case with samples manufacture from pre-forms).

b) According to the t-test, plasma treatment at 10 W had no significant effect on σ^{10}_{u} whereas treatment at 30 W did.

c) From 20 W onwards there is a downward trend in σ^{10}_{u} and σ^{10}_{uN} and at 50 W resulted in a significant reduction

d) According to the t-test, plasma treatment had no effect on the normalised elastic modulus E^{10}_{N}.

e) According to the t-test, plasma treatment had little effect on ε^{10}_{uN} (except in the case of 20 W treatment), from which point onwards there was a downward trend in ε^{10}_{uN} and after treatment at 50 W ε^{10}_{uN} was significantly reduced.

Explanations for each of these points are stated below:

a) As with the samples manufacture from pre-forms, plasma treatment at 20 W provided the optimal level of interfacial adhesion for this material system and test method. Table 4.9 shows that samples treated at 20W had the highest O/C ratio (0.41), and it was stated previously that oxygen functionality on the fibre can provide sights for chemical bonding with the matrix [46].

b) Again this is explained in the same way as the results manufactured from pre-forms of 10 and 28 W treated samples. The relative contributions of surface oxygen functionality and either fibre damage or increased surface roughness resulted in samples treated at 10 and 30 W having σ^{10}_{uN} values not too different from that of the untreated control.

c) Fibre damage caused by overtreatment explains the low σ^{10}_{uN} value for the 50 W treated samples. Samples treated at 40 W had a lower σ^{10}_{uN} than the untreated control (and indeed the 10, 20 and 30 W treated samples) however relatively it is not as low as σ^{10}_{uN} for the 35 W treated samples manufactured from pre-forms. This is best explained by the physical and manufacturing differences of the 2 samples (see Section 5.9).

d) All mean values for E^{10}_{N} fall within one standard deviation of the mean value for the untreated control. This is because composite stiffness is a function of V_f.

e) The trends in ε^{10}_{u} and ε^{10}_{uN} follow similar patterns to those of σ^{10}_{u} and σ^{10}_{uN} respectively. As E^{10} and E^{10}_{N} are fairly constant, it follows that ε^{10}_{u} and ε^{10}_{uN} vary with σ^{10}_{u} and σ^{10}_{uN} as $\varepsilon = \sigma/E$.

5.7.4 – Comparing Samples Manufactured from Pre-Forms and Samples Manufactured From Individual Veils

Overall the patterns in the tensile test data for both sets of samples is very similar. However, there are key differences between each sample set. The mean value of σ^{10}_u for samples manufactured from pre-forms is 230.8 MPa, compared to just 116.8 MPa for those manufactured from individual veils. This is explained by their differing V_f's, of 15.58 and 9.55 %. As σ^{10}_u is approximately double for the pre-form samples, this shows that the relationship between V_f and σ^{10}_u is not linear. Nor is the relationship between V_f and E^{10}, as the pre-form samples are approximately 3 times stiffer than the individual veil samples. The higher mean ε^{10}_u value (4.54 c.f. 2.77 %) for the individual veils samples is explained by their higher relative resin (matrix) content, as $\varepsilon_m \gg \varepsilon_f$. The minimum V_f required for reinforcement was achieved, as the σ^{10}_u and E^{10} of the cured resin system was 47 MPa and 2.4 GPa respectively (Table 3.1).

Despite these absolute differences, the patterns in the data with respect to plasma treatment are very similar. It is reasonable to expect that the pre-form samples would exhibit greater dependence on plasma treatment with respect to their tensile properties, as they have a higher V_f there is a greater dependence on interfacial performance in these samples. What explains the similar data patterns is 'shadowing'. Although it is a gas phase treatment it is possible that the outer layers of the pre-form were treated to a greater extent than the inner layers. The samples manufactured from individual veils were not affected by shadowing as each fibre veil was consistently treated. Thus the combined influences of V_f (degree of interface dependence) and shadowing explain the similar patterns in the data for both sample sets.

5.8 Fibre Surface Wettability

It can be seen from Table 4.6 and Figure 4.12 that fibre surface wettability had no effect interfacial performance. Plasma treatment at 10 W dramatically reduced the ethanol contact angle from 47.64 to 17.97^{o}. Despite this the tensile properties of samples treated at 10 W were very similar to those of the untreated control. Treatment at 20 W reduced the contact angle to 38.65^{o}. This is much higher than that for the 10 W treated yet resulted in the most improved mechanical properties. These values are unexpected as treatment at 20 W led to the highest O/C ratio on the fibre surface. Overtreatment at 35 W led to the highest value of contact angle. Although the plasma treatments have had a large effect on the wettability of the fibre, this has not translated into interfacial performance except in the case of the 35 W treated sample. Good or favourable wettability does not imply an improved interface, only an indication of the compatibility of the fibre with matrices. Although this varies widely across different treatments it can be stated that poor (or relatively poor) wettability is not a limiting factor in composite interface performance. Further work is required in this area to draw any firm conclusions about the relationship between wettability and composite performance.

5.9 Sources of Error

This section discusses the sources of error that arose at each stage of the data interpretation, tracing them back to the affects they had on the data analysis and what was done to minimise them.

5.9.1 Plasma Treatment

- Reactant Flow Rate – Flow rate was kept as constant as possible (Section 3.3.3). The oxygen was introduced to the chamber and stabilised at the same base pressure of 0.06 mbar. The shut-off valve was closed for 30 seconds and the final pressure reached 0.6 mbar each time. In theory the flow rate was therefore constant across all treatments. However there may have been small variations as it could take 1 to 2 seconds to fully close the shut-off valve and starting the timer exactly when the valve was closed may have varied slightly. Also, the Edwards Pirani pressure gauge is only accurate to +/- 15 %. Thus flow rate was not used as a treatment variable as changes would be difficult to quantify.

- Plasma Power – The display on the RF generator only quoted integers, so the power could only be set to an accuracy of +/- 0.5 W. This is fairly insignificant however as plasma power was differed by a minimum of 7 W (usually 10 W) in each treatment.

5.9.2 Composite Lay-up

- The nature of hand lay-up makes it impossible to manufacture 2 samples exactly the same. The resin components were weighed out on a 2-place balance and thus with an accuracy +/- 0.005g. Such variations can lead to slightly different ratios of resin to hardener in each mixture, so care was taken to weigh them accurately. When laying up it is impossible to use the exact same amount of resin for each panel. They were made in a way that ensured the fibres were fully wet out and it was left to the vacuum consolidated cure to impart consistency. In any case this would still lead to variations in V_f, however such variations were small across

each data set, and mechanical properties were normalised for V_f to account for this.

- The nature of FRPs is that no 2 specimens are the same. In each sample there will be differing degrees of alignment distributed through the sample, fibre bundles, resin rich areas, defects and voids. Larger test specimens average out homogeneity better than smaller ones, but the best way to obtain representative results was to perform repeat tests and calculate the mean and statistical distribution of the data.

5.9.3 Mechanical Testing

- Sample and Machine Alignment – Mechanical characterisation tests were performed so that the fibres bore the load longitudinally. Any variation from 0° could affect the results, so care was taken to align samples parallel to the load direction. Also, 0° tests assume that the fibres were cut, laid up and then the samples themselves cut *all at 0°*, and although care was taken at each stage to ensure this, there is an element of human error throughout the process that is difficult to quantify.

- Sample geometries were measured using Vernier calipers, which have an accuracy of +/- 0.005mm. Thus a cross-sectional area could have an error of +/- 0.000025mm, small enough to be ignored. The bigger problem was variations in width and thickness of individual test specimens. This was combated by taking 3 measurements of each and using the mean value.

- The load cells used were accurate to +/- 0.5 N, which may result in small errors in mechanical data.

5.9.4 Fibre Surface Variability

- The non-woven was manufactured from recycled carbon fibres that were first dispersed in solution prior to veil manufacture, and thus there will be local variations in fibre density, concentration of bundles, fibre alignment and surface chemistry. These are illustrated in Figure 5.10.

- Density – Small variations in fibre density can affect the localised V_f of manufactured samples, though they should be small enough to be compensated for by the size of the test specimens. Density variations would not affect the results of XPS spectra as elemental and chemical state compositions are relative to each other for a given spectrum.

- Bundles – The presence of fibre bundles in the veil is inevitable as it is almost impossible to achieve complete dispersion on the single fibre scale in solution prior to veil manufacture. A concentration of bundles in a small area could result in a higher V_f in a given test specimen, and was accounted for by normalising the mechanical data for V_f.

- Alignment – Local variations in degree of fibre alignment are likely present but difficult to quantify. Again for test specimens these should be averaged out by the size of the specimens. However for XPS analyses, where only a small area was analysed, differing degrees of alignment could result in different degrees of peak broadening across spectra.

- Surface Chemistry – The fibre surface chemistry could be inconsistent from the start, as the pyrolysis process is proprietary there is no data from testing of the surface chemistry to prove its consistency (or otherwise). The plasma treatment process may also inconsistently treat the surface within a specimen, although this was minimised as much as possible (Section 5.9.1)

Figure 5.10 – Micrograph of fibre veil showing variations in density, alignment and bundle concentration.

5.9.5 XPS Analysis

- Fibre surface chemistry inevitably varies in each specimen. Plasma treatment complicates the matter in that its effects on the surface will not be uniform for a given specimen. Thus in each XPS analysis 3 points per sample were analysed to give more representative results of the surface chemistry.

- No surface is perfectly smooth, thus the take-off angle of ejected photo-electrons varies and results in peak broadening. This is can be limited if not eradicated by analysing several points per sample.

- The curve fitting in XPS narrow scans is open to interpretation. Peaks can be assigned based on expected chemical environments at BEs corresponding to those of standard compounds. The software can then 'fit' these curves to the experimentally observed peak but it is open to judgement whether such an assignment is accurate or even representative of the sample and/or spectra. The fitting of the user defined (brown) peak with the experimental (red) peak is

purely mathematical and unrelated to surface chemistry considerations. Care must be taken when drawing conclusions.

Chapter 6

Conclusions and Further Work

6.1 Conclusions

The 2 main functions required of a fibre treatment or sizing are; to protect the fibres from damage during handling, storage, transportation and manufacture into composites and; to enhance the interface with respect to fibre-matrix adhesion to maximise mechanical performance. This work has demonstrated that an oxygen plasma treatment can perform the second function. Treatment at an intermediate power of 20 W resulted in the best interfacial performance in the composites, and this correlated to the highest proportion of surface oxygen content, thus providing the most sites for chemical bonding at the interface. Specifically the 10° off-axis tensile strength was increased by 20 % after treatment at 20 W for samples manufactured from pre-forms and by 29 % for samples manufactured from individual veils when compared to the untreated control. The O/C ratio increased from 0.29 for the untreated control to 0.41 after treatment at 20 W, an increase of 41 %. Treatment at higher powers did not result in higher surface oxygen content. Although this may be expected as there would be a greater number of reactive species in the plasma at higher powers, the effect of this treatment was the exposure of fibre surface functionality underneath the binder, not the deposition of reactive species from the plasma. This was shown by the increasing intensity of the π-π^* peak with increasing plasma power, demonstrating the exposure of the fibres. It is

possible that some deposition of oxygen did occur, however the net effect of binder removal (and fibre surface functionality removal at higher powers) and oxygen deposition (if any) was optimal at 20 W plasma power. As for the first function (protection) the polyester binder performs this function by holding the fibres together in the formation of a handle-able, workable veil. The effects of the plasma treatment process on this function are beyond the scope of this work, however post-treatment the veils were still easily handle-able and workable.

Composites manufactured by hand lay-up from a non-woven veil of recycled carbon fibre and cured under with vacuum consolidation have the potential to be used as an engineering material as their mechanical properties are comparable with other common composite materials (with the exception of pre-pregs) when normalised for V_f. With their properties being intermediate between those of 'low-end' chopped strand mat and 'high-end' CFRP pre-preg they will mostly compete with woven fabrics used for hand lay-up. Currently hand-laid woven CFRP-epoxy composites outperform the recycled carbon fibre system (for example its Young's modulus is 35.47 GPa compared to 22.16 GPa). However this is largely due to discrepancies in V_f. (40 % $\gg$ 15.7%). Improvements to fibre alignment will enhance their properties further as this will allow higher V_f composites (and thus better mechanical properties) to be achieved. This is essential for the recycled material to compete with woven CFRP as the woven material has the advantage of providing reinforcement properties in 2 directions. Further improvements could be achieved by incorporation of the oxygen plasma treatment system into the veil manufacturing process, however this would require research into up-scaling the lab-scale system to that of the industrial process.

Surface analysis showed that there was almost complete coverage of the veil by the binder. This was shown by the similar elemental compositions in the XPS survey scan, similar peak speciation in the C1s narrow scan and by the ToF-SIMS Na^+ image, which illustrated that the binder completely covered the fibres. The presence of silicon in the binder can be attributed to PDMS, a common contaminant of industrial water whose characteristic peaks were present in the ToF-SIMS spectra. Silicon on the fibre surface can be attributed to silica contamination (possibly as a result of the pyrolysis process) or possibly the oxidation of PDMS by the plasma treatment process as the Si2p narrow scans indicated the presence of SiO_2 and SiOH. Conclusions regarding the nature of silicon contamination are difficult to conclude without an analysis of the fibre surface chemistry prior to the veil making process, the scope for further work which is discussed in Section 6.2

6.2 Recommendations for Further Work

- Investigate further the changes in fibre surface morphology resulting from the plasma treatment process. SEM images of treated fibres would allow a qualitative assessment of possible fibre damage and/or surface roughening to be performed. This would provide a more detailed analysis of the relative contributions of each mechanism of interfacial bonding.

- Analyse the treated fibre surface chemistry at intervals post-treatment to determine the time-frame in which the treated samples are useable for composite manufacture. Ideally the plasma treatment process would be performed in situ with the veil making process, however should the effects of the treatment on the

fibre surface 'wear off' over time this would become impractical. Different storage methods of the treated fibres could also be tested. For example, the surface chemistry of a treated fibre veil stored at ambient temperature and pressure may change differently over time to one stored under vacuum.

- Treatment at higher plasma powers (>50 W) would be a simple extension to the current work, and may provide further insight into the interfacial phenomena of the material system. Such treatments were not performed as 50 W was the practical limit of the RF inducer.

- Mechanical testing of other properties (particularly ILSS as its value is highly sensitive to interfacial performance) of composites manufactured from treated samples. This would give a fuller account of the effects of the treatment on material performance.

- Surface analysis of the fibres prior to the veil making process. An analysis of the initial surface chemistry would greatly aid the analysis of the treated fibre surfaces, particularly with respect to silicon contamination. Quantification of surface Si would allow a more conclusive analysis to be made on the sources of Si and the effects on Si species brought about by the plasma treatment process. It would also allow the O/C ratio to be determined and therefore the extent to which the optimal plasma power (20W) achieves this.

References

1. **W.D. Callister and D.G. Rethwisch,** "Fundamentals of Materials Science and Engineering," 3rd Edition, *Wiley Publishing,* 2008.

2. **A. K. Kaw,** "Mechanics of composite materials", *CRC Press*, 1997.

3. http://www.technologyreview.com/review/417605/reinventing-the-commercial-jet/, D. Talbot, April 2010, accessed 09/07/2012.

4. **D. Hull,** "An Introduction to Composite Materials*", Cambridge University Press*, 1981.

5. **G.N. Naik, S. Gopalakrishnan and R. Ganguli,** 2007, "Design Optimization of Composites Using Genetic Algorithms and Failure Mechanism Based Failure Criterion", *Composite Structures,* **83,** 354-367.

6. **N. Pai, A. Kaw and M. Weng,** 2003, "Optimization of Laminate Stacking Sequence for Failure Load Maximization Using Tabu Search", *Composites Part B,* **34,** 405-413.

7. **M. Carus,** "Bio-Composites: Technologies, Applications and Markets", *ECOCOMP Conference*, Birmingham, UK, 2011.

8. http://www2.dupont.com/Kevlar/en_US/assets/downloads/KEVLAR_Technical_Guide.pdf, accessed 10/07/2012

9. **M.G. Dobb** in "Handbook of Composites", Vol. 1, eds W.Watt, and B.V. Perov, *Elsevier,* 1985.

10. **A.R. Bunsell and J. Renard,** "Fundamentals of Fibre Reinforced Composite Materials", *CRC Press,* 2005.

11. **A.A. Grffith,** 1921, "The phenomena of rupture and flow in solids", *Philosophical Transactions of the Royal Society of London,* A**221,** 163-198.

12. **W.Watt, L.N. Phillips and W. Johnson,** 1966, "High-strength high-modulus carbon fibres", *The Engineer,* **221,** 815-816.

13. **D.C. Leach** in "Advanced Composites", ed I.K. Partridge, *Elsevier,* 1989.

14. **R.S. Bailey** in "Handbook of Polymer Fibre Composites", ed. F.R. Jones, *Longman Scientific and Technical,* 1994.

15. **C.A. Arnold, P.M. Hergenrother and J.E. McGrath,** "An Overview of Organic Polymeric Matrix Resins for Composites", *ACS Symposium*, T.Vigo and B.Kinzig, Ed., 1990.

16. **N.J. Johnston, T.W. Towell and P.M. Hergenrother,** "Physical and Mechanical Properties of High Performance Thermoplastic Polymers and Their Composites", in *Thermoplastic Composite Materials,* Vol 7, L.A. Carlsson, Ed., *Elsevier,* 1991.

17. **F.R. Jones,** "Composites Technology Lecture Course", *The University of Sheffield*, 2008.

18. **H.L. Cox,** 1952, "The elasticity and strength of paper and other fibrous materials", *British Journal of Applied Physics,* **3,** 72-79.

19. **E. Witten,** "The composites market in Europe: market developments, challenges and opportunities", *AVK Online Report,* 2008.

20. **S. Job,** "Where we are with composites recycling in the UK", *Composites UK Recycling Working Group Kick Off Meeting*, Kenilworth, UK, 2011.

21. **K. Jang, W. Cho and C. Ha,** 1999, "Influence of processing method on the fracture toughness of thermoplastic-modified, carbon-fiber-reinforced epoxy composites", *Comp. Sci. and Tech.,* **59,** 995-1001.

22. **B.Z. Jang,** "Advanced Polymer Composites: Principles and Applications," *ASM International,* 1994.

23. **Directive on End-of-Life Vehicles (2000/53/EC),** 2000, "Official Journal of the European Union", **L**, 269/34.

24. **Directive on Waste Electrical and Electronic Equipment (2002/96/EC),** 2003, "Official Journal of the European Union", **L,** 37/24.

25. **V. Goodship,** "An Introduction to Plastics Recycling", 2nd Edition, *Smithers Rapra,* 2007.

26. **S.J. Pickering, T.A. Turner and N.A. Warrior,** 2006, "Moulding compound development using recycled carbon fibres", *Proceedings of SAMPE Fall Technical Conference,* Dallas, USA, November 2006.

27. **S.J. Pickering** in "Management, Recycling and Reuse of Waste Composites", ed V. Goodship, *Woodhead Publishing,* 2010.

28. **S.J. Pickering,** 2006, "Recycling technologies for thermoset composite materials – current status," *Comp. Part A, App. Sci. and Manufacturing,* **37**(8), 1206-1215.

29. **D. Kunii and O. Levenspiel,** "Fluidization Engineering", 2nd edition, *Butterworth-Heinemann,* 1993.

30. **S.J. Pickering, R.M. Kelly, J.R. Kennerley and C.D. Rudd,** 2000, "A fluidised bed process for the recovery of glass fibres from scrap thermoset composites", *Comp. Sci. and Tech., 60, 509-523.*

31. **Y. Yin, J.P.B. Binner, T.E. Cross and S.J. Marshall,** 1994, "Oxidation behaviour of carbon fibres", *Journal of Materials Science,* **29,** 2250-2254.

32. **H.L.H. Yip, S.J. Pickering and C.D. Rudd,** 2002, "Characterisation of carbon fibres recycled from scrap composite using fluidized bed process", *Journal of Plastics, Rubbers and Composites,* **31**, 278-282.

33. **Oxford Dictionary of Chemistry,** 5th Edition, ed. J. Daintith, *Oxford University Press,* 2004.

34. **M. Blazso** in "Management, Recycling and Reuse of Waste Composites", ed V. Goodship, *Woodhead Publishing,* 2010.

35. **K. Ushikoshi, N. Komatsu and M.Sugino,** 1995, "Recycling of CFRP by pyrolysis method", *J. Soc. Mat. Sci. Japan,* **44**, 428-431.

36. **K.H. Wong, S.J. Pickering and R. Brooks,** 2007, "Recycled carbon fibre reinforced polypropylene composites: effect of coupling agents on mechanical properties", *CIC Conference,* Barcelona, ESP, October 2007.

37. **K.H. Wong, G.Z. Jiang, S.J. Pickering and C.D. Rudd,** 2005, " Effects of fibre length and loading on electromagnetic shielding of thermoset composite reinforced with virgin or recovered fibres", *ICCM15,* Durban, RSA, June 2007.

38. **A.Kelly and W.R. Tyson,** 1965, "Tensile properties of fibre-reinforced metals: Copper/tungsten and copper/molybdenum", *J. Mech. Phys. Solids,* **13,** 329-350.

39. **R.E. Swain, K.L. Reifsnider, K. Jayaraman and M.Elzein,** 1990, "Interface/Interphase Concepts in Composite Material Systems", *J. Thermoplastic Comp. Mat.,* **3**(1), 13-23.

40. **L.T. Drzal,** 1990, "The role of the fiber-matrix interphase on composite properties", *Vacuum,* **41,** 1615-1618.

41. **L.T. Drzal and M. Madhukar,** 1993, "Fibre-matrix adhesion and its relationship to composite mechanical properties", *J. Mat. Sci.,* **28,** 569-610.

42. **F.R. Jones,** 2010, "A Review of Interphase Formation and Design in Fibre-Reinforced Composites", *J. Adhes. Sci. and Tech.,* **24,** 171-202.

43. **G. Dorey,** 1986, "Carbon Fibres and Their Applications", *J. Phys. D: App. Phys.,* **20**, 245-256.

44. **C. Kozlowski and P.M.A. Sherwood,** 1987, "X-ray photoelectron spectroscopic studies of carbon fibre surfaces VIII – A comparison of type I and type II fibres and their interaction with thin resin films", *Carbon,* **25,** 751-760.

45. **P.Marshall and J. Price,** 1991, "Topography of carbon fibre surfaces", *Composites,* **22,** 388-393.

46. **E. Fitzer and R. Weiss,** 1987, "Effect of surface treatment and sizing of carbon fibres on the mechanical properties of carbon fibre reinforced thermosetting and thermoplastic polymers", *Carbon,* **25,** 455-467.

47. **T.J. Swait,** 2009, "Interfacial Optimisation of Glass Fibre Reinforced Composites by Plasma Polymerisation", PhD Thesis, *University of Sheffield*.

48. **Z. Liu, F.Zhao and F.R. Jones,** 2008, "Optimising the interfacial response of glass fibre composites with a functional nanoscale plasma polymer coating", *Comp. Sci. and Tech.,* **68**, 3161-3170.

49. **A.P. Kettle, A.J. Beck, L. O'Toole, F.R. Jones and R.D. Short,** 1997, "Plasma polymerisation for molecular engineering of carbon-fibre surfaces for optimised composites", **57**, 1023-1032.

50. **N. Loppatananon, A.P. Kettle, D. Tripathi, A.J. Beck, E. Duval, R.M. France, R.D. Short and F.R. Jones,** 1999, "Interface molecular engineering of carbon-fiber composites", *Comp. Part A: App. Sci. and Manuf.,* **30,** 49-57.

51. **N. Dilsiz, E. Ebert, W.Weisweiler and G. Akovali,** 1995, "Effect of Plasma Polymerization on Carbon Fibers Used for Fiber/Epoxy Composites", *J. Colloid and I'face Sci.,* **170**, 241-248.

52. **G. Dagli and N.H. Sung,** 1989, "Properties of Carbon/Graphite Fibers Modified by Plasma Polymerization", *Polymer Composites,* **10,** 109-116.

53. **S. Mujin, H. Baorong, W. Yisheng, T. Ying, H. Weiqiu and D. Youxian,** 1989, "The Surface of Carbon Fibres Continuously Treated by Cold Plasma", *Comp. Sci. and Tech.,* **34,** 353-364.

54. **L. Tang and J. Kardos,** 1997, "A Review of Methods for Improving the Interfacial Adhesion Between Carbon Fibre and Polymer Matrix", *Polymer Composites*, **18,** 100-113.

55. **T.C. Chang,** 1999, "Plasma Surface Treatment in Composites Manufacturing", *J. Industrial Tech.,* **15,** 1-7.

56. **A. Bismarck, M.E. Kumru and J. Springer,** 1999, "Influence of Oxygen Plasma Treatment of PAN-based Carbon Fibres on Their Electrokinetic and Wetting Properties", *J.Colloid and Interface Science,* **210,** 60-72.

57. **Y.D. Huang, J.H. Qiu, L.X. Liu and Z.Q. Zhang,** 2003, "The Uniform Treatment of Carbon Fiber Surface in Three-Directional Orthogonal Fabric by Oxygen-Plasma", *J. Mat. Sci.,* **38,** 759-766.

58. **M.A. Montes-Moran, A. Martinez-Alonso, J.M.D. Tascon and R.J. Young,** 2001, "Effects of plasma oxidation on the surface and interfacial properties of ultra-high modulus carbon fibres", *Comp. Part A: App. Sci. and Manuf.,* **32**, 361-371.

59. **A. Proctor and P.M.A. Sherwood,** 1982, "X-ray photoelectron spectroscopic studies of carbon fibre surfaces. 1. Carbon fibre spectra and the effect of heat treatment", *J. Electron Spectr. Rel. Phenom.,* **27**, 39-56.

60. **A. Ishitani,** 1981, "Application of X-ray photoelectron spectroscopy to surface analysis of carbon fiber", *Carbon*, **19,** 269-275.

61. **G.A. Beitel,** 1971, "The Use of Graphite in High and Ultrahigh Vacuum: A Review" *J. Vac. Sci. and Tech.,* **8**, 647.

62. **C. Jones,** 1991, "The chemistry of carbon fibre surfaces and its effect on interfacial phenomena in fibre epoxy composites", *Comp. Sci. and Tech.,* **42,** 275-298.

63. **M.R. Alexander and F.R. Jones,** 1995, "Effect of electrolytic oxidation upon the surface chemistry of type A carbon fibres – Part II, analysis of derivatised surface functionalities by XPS, and TOF SIMS", *Carbon,* **33**, 569-580.

64. **D. Briggs and M.P Seah,** "Practical Surface Analysis: Volume 2 – Ion and Neutral Spectroscopy", 2nd Edition, *Wiley Publishing,* 1992.

65. **P.E Vickers, M.E. Turner, M.-L. Abel and J.F. Watts,** 1998, "The interaction of organic molecules with carbon fibre surfaces: a ToF-SIMS study", *Comp. Part A.,* **29A**, 1291-1304.

66. **T. Young,** 1805, "An essay on the cohesion of fluids", *Philosophical Transactions of the Royal Society of London,* **95,** 65-87.

67. **N. Eustathopoulos, M.G. Nicholas, and B. Drevet,** 1999, *Wettability at high temperatures,* Oxford UK: Pergamon.

68. **T.Ogawa and M. Ikeda,** 1993, "Determination of the contact angle of a liquid droplet on a carbon fibre", *J. Adhesion,* **43,** 69-78.

69. **H.W. Chang, R.P. Smith, S.K. Li and A.W. Neumann** in "Molecular Characterisation of Composite Interfaces", eds. H.Ishida and G.Kumar, *Plenum New York*, 1985.

70. **A. Hamaraoui and T. Nylander,** 2002, "Analytical Approach for the Lucas-Washburn Equation", *J. Coll. and I'face Sci.,* **250**, 451-421.

71. **T. Dang-Vu, J. Hupka,** 2005, "Characterization of Porous Materials by Capillary Rise Method", *Physiochem. Prob's of Mineral Processing,* **39,** 47-65.

72. **S. Zhandarov and E. Mader,** 2005, "Characterization of fiber/matrix interface strength: applicability of different tests, approaches and parameters", *Comp. Sci. and Tech.,* **65**, 149-160.

73. **B. Miller, P. Muri and L. A. Rebenfeld,** 1987, "Microbond method for determination of the shear strength of a fiber-resin interface", *Comp. Sci. and Tech.,* **28,** 17-32.

74. **S. Zhandarov and E. Mader,** 2003, **"**Indirect estimation of fiber/polymer bond strength and interfacial friction from maximum load values recorded in the microbond and pull-out tests. Part II: Critical energy release rate", *J. Adh. Sci. and Tech.,* **17,** 967-980.

75. **D. Tripathi and F.R. Jones,** 1998, "Single fibre fragmentation test for assessing adhesion in fibre reinforced composites; review", *J. Mat. Sci.,* **33**, 1-16.

76. **M.R. Piggott,** 1997, "Why interface testing by single-fibre methods can be misleading", *Comp. Sci. and Tech.,* **57,** 965-974.

77. **R.J. Young,** 1996, "Evaluation of composite interfaces using Raman spectroscopy", *Key Eng. Mat.,* **116-117**, 173-192.

78. **BS ISO 14127:** 2008, "Carbon-fibre-reinforced composites – Determination of the resin, fibre and void contents", *British Standards Institution*.

79. **BS EN ISO 527-1:** 1996, "Plastics – Determination of tensile properties – Part 1: General principles", *British Standards Institution*.

80. **BS EN ISO 527-5:** 2009, "Plastics – Determination of tensile properties – Part 5: Test conditions for fibre-reinforced plastic composites", *British Standards Institution.*

81. **BS EN ISO 14125:** 1998, "Fibre-reinforced plastic composites – Determination of flexural properties", *British Standards Institution.*

82. **BS EN ISO 14130:** 1998, "Fibre-reinforced plastic composites – Determination of apparent interlaminar shear strength by short-beam method", *British Standards Institution.*

83. **K.R. Barton,** 1979, "Polyester Binders for Polyester Nonwovens", *Nonwovens Industry*, **May 1979.**

84. **A. Thibault, A.D. Lafferty, A. Hodzic and C. Soutis,** 2010, "Properties of Carbon Fibre/Epoxy Composites Modified with 1%wt Carbon Nanotubes", *Unpunlished.*

85. **HexPly 8552 Product Data Sheet,** *Hexcel.*

86. **B. Harris,** "Engineering Composite Materials", *The Institute of Materials,* London, 1999.

87. **Tenax HTA filament yarn product data sheet,** *Toho Tenax.*

88. **G. Li, C. Zhang, Y. Wang, P. Li, Y. Yu, X. Jia, H. Liu, X. Yang, Z. Xue and S. Ryu,** 2008, "Interface correlation and toughness matching of phosphoric acid functionalised Kevlar fiber and epoxy matrix for filament winding composites", *Comp. Sci. and Tech ,* **68,** 3208-3214.

89. **C. Moreno-Castilla,** 2004, "Adsorption of organic molecules from aqueous solutions on carbon materials", *Carbon*, **42,** 83-94.

90. **T. Choudhury and F.R. Jones,** 2006, "The interaction of silanes with amorphous silicon oxide surfaces", *Int. J. of Adhesion and Adhesives,* **26,** 79-87.

91. **D.Briggs and M.P. Seah,** "Practical Surface Analysis, Second Edition, Volume 1 – Auger and X-ray Photoelectron Spectroscopy", *Wiley Publishing,* 1990.

92. **J. C. Vickerman and D. Briggs,** "ToF-SIMS – Surface Analysis by Mass Spectrometry", *IMPublications,* 2001.

93. **A. Delcorte, S. Befahy, C. Poleunis, M. Troosters and P. Bertrand,** 2004, "Improvement of metal adhesion to silicone films: a ToF-SIMS study", *Adhesion Aspects of Thin Films,* **2**, 1-12.

Appendix A

Compliance Data
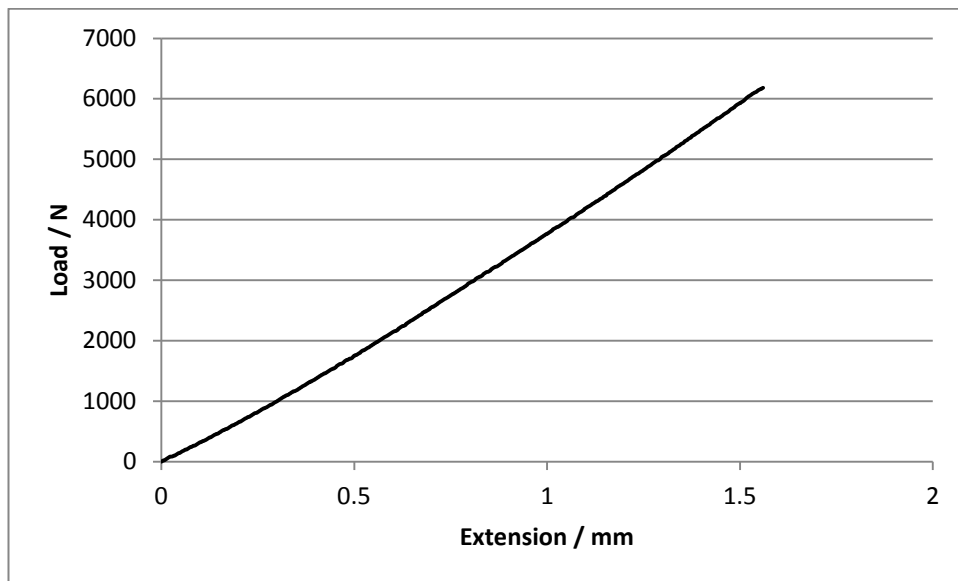
Figure A.1 – Load/extension plot of tensile test of steel bar

Average Compliance $C = 2.43 \times 10^{-4}$ mmN^{-1}

Appendix B

Samples Manufactured from Pre-Forms

Table B.1 – Individual 10° off-axis tensile test data of samples manufactured from untreated pre-forms

Sample	σ^{10}_u / MPa	E^{10} / GPa	ε^{10}_u / %	V_f (%)
1	249.2	16.39	2.69	15.9
2	236.9	15.80	3.59	14.8
3	250.2	15.74	2.58	15.4
4	196.8	14.79	2.55	15.7
5	221.1	15.41	2.42	16.1

Table B.2 – Individual 10° off-axis tensile test data of samples manufactured from 10 W treated pre-forms

Sample	σ^{10}_u / MPa	E^{10} / GPa	ε^{10}_u / %	V_f (%)
1	251.6	17.51	2.36	14.3
2	275.2	16.76	2.70	15.9
3	266.2	14.48	2.47	13.9
4	216.5	11.36	3.15	13.5
5	231.5	13.72	2.76	15.0

Table B.3 – Individual 10° off-axis tensile test data of samples manufactured from 20 W treated pre-forms

Sample	σ^{10}_u / MPa	E^{10} / GPa	ε^{10}_u / %	V_f (%)
1	264.3	13.22	3.16	14.1
2	254.8	12.33	2.42	14.5
3	273.1	17.08	2.21	15.4
4	296.6	17.14	3.39	16.1
5	246.1	14.56	1.95	14.8

Table B.4 – Individual 10° off-axis tensile test data of samples manufactured from 28 W treated pre-forms

Sample	σ^{10}_u / MPa	E^{10} / GPa	ε^{10}_u / %	V_f (%)
1	217.7	13.96	2.57	14.5
2	234.4	15.06	2.58	14.7
3	235.1	13.46	2.76	14.7
4	260.4	15.34	3.53	15.2
5	251.1	15.21	2.36	15.9

Table B.5 – Individual 10° off-axis tensile test data of samples manufactured from 35 W treated pre-forms

Sample	σ^{10}_u / MPa	E^{10} / GPa	ε^{10}_u / %	V_f (%)
1	157.9	12.62	1.41	15.4
2	137.8	12.56	1.54	14.8
3	177.6	14.57	1.64	14.8
4	130.1	15.51	1.51	15.0
5	152.6	13.92	1.76	15.2

Table B.6 – Individual 10° off-axis tensile test data of samples manufactured from 50 W treated pre-forms

Sample	σ^{10}_u / MPa	E^{10} / GPa	ε^{10}_u / %	V_f (%)
1	183.0	16.01	2.08	14.7
2	163.2	14.00	1.68	16.6
3	195.2	15.75	1.72	15.0
4	161.3	15.63	1.89	14.8
5	162.0	15.71	2.01	14.8

Appendix C

Samples Manufactured from Individual Veils

Table C.1 – Individual 10° off-axis tensile test data of samples manufactured from untreated individual veils

Sample	σ^{10}_u / MPa	E^{10} / GPa	ε^{10}_u / %	V_f (%)
1	110.6	3.26	4.74	9.14
2	117.5	3.79	4.51	9.14
3	105.3	4.91	4.06	9.77
4	120.6	4.46	5.26	9.94
5	129.9	5.30	4.13	9.77

Table C.2 – Individual 10° off-axis tensile test data of samples manufactured from 10 W treated individual veils

Sample	σ^{10}_u / MPa	E^{10} / GPa	ε^{10}_u / %	V_f (%)
1	101.7	3.46	5.08	8.79
2	121.3	4.13	4.77	8.34
3	123.6	4.70	4.37	8.16
4	135.7	5.12	3.47	9.77
5	116.4	4.01	4.33	8.79

Table C.3 – Individual 10° off-axis tensile test data of samples manufactured from 20 W treated individual veils

Sample	σ^{10}_u / MPa	E^{10} / GPa	ε^{10}_u / %	V_f (%)
1	142.9	3.95	4.95	8.16
2	135.6	3.93	4.47	8.16
3	123.2	4.33	4.24	8.34
4	124.3	4.47	4.81	9.29
5	155.1	3.95	4.76	9.29

Table C.4 – Individual 10° off-axis tensile test data of samples manufactured from 30 W treated individual veils

Sample	σ^{10}_u / MPa	E^{10} / GPa	ε^{10}_u / %	V_f (%)
1	126.6	4.48	3.80	9.0
2	107.4	3.90	4.26	8.16
3	123.6	3.77	4.86	8.16
4	102.5	4.30	3.72	7.77
5	114.4	3.41	4.28	8.16

Table C.5 – Individual 10° off-axis tensile test data of samples manufactured from 40 W treated individual veils

Sample	σ^{10}_u / MPa	E^{10} / GPa	ε^{10}_u / %	V_f (%)
1	84.4	2.85	3.77	8.16
2	111.7	4.13	4.02	9.29
3	91.3	3.52	3.58	8.59
4	91.0	3.10	4.54	8.79
5	103.9	4.05	3.65	8.16

Table C.6 – Individual 10° off-axis tensile test data of samples manufactured from 50 W treated individual veils

Sample	σ^{10}_u / MPa	E^{10} / GPa	ε^{10}_u / %	V_f (%)
1	75.0	3.83	3.04	10.39
2	96.3	4.83	2.60	10.39
3	85.9	4.53	2.78	10.11
4	90.1	3.60	3.07	9.77
5	95.6	4.40	3.00	10.11

Appendix D

Example t-test Calculation

Samples manufactured from pre-forms, test for significant difference between the mean
($\overline{x}$) $\sigma^{10}{}_{\text{uN}}$ of untreated (a) versus 10 W plasma treated (b) samples. The t-test equation is
given below:

$$t = (\overline{x}_a - \overline{x}_b)/\sqrt{V_a/n_a + V_b/n_b} \qquad \text{[D.1]}$$

Where:

$\overline{x}_{a/b}$ = the mean value of data set a/b (a = 222.9, b = 257.3 – Table 4.3)

$V_{a/b}$ = the variance (square of the standard deviation) of data set a/b (a = 372.49, b =
506.25)

$n_{a/b}$ = number of results in data set a/b (5 in both cases).

$$t = \frac{34.4}{13.26} = 2.59 \qquad \text{[D.2]}$$